INFORMATION TO USERS

This manuscript has been reproduced from the microfilm master. UMI films the text directly from the original or copy submitted. Thus, some thesis and dissertation copies are in typewriter face, while others may be from any type of computer printer.

The quality of this reproduction is dependent upon the quality of the copy submitted. Broken or indistinct print, colored or poor quality illustrations and photographs, print bleedthrough, substandard margins, and improper alignment can adversely affect reproduction.

In the unlikely event that the author did not send UMI a complete manuscript and there are missing pages, these will be noted. Also, if unauthorized copyright material had to be removed, a note will indicate the deletion.

Oversize materials (e.g., maps, drawings, charts) are reproduced by sectioning the original, beginning at the upper left-hand corner and continuing from left to right in equal sections with small overlaps. Each original is also photographed in one exposure and is included in reduced form at the back of the book.

Photographs included in the original manuscript have been reproduced xerographically in this copy. Higher quality 6" x 9" black and white photographic prints are available for any photographs or illustrations appearing in this copy for an additional charge. Contact UMI directly to order.

UMI®

Bell & Howell Information and Learning
300 North Zeeb Road, Ann Arbor, MI 48106-1346 USA
800-521-0600

Measurement of the Evoked Vascular Response to Cerebral Activation with PET

Bing Wang, M.Sc.

Department of Physics
McGill University, Montreal

June, 1997

A thesis submitted to the Faculty of Graduate Studies and Research in partial fulfilment of the requirements of the degree of Doctor of Philosophy in physics

---

ABSTRACT

A technique to measure the evoked vascular response in the human brain has been developed for a Scanditronix PC2048-15B PET scanner. New hardware and software have been designed to enable the scanner to acquire image data in 8 distinct segments of the acquisition memory sequentially and repetitively when gated by an auxiliary signal. For PET activation studies, these modifications facilitate the application of a stimulation pattern consisting of 8 phases. By synchronizing the phases with the acquisition, the time course of the response to the stimulation is measured. Simulation and phantom tests were performed to verify the system performance before applying it to human subjects. A ^{11}C-CO generator was developed in order to supply gaseous ^{11}C-CO to be administered to the subjects with bolus inhalation. A multiple inhalation method was devised which increases the efficiency of the uptake of the radioactive tracer by up to a factor of 2 when compared with the conventional single bolus inhalation method, which results in an increase in SNR by a factor of 1.4. The EVR technique has been applied to CBV measurements using vibrotactile stimulation to the fingers of the right hand of the subject. The averaged results among 4 subjects show a clear response in the somatosensory right-hand area, with a measured rise time of 7.2±1.9s and a decay time of 13.2 ±2.2s. The technique maybe applied to other PET activation studies such as visual, auditory and olfactory studies.

Acknowledgements

Glory to my Lord Christ Jesus for healing me of insomnia at the time when I was baptized in August 18, 1993, otherwise I was not able to finish this work.

Thanks to my supervisor Christopher Thompson for his practical advice, constant encouragement and support from his MRC SP30 grant. From him I not only learned a lot on science but also on humanity. I also owe thanks to my co-supervisor, Dr. Jonathan Lee for his advice, care, and encouragement.

I would like to thank Mike Mazza, Ray Clancy for their solid Electric Engineering knowledge which helped me to make my design more elegant. Many thanks to Dean Jolly, Brian Naud, Ed Errington, Shadreck Mzengeza and Don Porter for their labour on suppling ^{11}C-CO tracer; to Gary Sauchuk, Richard Fukasawa and Andre Casavant for the aid during the PET scans.

Dr. David Reutens, Dr. Ernst Meyer, Dr. Thomas Paus, Dr. Yilong Ma gave me a lot of insights in the discussion with them. Peter Neelin, Greg Ward, Yani Picard, Jorge Moreno-Cantu, Kavita Muthy, Alanah Bergman offered their most friendly help. The author is grateful to all of them.

James Robar, my friend and fellow student, faithfully proof-read my whole thesis by correcting the English grammar. His labour is appreciated from the bottom of my heart.

I owe so much to my parents for their sacrificial love without which I could not imagine if I can finish this thesis.

RESUME

Une technique pour mesurer la réponse vasculaire induite (RVI) dans le cerveau humain a été développée pour le tomographe à émission de positrons (TEP), le Scanditronix PC2048-25B de l'Institut Neurologique de Montréal (INM). De nouvelles composantes électroniques (hardware) et de programmation (software) ont été agencées afin de permettre au tomographe d'acquérir répétitivement et séquentiellement des données d'imagerie en 8 segments de mémoires distincts lorsque géré par un signal auxiliaire. Pour des études d'activation en TEP, ces modifications facilitent l'application d'un pattern de stimulations en 8 phases. En sinchronisant les phases avec l'acquisition, la course temporelle de la réponse induite par la stimulation est mesurée. Les tests de simulation et ceux utilisant des fantômes ont été effectués pour vérifier la performance du système avant son application sur des sujets humains. Un générateur de ^{11}C-CO a été développé afin de fournir ce gas radioactif qui doit etre administré aux sujets par une méthode de multiple inhalations. Ceci permet de doubler l'efficacité de l'absorption du marqueur radioactif en comparaison avec la technique conventionnelle de l'inhalation d'un simple bolus conduisant à une augmentation du rapport signal sur bruit (RSB) par un facteur de 1.4. La technique RVI a été utilisée pour mesurer des changements de volumes sanguins célébraux suite à des stimulations vibrotactiles aux doigts de la main droite du sujet. Les résultats moyens obtenus à partir de quatre sujets ont montré une réponse claire dans l'aire somatosensorielle associée à la main droite avec un temps d'ascension de 7.2±1.9s et de descente de 13.2±2.2s. De plus, la technique peut etre appliquée à d'autres études d'activation en TEP comme au niveau visuel, auditif ou olfactif.

Figure List

(Figures are at the end of each chapter)

Table of Abbreviations

AVM	Arteriovenous Malfunction
BOLD	Blood Oxygenation Level Dependent
Cyt-O_2	Oxygenated cytochrome-oxidase
CBF	Cerebral Blood Flow
CBV	Cerebral Blood Volume
EVR	Evoked vascular response
HbR	Concentration of deoxygenated hemoglobin
HbO_2	Concentration of oxygenated hemoglobin
LOR	Line of Response
MNI	Montreal Neurological Institute
MRI	Magnetic Resonance Imaging
fMRI	Functional Magnetic Resonance Imaging
NIRS	Near Infrared Spectroscopy
PET	Positron Emission Tomography
PROM	Programmable Read-Only Memory
ROI	Region of interest
TAC	Time activity curve
VOI	Volume of interest

Table of Contents

1. Introduction

>>>

1.1. Positron emission tomography (PET)

1.1.1. What is PET

PET (Positron Emission Tomography) is a medical imaging technology developed since late 1970s [Ter-Pogossian MM, 1980]. It provides quantitative, three-dimensional images for the study of specific biochemical and physiological processes in humans or animals. The PET imaging technique is based on the detection of the two 511keV γ-rays emitted in opposite directions when a positron, emitted from a radioactive tracer, annihilates with an electron in the tissue or organs in the body. The detection of the two coincident γ-rays makes it possible to define a line on which the annihilation occurs, from which we can derive an image of the distribution of the radioactive tracer.

A conventional PET system consists of a camera, a set of data acquisition electronics and a computer system. A medical cyclotron and a radiochemistry department are also indispensable for the provision of radioactive isotopes. As shown in Fig. 1.1, a camera consists of several rings of detectors which are used to record events by detecting the γ-rays emitted from a part of the body of a subject. Each detector consists of a block of crystal scintillator such as bismuth germinate (BGO) [Thompson CJ, 1979] coupled to a photomultiplier tube. The data acquisition electronics reads and processes the signals from the anodes of all the photomultipliers to provide timing, energy discrimination and

coincidence detection information. The chord between the detectors in which the coincident events occur defines a line of response (LOR). The angular position and the locations of the LORs for detected events are stored into matrices which are called "sinograms". A complete sinogram is used to reconstruct a three dimensional PET image by employing a filtered back-projection algorithm. In a PET image, the intensities of pixels indicates the spatial distribution of the concentration of the radioactive tracers. The image can be used for further physiological interpretation, such as blood volume, blood flow, oxygen consumption measurement, protein synthesis, or tumour detection [Grubb RL, 1978; Raichle ME, 1983; Fox PT, 1986].

A PET scanner can operate in different acquisition modes according to the requirements of temporal and spatial resolution. As an example, the Scanditronix PC2048B scanner presently has two modes available: one is "stationary", for which all the detectors are at rest, and the other is "wobbled", for which each detector moves along the circumference in a small circle to improve the spatial resolution [Scanditronix PC2048-15B software manual]. This thesis introduces a third mode on the Scanditronix PC2048B and named as "EVR" (Evoked Vascular Response) mode, at which the phases of the stimulation given to the subject are synchronized with the sequence of the acquisition, and the data can be acquired to a series of phase-dependent memory regions. The EVR mode is mainly designed for PET activation studies to measure vascular response with a reasonably good temporal resolution without a trade-off in spatial resolution.

1.1.2. Radiochemistry and PET applications

The application of PET to specific physiological functions requires specific radiopharmaceuticals labelled with various positron-emitters. Table 1 summarizes some commonly-used positron emitters, their basic properties and the methods used for their production.

Table 1. A list of positron emitters with their properties and producing methods

Radio-isotope	Half-life (minutes)	Target material	Nuclear reaction	Energy required (Mev)
^{15}O	2.07	N_2	$^{14}N(d,n)^{15}O$	6
^{13}N	10.0	graphite	$^{12}C(d,n)^{13}N$	6
		water	$^{16}O(p,\alpha)^{13}N$	10
^{11}C	20.4	boron	$^{10}B(d,n)^{11}C$	6
		enriched ^{11}B	$^{11}B(p,n)^{11}C$	10
		N_2	$^{14}N(p,\alpha)^{11}C$	10
^{18}F	109.8	Ne	$^{20}Ne(d,\alpha)^{18}F$	6.1
		H_2O	$^{16}O(^3He,p)^{18}F$	20
		H_2O	$^{16}O(^4He,pn)^{18}F$	35
		$H_2{}^{18}O$	$^{18}O(p,n)^{18}F$	9
^{77}Kr	74.8	NaBr	$^{79}Br(p,3n)^{77}Kr$	35
^{68}Ga	68.3	$^{68}Ge/^{68}Ga$ generator		
^{82}Rb	1.25	$^{82}Sr/^{82}Rb$ generator		
^{62}Cu	9.8	$^{62}Zn/^{62}Cu$ generator		

The positron-emitting isotopes such as ^{11}C, ^{13}N, ^{15}O, ^{18}F, can be produced by small medical cyclotrons by bombarding a target with accelerated particles, such as protons or deuterons. These short-lived positron-emitters can be used as labels without causing problems to the structure or metabolism of the biomolecule. In particular carbon, oxygen and nitrogen are constituents of living organisms and are useful in creating molecules which mimic the functions of naturally-occurring agents. The short half-life of these positron emitters used makes it possible to perform repetitive studies and to minimize the exposure of the subject.

Several other positron-emitters have considerably greater half-lives, but are used less commonly, and are more complicated to produce. These include ^{77}Kr (half-life 74.8 min) and ^{75}Br (half-life 95.5 minutes), which require higher energy cyclotrons for their production [Diksic M, 1977]. ^{68}Ga (half-life 68.3 minutes) is obtained from a ^{68}Ge-^{68}Ga generator, and ^{82}Rb (half-life 1.25 minutes) from a ^{82}Sr -^{82}Rb generator.

The lighter positron-emitters, such as ^{11}C, ^{13}N, ^{15}O, ^{18}F, and their radio-pharmaceuticals are normally produced and used to study quantitatively a variety of functions, such as blood flow, blood volume, oxygen metabolism and glucose metabolism, in the human brain in vivo, and they are used in most of the PET centres such as the Brain Imaging Centre in Montreal Neurological Institute (MNI). Because only a small cyclotron is required, it is relatively affordable and convenient. The following discussion will focus on the application of these more commonly-used positron-emitters.

^{15}O has a half-life of only 2 minutes. It is very commonly used to label water for blood flow measurements. PET activation studies based on regional blood flow changes employing ^{11}O labelled water have been used effectively to map different functions of the human brain.

[Raichle ME, 1976; Herscovitch P, 1983; Raichle ME,1983; Doyon J, 1996; Owen AM, 1996; Hurtig R, 1994]. ^{15}O is used also to label gases such as $C^{15}O$ for blood volume studies [Grubb RL, 1974, Martin WRW, 1987], ^{15}O labelled CO_2 for CBF studies and O_2 for oxygen consumption studies. The longer half-life of ^{11}C (20 minutes) is used for studies involving repetitive stimulation or longer observation periods, yet it is short enough to diminish totally in a day. ^{11}C can also be used to label CO_2 for blood flow and CO for blood volume studies. ^{18}F is a very important positron emitter. ^{18}F- labelled fluoro-2-deoxy-2-D-glucose (FDG) is used commonly to visualize glucose metabolism, F Dopa is used to study dopaminergic receptors etc [Barrio JR, 1996; Cumming P, 1993].

While PET has been used extensively in research for the study of physiological and biochemical processes, it also has a role in clinical applications by providing quantitative three-dimensional images in vivo. Since glucose and oxygen are almost exclusively the substrates for cerebral metabolism, both ^{18}F-FDG and ^{15}O labelled compounds are popular in clinical studies to examine cerebrovascular diseases [Grubb RL,1979], epilepsies [Yamamato YL, 1983], brain tumours, cardiac diseases [Allemand R, 1980], Breast cancer [Thompson CJ, 1995] and other kinds of brain disorders [Di Chiro G,1981, Owen AM, 1996].

Among all of the applications of PET, activation study has become a very active field, in which subjects are required to perform some given task during the scan. The following section introduces the concept of the activation study, its PET methodology, its goals and limitations.

1.2. Activation studies with PET

1.2.1. Physiology for activation studies

Physiological, anatomical and cognitive behavioural studies have demonstrated that the brain possesses anatomically-distinct processing regions, and that networks of neurons residing in strictly localized areas perform mental processes. In any mental process, glucose and oxygen are utilized by neurons and cerebral perfusion is also influenced by neuronal activities. The physiology of the nervous system is strictly related to the close relationship between blood perfusion, metabolism and neuronal function. Measuring these variables and their relationships thus illuminate various mechanisms of brain.

During cognitive tasks, local alterations in neuronal activity induce local changes in glucose metabolism, oxygen metabolism, cerebral blood flow and blood volume. These changes can be measured with PET quantitatively and they can be used to map the functional loci of mental operations. Glucose utilization is usually quantified by the cerebral metabolic rate for glucose (CMRGlc) and oxygen consumption is measured as the cerebral metabolic rate for oxygen ($CMRO_2$). Cerebral perfusion is indicated by cerebral blood volume (CBV) and cerebral blood flow (CBF) measurement. CBV is defined as an intravascular volume of blood in unit weight of brain tissue. Its change can be caused by volumetric expansion in vessels already perfused [Ngai AC, 1988] or by increasing the proportion of vessels actually perfuses [Shockley RP, 1988]. CBF, on the other hand, quantifies the dynamic alteration in the delivery of blood to a certain mass of brain in unit time. With PET, CBF change is measured by detecting the increased amount of radioactive water which diffuse out of the vessels [Raichle ME, 1994].

Among all the PET activation studies available, CBF is the most frequently measured

variable because increase in blood flow is commonly observed. CBV is less frequently measured because of its comparatively small magnitude of change. For example, in the experiments by Fox et. al. [Fox PT, 1986, Murase K, 1995] on 9 subjects using vibrotactile stimulation, the regional CBF demonstrated a change of 29% with a standard deviation of 9%, while in comparison the regional CBV magnitude of change was 7% with a standard deviation of 6%. Similar studies by other authors also show the same trend [Murase K, 1995]. More sensitive methods to measure regional CBV changes are still required.

1.2.2. PET methodology for activation studies

PET activation studies involving cognitive tasks have become a well-known means to map the human brain and to investigate the neuronal activities in relations to behaviour. It specially facilitates the study of sensory, motor, and cognitive functions in human subjects. After administering the tracer to the subject, scans with and without tasks are acquired. The scans without tasks are referred as "base-line", "rest state" or "control state", and the scans involving tasks as "activation" or "task state". Because the cerebral hemodynamic state in nonactivated brain areas is quite stable over time, a control state perfusion image can be subtracted from a task state image to create a new functional image to present local changes caused by activation tasks. These functional images can be further interpreted to explain neuronal phenomenon with mathematical models. For some studies, more than one subject is scanned in order to increase the signal-to-noise ratio, or to remove individual physiological variations.

Figure 1.2 is an illustration of the methodology of the PET activation study [Raichle ME,

1994]. In this study, ^{15}O-labelled water bolus was administered to the subjects and visual stimulation tasks were performed.

Commonly, magnetic resonance Imaging (MRI) scans are conducted to provide an image of detailed anatomical brain structure for the purpose of comparative study and rescaling the images of each subject into a standard space in order to perform averaging and statistical analysis among multiple subjects.

1.2.3. Application of PET activation studies

A large number of studies have been done to map the locations and to study the function of visual, somatosensory, sensory-motor, auditory, olfactory and other cortices.

Visual PET activation studies have revealed some of the physiological response characteristics of the human visual cortex by measuring CBF employing ^{15}O labelled water bolus or by measuring glucose utilization employing ^{18}F-labelled FDG. These studies provide images indicating the spatial dependence of the response of the human visual cortex to the site and size of retinal stimulation. These approaches have demonstrated the relationship between the complexity and the magnitude of the change of the blood flow and oxygen consumption in the visual cortex, the correspondence of the input of each eye to specific regions of visual cortex [Fox PT, 1987a; Roland PE, 1994].

Auditory PET activation studies employing FDG as a tracer have shown a correlation between the distribution of glucose utilization and the pattern of the stimuli presented to the subject. Complex patterns of responses to auditory stimuli were observed when experiments on pitch perception, speech, attention were conducted [Perry DW, 1996; Zattore RJ, 1996].

PET images resulting from CBF studies using ^{15}O labelled water, together with MRI images have been useful in the preoperational assessment of patients with cerebral AVMs (arteriovenous malfunctions) in regions corresponding to speech [Leblanc R, 1992].

Language studies with PET have contributed to identify the anatomic basis of language processing and the neural basis of the language deficits such as Alzheimer's Disease [Grady CL, 1993].

Olfactory cortices are usually thought to be poorly understood. PET activation studies involving CBF measurements with ^{15}O labelled water while presenting olfactory stimulation, have contributed to the localization and lateralization of the olfactory cortices [Zatorre RJ, 1992]. More recent studies on the interaction between olfactory and gustatory systems have demonstrated evidence of suppression of primary gustatory cortices when both taste and smell stimulations are applied at the same time [Small DM, 1996]

Vibrotactile PET activation studies, by measuring regional cerebral blood flow and regional cerebral oxygen consumption, are used to map somatosensory cortices corresponding to a large number of tactile-responsive regions in the human body, including fingers, lips, toes [Fox PT,1987b]. Such studies also have revealed physiological response characteristics of the cortex, such as undivided attention [Drevet WC, 1995; Seitz RJ, 1992], and the coupling between brain function and cerebral perfusion [Lou HC, 1987]. Since vibrotactile stimulation generates intense and consistent focal rCBF increases in the corresponding cortex, and because experiences and a large amount of data on studies with vibrotactile stimulation are available in MNI, it is a quite feasible way to investigate physiological and pathological changes of local neural activity, and to test new techniques for neuronal activation studies.

Clinical applications of PET activation studies are also imminent. PET can be employed for the diagnosis of various cerebral disorders and diseases, such as brain tumours, ischemic stroke and migraine diseases.[Maini CL, 1990].

1.2.4. Temporal requirements in activation studies

While the majority of methodologies used have aimed to reveal the magnitude and spatial nature of neuronal activities, very few have focused upon the temporal course of these activities. Previous studies have illustrated that the major challenge in measuring the time course arises from the complexity of the brain function itself. As an example, the speed of neuronal activity is incomparably faster than the speed of vascular response. A signal from one part of the brain may travel to another in less than 0.01 second, but the change of CBF, CBV and metabolism can occur over seconds [Raichle ME, 1994]. New techniques are required to explore the brain as a whole.

The examination of the temporal nature of cerebral activities introduces numerous new questions. For example, how rapidly do these activities occur following the stimulus? How are CBF, CBV, CMRGlc and $CMRGO_2$ related in response to different patterns of stimulation? How do different parts of the brain coordinate as a network to produce a certain behaviour? How does the time course vary with age, sex, or different abnormal neurological states? Does the temporal course of these responses contain information that would allow one to treat a disease more efficiently? Techniques other than PET exist and are employed to provide very good time resolution , yet, each presents its own advantages and disadvantages. None can replace PET because of its ability to provide three dimensional tomographic images

and to measure some neuronal functions directly. The following section briefly describes some of the techniques used to measure the time course of the neurological activation.

1.3. Some techniques for measuring time course of neurological activities

Near Infrared Spectroscopy (NIRS) is an optical technique which measures the absorption of infrared light by tissue. It is a noninvasive tool for the continuous monitoring of changes in CBV, oxyhemoglobin (HbO_2), and deoxyhemoglobin (HbR). It offers a time resolution of 0.5s [Villringer A, 1994] for assessing changes in cerebral hemodynamics during various functional states of the adult human brain. Kato et al [Kato T, 1993] and Villringer et al [Villringer A, 1994] have studied human cortical function by measuring hemodynamics and tissue oxygenation in response to cognitive stimulation, visual stimulation and epileptic seizure. An increase in local HbO_2 and blood volume with a decrease in deoxygenated haemoglobin are found during such physiological functional activation. A significant, spike-like increase in HbO_2 and blood volume was found during epileptic seizures. Both the temporal relationship between this sharp increase and the onset of epileptic seizure and the magnitude of the change in oxygenated cytochrome-oxidase may be insightful in localizing the epileptic focus. These phenomena might be clinically useful in the future. However, NIRS is limited by its insufficient SNR for an adult human head, since NIRS signals depend on the amount of infrared light penetrating and reflected through biological tissue. Also it does not provide tomographical images of the brain.

The Functional Magnetic Resonance Imaging (fMRI) technique has also been applied to brain functional studies [Ogawa S, 1990]. MRI imaging technique is based on detecting the absorption of radio-frequency energy by the magnetic moments of nuclei which are rich in the human tissue, such as hydrogen. The group of nuclei playing roles is characterized by the following parameters: the magnitude of the longitudinal and transverse magnetization, the phase of the transverse magnetization, frequency of the nuclear-magnetic resonance, longitudinal relaxation time T_1 and transverse relaxation time T_2. A neuronal function such as blood flow and oxygenation can cause a change in one of the above parameters. fMRI is developed to detect these changes to illuminate the corresponding neuronal function [Moonen C, 1990]. fMRI also has the ability to measure the time course of vascular response because of its ability to monitor the signal of oxygen level in blood in real time. With both visual and hand squeezing tasks, a rise-time of about 4 seconds for flow and of 8 seconds for oxygenation changes have been measured with a temporal resolution of about 3 seconds by Kwong et al. [Kwong KK,1992]. The rise-time may reflect the onset of the hemodynamic response following the task-induced neuronal activation. fMRI offers an advantage over electroencephalography (EEG) or magnetoencephalography (MEG) in that it provides high spatial resolution tomographical images showing anatomical and functional information, which makes it possible to accurately identify the activated regions. The other advantage is that it does not involve the administration of radioactive tracers as PET does. There are still quite a few questions remain about the fMRI technique, one of these is the brain vs vein debate [Segebarth C, 1994] which arises from the fact that fMRI provides micro-vascular information rather than macro-vascular information. The temporal resolution of fMRI is at

the level of 3 seconds, which is barely good for vascular response measurement and too slow for neuronal response measurements.

Methods such as EEG and MEG offer high temporal resolution to detect neuronal activities. The former detects brain electrical activity from the scalp and the latter measures the magnetic fields generated by electrical activity within the brain. Both are limited by poor spatial resolution and sensitivity, which degrade when detecting signals from deeper parts of the brain. These disadvantages limit EEG and MEG being used for mapping the brain.

Some other methods used in animals, such as electrophysiology aided by vascular florescence imaging, may also provide us useful knowledge in understanding similar neuronal activities in human brain [Narayan SM, 1995]. Narayan et al successfully measured the time course of CBV in response to stimulation to the foredigit of rats. It has been found that the CBV in the corresponding cortices increases at 1-1.5s and rises to a peak 2-2.5s after the onset of the stimulation. Though it may not be feasible to apply these methods to humans, the results are very valuable in guiding the approaches taken for human brain study.

For PET, the present challenge is the development of improved temporal resolution while presenting the established advantages of this modality. Some work related to temporal resolution has been done, such as performing multiple-frame dynamic CBF studies with the ability to measure very short times by making the frames short enough [Ter-Pogossian MM, 1994], but the SNR has been a problem for spatial resolution while obtaining very short frames. The vascular response could not be measured by repeating the scans, because the PET activation studies are limited to one repetition every several minutes since the half-lives of the positron-emitting isotopes are on the order of minutes (e.g. the half-life of ^{15}O is 2 minutes

). These limitations have prevented PET from measuring cerebrovascular transit times occurring on the order of seconds [Kwong KK, 1992] and instantaneous hemodynamic response time occurring on the order of hundreds of milliseconds [Fristig RD, 1990].

The "EVR" technique has been developed in order to meet the above needs.

1.4. The EVR technique

1.4.1. Principle

Currently the basic limitation of PET in the measurement of time course in the order of seconds is the poor signal to noise ratio (SNR) when a limited amount of radioactivity is administered to a subject. One way to increase SNR is to send the same signal repetitively to a noisy background. The theory of this method can be explained in the following formulae:

The signals of the total counts in a pixel in a PET image are results from radioactive decay, which can be described with a Gaussian distribution:

$$f(S_i, S)=\frac{1}{\sqrt{2\pi}\sigma_i}e^{-\frac{(S_i-S)^2}{2\sigma_i}} \quad , \quad i=1,2,.....n \tag{1.1}$$

$$SNR(i)=\frac{S_i}{\sqrt{\sigma_i^2}} \tag{1.2}$$

Where S_i is the signal measured during the measurement **I** and σ_i^2 is the variance. A total of

n measurements are done.

$$D(S_i)=\sqrt{\sigma_i^2} \tag{1.3}$$

Where **D** is the standard deviation.

The mean of the measured signal will be

$$\bar{S}=\frac{\sum_{i=1}^{n} W_i S_i}{\sum_{i=1}^{n} W_i} \quad , \qquad W_i=\frac{1}{\sigma_i^2} \tag{1.4}$$

W_i is the weight of the ith measurement.

According to the rules of the propagation of standard deviation:

$$D(ax_1 \pm bx_2)=[(a\sigma_{x_1})^2+(b\sigma_{x_2})^2]^{\frac{1}{2}} \tag{1.5}$$

We get

$$D(\bar{S})=\sqrt{\frac{1}{\sum W_i}} \tag{1.6}$$

and

$$\bar{\sigma}=\sqrt{D(\bar{S})}$$

$$=\frac{1}{\sqrt{\sum(\frac{1}{\sigma_i^2})}} \tag{1.7}$$

and

$$\overline{SNR}=\frac{\bar{S}}{\sqrt{\bar{\sigma}^2}}$$

$$=\frac{\sum_{i=1}^{n}\frac{1}{\sigma_i^2}S_i}{\sqrt{\sum_{i=1}^{n}\frac{1}{\sigma_i^2}}} \tag{1.8}$$

When the variable **S** is the radioactive counting rate, $S_i = N_i$, $\sigma_i \approx N_i^{1/2}$, $SNR(I)= N_i^{1/2}$, can be applied. and the mean SNR can be derived as:

$$\overline{SNR}=\frac{n}{\sqrt{\sum_{i=1}^{n}(\frac{1}{N_i})}} \tag{1.9}$$

The mean SNR is higher than SNR(I). When we make a simple assumption that each measurement is of equal precision, that is : $\sigma_1= \sigma_2 = ...= \sigma_n$, then

$$\overline{SNR} = \sqrt{nN_i} = \sqrt{n}\ SNR(i) \tag{1.10}$$

That means the SNR is $n^{1/2}$ times better if a measurement is repeated n times. For a PET study, a weight of

$$W_i = \frac{IN_i}{\sum_{i=1}^{I} N_i} \tag{1.11}$$

is counted for a measurement during the time interval t_{i-1} to t_i. Where N_i is the accumulated counts during $t_i - t_{i-1}$ and a total of I interval were measured.

The above theory suggests that a series of images can be acquired with high SNR, if a transient biological process can be repeated during several half-lives of the radioactive isotope. However, the number of repetition should be optimized, because the counts becomes very low and the improvement in SNR becomes insignificant several half-lives later. The above theory has been successfully applied to gated cardiac studies in nuclear medicine where data from the gamma camera are saved in 8 or 16 bins which are locked to phases of the cardiac cycles. Data accumulates in each frame over a large number of cycles. These can be played back as a movie loop with images of good quality.

Based on this concept of gated technique, we have developed the Evoked Vascular Response technique in order to acquire dynamic PET images in multiple phases with a adjustable phase-duration from milliseconds to several minutes and without compromising spatial resolution.

Figure 1.3 illustrates how the EVR technique works. The function of the stimulation and the location of the data in memory are phase dependent. There are 8 phases in total and the data is acquired from phase 1 to 8 in cycles in several half-lives. Eventually a loop of 8 images can be reconstructed for observing the time dependence of the activation in the brain. Hardware and software design is important to achieve this purpose. The details of this part is described in chapter 2 and 3.

In order to make the EVR technique possible, the following requirements have been considered:

1. A PET scanner with high spatial resolution and the potential for achieving high temporal resolution is required.

2. The hardware should have the ability to separate and store the acquired data to different regions of memory according to different phases of stimulation so that a movie loop of several discrete images can be reconstructed for the purpose of observing the time course of the measurement.

3. Stimuli must be synchronized with the acquisition so that the image acquired in each phase may be accurately related to a specific phase of the stimuli since time discrimination is critical for temporal resolution [Sandman CA, 1984].

4. The repetition of the synchronized stimuli and acquisition in one scan is required so that enough cycles of counts can be accumulated for each phase to achieve adequate SNR for a good quality PET image.

5. Software is required to organize the acquired data of each phase into a structure which can be reconstructed into conventional PET images for further analysis.

1.4.2. Implementation

In order to fulfil the above requirements, some modification has been done to the acquisition system of the Scanditronix PC-2048B scanner [Evans AC, 1991, Thompson CJ, 1990]. The following section is a brief description of the setup used for data acquisition and for the EVR technique. A more detailed account will be given in the following chapters.

1. We could not use the function for gated cardiac studies as it requires hardware which we do not have. But the hardware has the potential mechanism for gated studies. As introduced in section 1.1.1, there are two acquisition modes on the scanner presently: One is "stationary" and the other is "wobbled". When the scanner is operated at wobbled mode, it allocates five times more memory than needed for the stationary mode [Scanditronix PC2048-15B PET scanner software manual]. This large memory region can be used also for the storage of data for eight phases of stimulation. A new electronics circuit board to generate sinograms was designed for the EVR mode to allocate the large memory of wobbled mode phase-dependently, though the scanner remains stationary.

2. Some modifications were made to the controlling logic of the acquisition system for the EVR mode whereby the scanner remains stationary while the memory for wobbled mode is accessed. New logic electronics have been designed so that the scanner can switch between modes easily.

3. The EVR stimulator has been built. This is an electronic device to control the stimuli and to synchronize the stimuli with the acquisition. This ensures that the data can be accumulated in cycles in phase-dependent memory locations.

4. Programs have been written to process the data accumulated while scanning in EVR

mode to produce a series of 8 data files for the 8 phases. Eight images are subsequently reconstructed in a conventional way.

5. Programs have been written for activation ROI analysis and SNR analysis to investigate the activation significance and the temporal information.

1.4.3. Testing

The reliability of the EVR technique was examined with empirical simulation tests using a rotating radioactive source combined with a shaft encoder to ensure the electronics perform properly and that the data can be acquired according to the series of phases. Phantom studies also have been done to test the software to ensure the quality of images before the technique was used on human subjects. (For details, see Chapter 4)

1.4.4. Application

This technique was first applied using vibrotactile stimulation with ^{11}C labelled CO gas administered to subjects. The magnitude and time course of CBV changes in cortical regions corresponding to the phases of the stimulation were observed.

The following considerations have been taken into account in developing this protocol for the first trial.

1. Regional cerebral blood volume is proportional to the local radioactivity concentration in the brain, so that the time course of the activation can be measured without blood sampling, rather based on the measurement of relative changes of the CBV. The following formula is used :[Martin W, 1987]

$$CBV = \frac{C \; 100}{\int_{t_1}^{t_2} C_{bl} dt R d_t d_{bl}} \qquad (1.12)$$

Where , C is the accumulated counts per unit volume from the beginning (t_1) to the end (t_2) of the scan; C_{bl} is the blood activity integrated over the time of the scan; R is the ratio of cerebral small-vessel haematocrit to large-vessel haematocrit; d_{bl} is the density of the blood (g/ml), and d_t is the density of cerebral tissue (g/ml). A value of 0.85 is usually used for the ratio of cerebral small-vessel to large-vessel haematocrit and a value of 1.05g/ml is usually used for the density of both blood and cerebral tissue.

2. It has been proved by a lot of experiments that vibrotactile stimulation applied to the subjects' fingers produce very stable, reliable, significant changes in brain functions such as regional blood flow and blood volume [Fox PT, 1986; Fujita H, 1993; Murase K, 1995].

3. The choice of ^{11}C labelled CO gas as tracer was made for its relatively longer half-life which allows repetitive acquisition of data during a single scan.

4. We assume that any increase in the CO concentration will appear some time (rise-time) after the onset of the stimulus and decrease to normal in a certain period of time (decay time). For this reason there are four phases (phase 1-4) during which one hand of the subject was stimulated followed by 4 other phases during which the subject relaxed. By choosing carefully phase-duration we hope to estimate the rise-time and decay-time of the response. The phase-duration can be adjusted from 1 second to 40 seconds and a five-second phase duration was used in this particular set of scans. The details of the experiments and results are described

in Chapter 6 and 7.

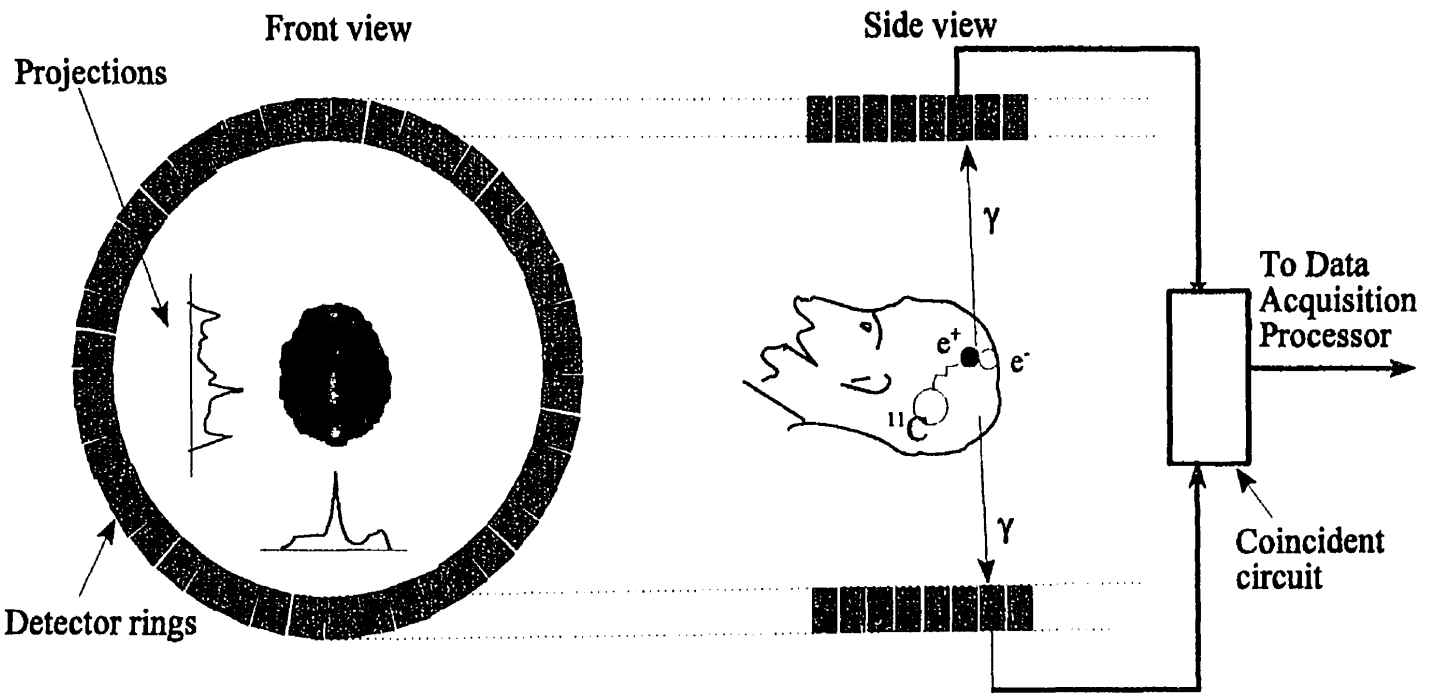

Figure 1.1 General principles of Positron Emission Tomogaraphy (PET).

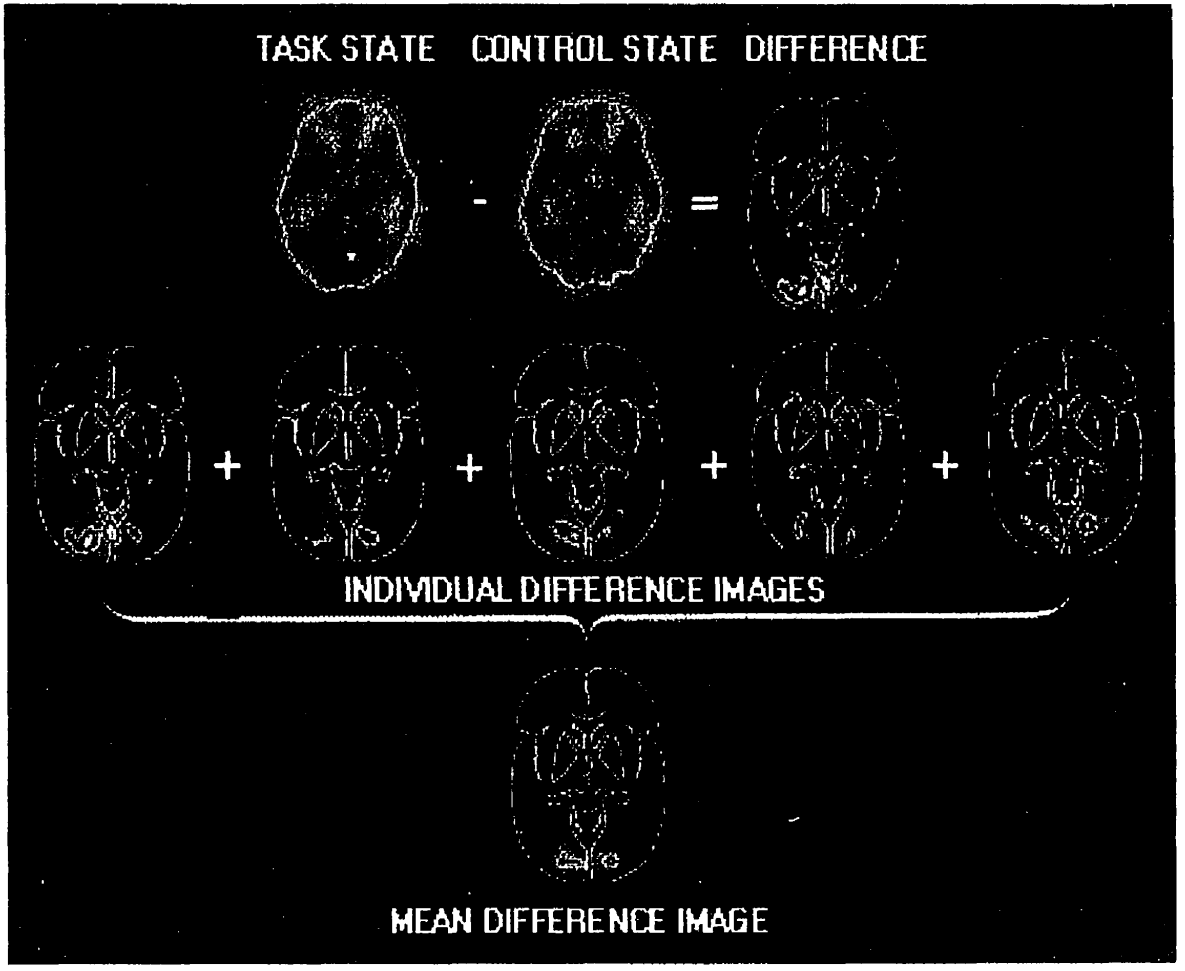

Figure 1.2 Image subtraction and averaging process in PET activation studies [Raichle ME, 1994]

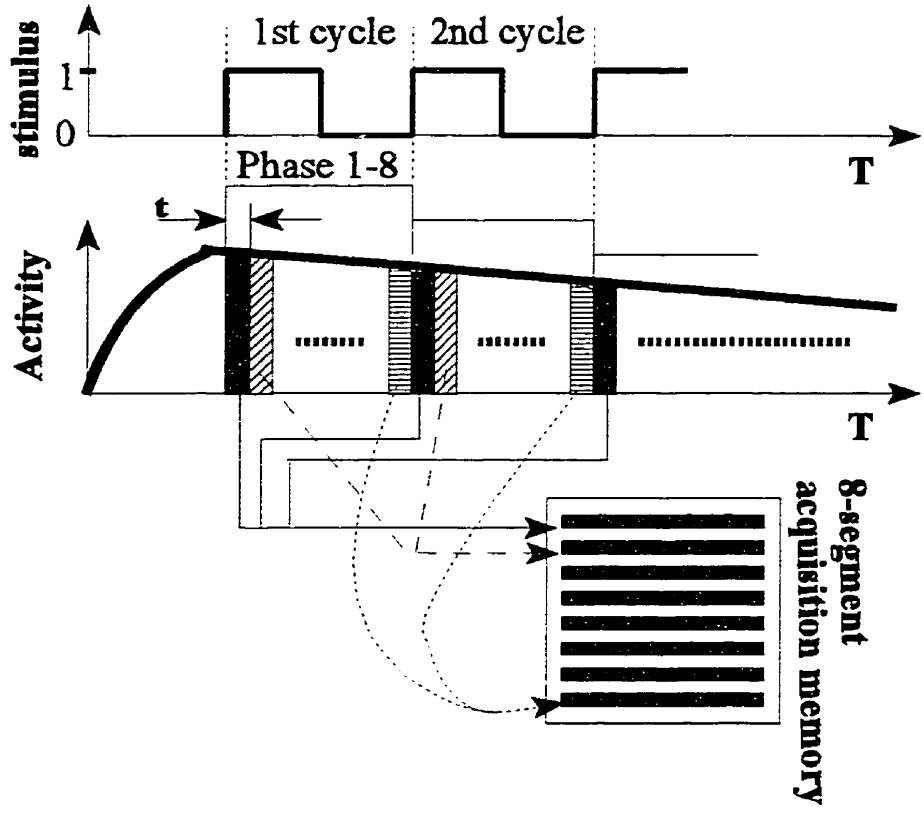

Figure 1.3 An illustration of the EVR acquisition. Where t is phase-duration, and T is the time after radioactive tracer administration.

2. Hardware design for the EVR technique

As was introduced in Chapter 1 section 1.4.1, in order to include the capability for the evoked vascular response, a PET scanner should have the ability to: (1) separate coincidence and singles data into distinct regions of memory according to different phases of the stimulation; (2) synchronize the stimulation with the acquisition; and (3) accumulate data repetitively. This chapter discusses the hardware design of the PET scanner for the EVR mode.

2.1. Theory for generating sinograms

From Chapter 1, section 1.1, we know that all useful coincident events are stored in matrices called "sinograms" and ready to be reconstructed into images with a back-projection algorithm. The X coordinate in a sinogram represents the position (d) and Y coordinates represents the projection angle (β) of a line-of-response. The following paragraphs explain how a sinogram is defined and obtained.

In Figure 2.1, D and B are two detectors on a ring of N detectors. A positron-electron annihilation event happens at point A, and the two emitted γ-rays are detected by a detector pair D and B. Then the event can be identified by d (position along the projection line) and β (the projection angle). The coincident events which are from all possible detector pairs allowed by the radial acceptance criteria will be sorted and stored in a matrix of (d, β) which

forms a sinogram.

The relationship of (d, β) with the detector number can be derived in the following way: Suppose a two-dimensional PET scanner has N detectors around each ring of a radius r. The detector numbers increase anticlockwise, starting from detector 0 on the x axis to detector N-1. An event is detected by detector pair D & B, where $0 \leq$ D or B $\leq$ (N-1). The angle of D and B should be $2\pi D/N$ and $2\pi B/N$ respectively. Considering that the triangle DOB is an isosceles triangle which is made up of two identical right-angled triangles DOC and BOC, and that the line in which the angle β is defined is parallel to OC, then the following relationship can be derived from the triangle DOB, BOC and the angle BOX.

$$d = r\cos\frac{\pi(D-B)}{N} \tag{2.1}$$

$$\beta = \frac{\pi(D+B)}{N} \tag{2.2}$$

We can see that d and β are derived from the "difference" and the "sum" of the two detector numbers. Practically, these calculations are performed by the hardware using adders. The cosine of the " difference" are stored in a table to find X coordinates (d), and the "sum" in another table to find Y coordinates (β). Negative numbers of (D-B) have N added to then to make them positive. The point in the sinogram matrix whose coordinates are calculated (d, β) is incremented if the event is a prompt coincidence. A Programmable Read Only Memory (PROM) is employed for these functions (PROM MPP in Figure 2.6 & 2.7).

Figure 2.2(a) and 2.3 use a simplified illustration to show how projections from all the

possible detector pairs are obtained and stored in a sinogram. For Scanditronix PC2048-15B scanner, projections with even and odd detector-number-difference (e.g. D-B) are stored separately in the sinogram. Figure 2.2(b) shows how the sampling precision can be increased by adding a wobble angular displacement ω when the scanner operates in wobbled mode (see section 1.1.1).

From Figure 2.1, triangle OAC, it can be derived that

$$d = s\cos(\beta - \alpha) \tag{2.3}$$

(where s is the distance of the annihilation point to the centre and α is its angle). The sinogram will show a cosine wave if the annihilation point is fixed (s and α are constants, e.g. a point source). This can be used to test the function of the hardware.

2.2. Data acquisition system of PC2048-15B PET scanner

The Scanditronix PC2048-15B PET scanner in MNI has a high spatial resolution and the potential to accumulate data in discreet phase-dependent memory regions, though the hardware for gated cardiac studies is not available. The following is an overview of the acquisition system of the scanner.

Figure 2.4 is a diagram of the acquisition system of the scanner. The computer configuration of this system is based on a VAX Station 4000/90. Data is acquired on a Data Acquisition Processor (DAP). The DAP communicates with the VAX over a private ethernet. The VAX system has fixed disks, optical disks and high capacity magnetic tapes for data handling. The code for the DAP is written in PLM286.

γ-rays emitted from the brain of the subject are detected by 2048 detector modules, which are in an array of eight rings, each ring has 256 detectors. Pulses from all the detector modules are fed to the discriminator rack, and each discriminator board processes signals from four detector modules. Each signal is split into two for timing and energy determination purposes. One signal is used to activate a leading edge discriminator, which triggers a monostable. The other signal is amplified and summed up with the three others in its module for energy discrimination, and compared with the other signal in the same row and column in separate comparators to identify the crystal in which the γ- ray was absorbed. Triggered by the monostable, a set of comparators identify the crystal and a second set of comparators at the output of the summing amplifiers selects the photopeak of the energy spectrum.

The timing and crystal identification signals are processed by a coincidence circuit. When a coincidence event occurs, the identification of the crystal pair is saved and sorted into parallel projections by a program stored in a PROM (PROM MPP in Figure 2.6). Axial and radial acceptance criteria are also selected by the same PROM. The radial criteria limits the projection length, only LORs whose distance from the centre is less than 15cm are accepted. The axial criteria are set to accept coincidence events which only occur in the direct and the adjacent plane, so a total number of 15 slices can be acquired for an image. Figure 2.5 shows how and why these criteria are set. The identification of detector rings are sorted by another PROM (PROM RPP in Figure 2.6).

In wobbled studies, the detectors are wobbling in the radial plane in order to increase the density of sampling in each projection (Figure 2.2(b)). The diameter of the wobble circle is fixed at 6mm, while the wobble speed can be set from 1 to 60 rpm. There are five wobble

angular position (ω) which are sorted by the third PROM (PROM WDP in Figure 2.6) and then added as a displacement to the projection.

All the above functions are performed by several groups of PROMs (RPP, MPP and WDP) which are mounted on an electronic circuit board called the PROM Circuit Board. Figure 2.6 is an illustration of the PROM board. All the information from the three PROM groups come together to generate sinograms. It should be noticed that there are four auxiliary bins (S0, S1, S2, S3) on PROM RPP, which were put there for cardiac gating studies originally but were not used. the input of these bins can shift the memory locations according to the signal of the input. This function is made use of by the EVR technique, and a new PROM circuit board has been built for the EVR mode including all the capacity of the previous PROM board.

2.3. A new programable read only memory circuit board

When the scanner operates in the new mode EVR, the phase-dependent memory locations are specified by feeding the "phase signal" into the four inputs (S0, S1, S2, S3) of the PROM RPP. As shown in Figure 2.8, a signal W/S, issued by the DAP, signals the PROM board whether the scan mode is stationary (W/S = 0) or wobble (W/S = 1). This signal is set when the acquisition protocol is loaded. In order to allow the scanner to function in the EVR mode, while not interfering with the capacity to switch to stationary or wobbled modes, the signal W/S is converted into W/S' to control the PROMs, while the W/S signal controls the rest of the scanner. This conversion to W/S' is made by a logic circuit, the inputs of which are W/S and P (power of the stimulator, P=1 when power on, P=0 when power off. See 2.4

"Stimulator"). W/S', working together with W/S, triggers the scanner to work at only one of the three modes according to the following truth table:

Table 2.1 The truth table to set the modes on the new PROM circuit board

W/S	P	W/S'	mode
0	0	0	stationary
0	1	0	stationary
1	0	1	wobble
1	1	0	EVR

From the truth table, it is found that W/S and W/S' are opposite only when the scanner operates in the EVR mode. In this situation, W/S'=0 tells the PROM Board not to add wobble position displacement to the projections, while W/S=1 tells the DAP to allocate memory for a wobble scan. Then singles and coincidence data will be accumulated in separate memory locations. The sequence of the location is according to the signal input from S0, S1, S2, S3 (See Figure 1.3). The data structure will be discussed in the next chapter "Software".

A stationary scan can be done whether the stimulator is on, but a wobble scan is only possible with the stimulator off. An EVR scan can be done by applying power to the stimulator, turning off the wobble motor manually, but choosing an unaltered wobble acquisition protocol.

Four LEDs are mounted on this circuit board to monitor the phase signals, and a fifth LED is mounted to monitor the modes.

An OR logic is used to generate a signal E (E = OR[S0, S1, S2, S3]). This signal is fed

to the Logic Control Circuit Board to control the exchanging between stationary, real wobbled and pseudo-wobbled (EVR) modes. (For details, see next section)

2.4. Modifications on the logic control circuit board

When operating the scanner in the wobbled mode, DAP will issue a command to turn the wobble motor on as in the case of a real wobble mode, and a wobble position encoder is used to detect the motion of the wobble motor and send the position information through an eight-bit counter to the DAP. The scan can be enabled only if the DAP detects a continuous position change. Otherwise, the DAP issues an error message and prompts the user to restart or cancel the scan. In order to disable the wobble motor for this "pseudo-wobble" scan while avoiding this error, another circuit on the logic control circuit board was modified to provide the missing input from the counter. (The logic control circuit board is used to control the time sequence of the data acquisition).This part of the hardware modification is described in the following paragraph.

As shown in Figure 2.9 and 2.10, on the original logic control circuit board, one octal buffer (74LS244, OB1) was employed to work as a bus driver to enable the pulses from the wobble motor encoder to be read by the DAP. For the special purpose of the new EVR mode, the circuit has been modified to generate a series of pseudo-wobble pulses. these pulses may be started and stopped at the code which corresponds the code of the home position of the wobble motor (Figure 2.11). The home position is the position at which stationary scans, blank scans and transmission scans are taken and also is the physical position for EVR scans. The coordinates in the world of the reconstructed PET images are also set up according to

the home position.

Fig. 2.10 shows the new circuit used to implement the functions described above. For the pseudo-wobble encoder, a series of TTL pulses are generated by a timer (NE555) to simulate the pulses from the wobble encoder. The frequency of the pulses is 128 pulses per second which is equivalent to the wobble speed 30 rpm. This signal goes to an eight-bit counter (74LS393N) and the eight-bit signals are transmitted by an octal buffer OB2 (74LS244N) to the bus to DAP I/O. This bus originally serves to receive the signal from the wobble encoder through octal buffer OB1. Either of the two octal buffers must be enabled so that the bus can carry the signal either from the wobble encoder or from the pseudo-wobble encoder. An RS flip-flop is employed to enable either of the two octal buffers according to whether the EVR mode has been selected. OB2 is opened for the EVR mode while OB1 is closed; OB1 is opened for wobble and stationary modes while OB2 is closed. (The time sequence of this logic is shown in Figure 2.11). The signal E from PROM board will be high if any of the 4 bits is high, which happens only if the EVR stimulator is working at the EVR mode and one of the 8 phases are active (see section 2.4 " EVR stimulator"). Another signal Home is computed by taking the AND of all the eight wobble position bits, which occurs only once in every 256 pulses. NOR(E) is used as a R (reset) and NOR(NOR(E).AND.NOR(Home)) is sent to the S (set) of the RS flip-flop. This logic also automatically corrects the unstable state caused by the situation when both R and S are 1. Because the pseudo-wobble encoder signal is always running, a Home signal will be generated to set OB1 open and make the wobble position code to the DAP stay at Home, so that the scanner is always ready to be used for stationary or wobble modes.

2.5. EVR Stimulator

In order to provide the correct experimental sequence during EVR studies, an electronic device called EVR Stimulator has been designed for the EVR technique (Fig. 2.12 - 2.15) to: (1) generate the phase signals (S0, S1, S2, S3) to gate the PROM Board with a given phase-duration; (2) assist to set the scanner to EVR mode (See section 2.3 "Logic Control Board"); (3) synchronize the acquisition phases with the stimuli given to the subject; (4) set the pattern of the stimuli; (5) modulate the sweeping frequency of the stimuli to provide choices to deal with physiological adaptation effects.

The following paragraphs describe the electronic circuits designed for this device.

2.5.1. The main circuit

As shown in Fig. 2.13, the main circuit of the EVR stimulator employs an astable (NE555) to generate pulses with an adjustable frequency from 0.25Hz to 5Hz. The signal splits to provide three outputs after processed by two decade counters. One output is fed to the 4 bins (S0, S1, S2, S3) on the PROM RPP. Another output is sent to a numeric display which indicates the present phase. The third output is sent to two comparators (74LS85) where the present phase is compared to the "start" and "stop" codes which are set by two manual switches. (The "start" and "stop" codes can be set at any number from 1 to 8). Then one or two sets of stimuli are enabled to begin at the "start" phase and to stop at the beginning of the "stop" phase. Two sets of phase-dependent stimuli can be applied at the same time if necessary. Two LEDs are mounted on the housing to monitor which of the two stimuli

is on. For studies involving vibrotactile stimulation, two solid state relays can be gated by the "start" and "stop" phase to switch the power of the two vibrators on and off. There is also a manual switch on the housing to set the stimulator on either "EVR" or "Normal". The "Normal" position is reserved for stationary scans (Figure 2.13).

The phase duration is critical for the observation of the vascular or neuronal response. it is now set to be adjusted from 2 seconds to 40 seconds. Four values can be preset with the trimmpots which represent Ra (Figure 2.13), and can be easily varied by a switch mounted on the circuit housing. Two ranges (a "fast" and a"slow") for the duration are set by exchanging the capacitance C, which is by a switch on the housing too.

The frequency is given by [TTL Data Book ; TTL Data Book supplementary.]:

$$f=\frac{1.44}{(R_a+2\times R_b)\times C} \quad (Hz) \tag{2.4}$$

And the phase duration will be:

$$p=\frac{10}{f}=6.93(R_a+2R_b)\times C \quad (s) \tag{2.5}$$

Presently, two phase-duration ranges are available. The "fast" range is from 2s to 5s, and the "slow" range is from 5s to 40 s. These ranges can be easily adjusted by replacing Ra, Rb and C if necessary.

2.5.2. The circuit to modulate the stimuli

In order to achieve the optimum activation for the purpose of functional brain studies, some physical variables of the stimuli must be carefully adjusted. Some of these variables include: (1) amplitude of the stimulation; As an example the head of the vibrators can vibrate with an amplitude of 2mm. (2) Intrinsic frequency; As an example the vibration frequencies of the vibrators provided by the manufacture are 60 Hz and 120 Hz. Thus the amplitude can change 60 or 120 times in a second; (3) modulation frequency; (4) duty cycle of modulation ($T_L /(T_L + T_H)$ in Figure 2.7) [TTL Data Book supplementary]. Both modulation frequency and modulation duty cycle are for obtaining desirable physiological effects. Figure 2.16 shows a stimulation pulse from a vibrator with its amplitude, intrinsic frequency, modulation frequency and modulation duty cycle. Similar variables are also critical for other kinds of stimulation such as visual, auditory stimulation. Figure 2.15 shows an auxiliary circuit built on the circuit board of the stimulator for the purpose of modulating some of the above parameters. A dual timer (LM556) is employed. One works as an astable to generate a series of pulses at a certain frequency, which is the modulation frequency of the stimuli. This frequency can be adjusted with a trim-potentiometer R-VAR-1. the pulse is fed into the other timer so that the duty cycle can be adjusted by a second trim-potentiometer R-VAR-2. This modulated pulse, sent with the output of the comparator to a logic AND, controls the stimulation given to subjects. A switch (SW-M) may be used to override the stimulus modulation as well. Amplitude and intrinsic frequency are not varied by this circuit. Rather, they are adjusted on the apparatus which generate the stimuli.

The EVR Stimulator was applied to the EVR studies with vibro-tactile stimulation, which will be described in details in Chapter 6. It can be also used to control apparatuses for other kinds of stimulation such as visual and auditory stimulations.

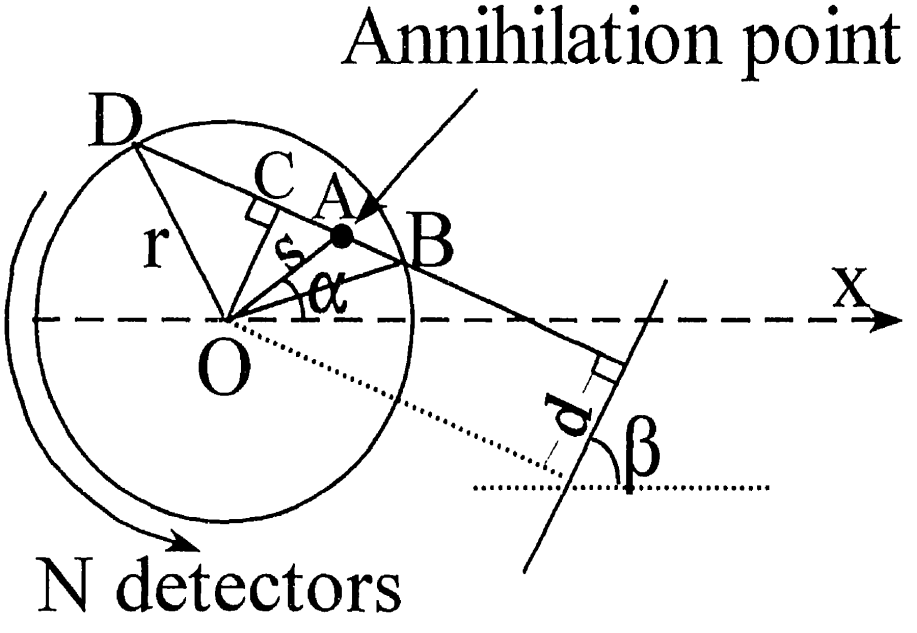

Figure 2.1 The geometry for calculating the projection angle (β) and the position along projection line (d) for each detector pair. The detector numbers increase anticlockwise starting from detector 0 on the x axis to detector N-1.The detectors are numbered from 0 to N-1. B and D are two detectors, r is the radius of the detector circle. α is the angle of the annihilation point, s is the distance from the annihilation point (A) to the centre (O).

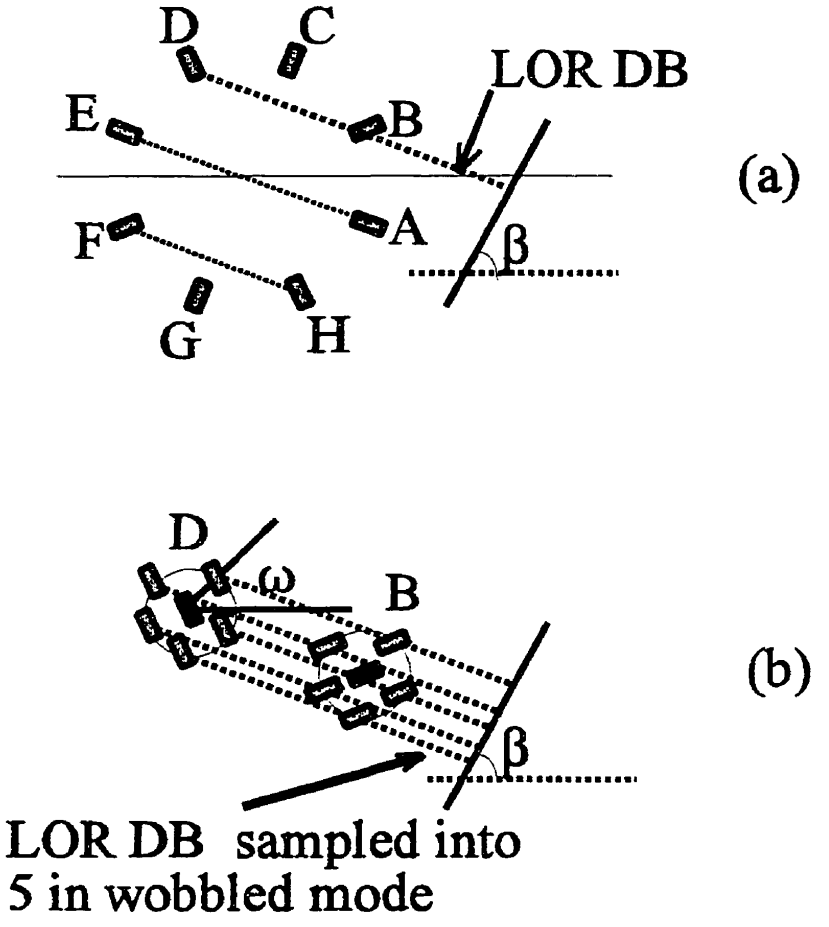

Figure 2.2 (a) A simplified illustration of detector pairs to generate sinograms in Figure 2.3. **(b)** the 5 positions of a detector pair when the scanner operates in the wobbled mode, which samples each LOR into 5.

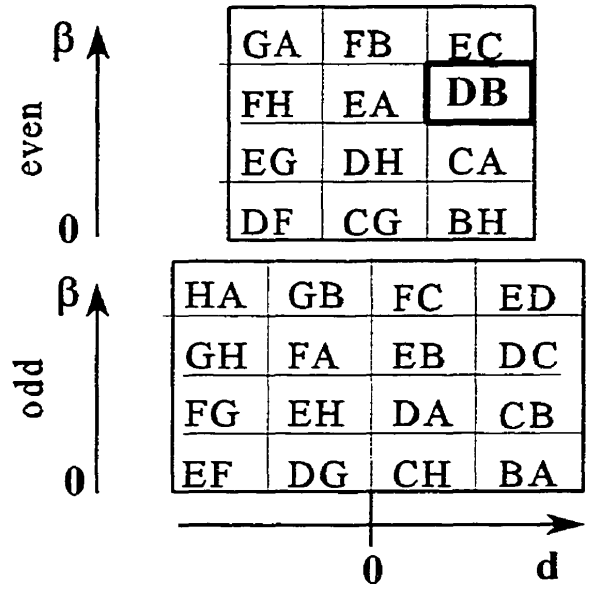

Figure 2.3 A sinogram generated by all possible detector pairs in Figure 2.2 (a). The projections from detector pairs with even and odd number-differences (e.g. D - B) are written separately for Scanditronix PC2048-15B.

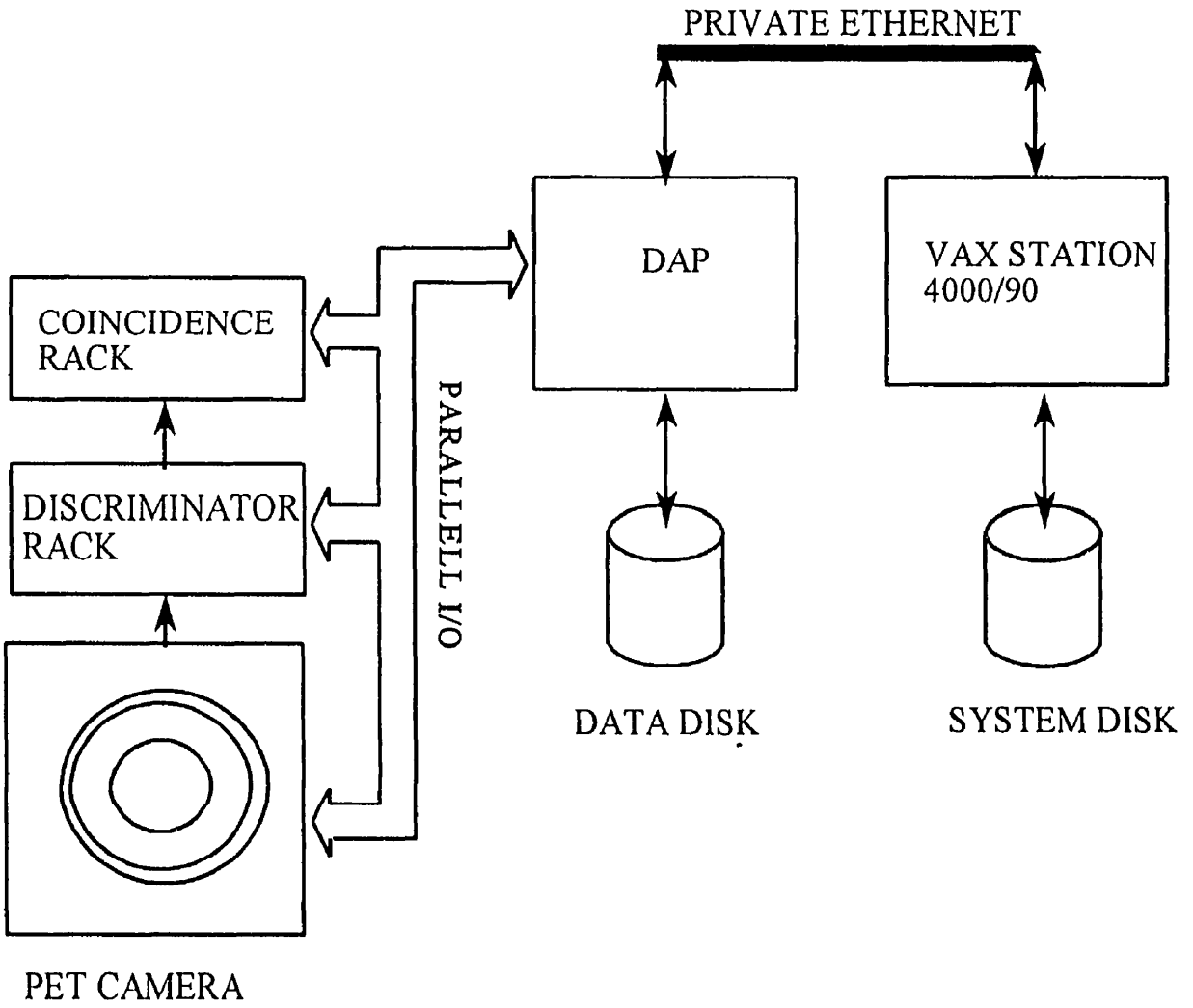

Figure 2.4 Hardware systems of the Scanditronix PC2048-15B PET scanner. The PROM circuit board and the logic control circuit board are mounted in Coincidence Rack.

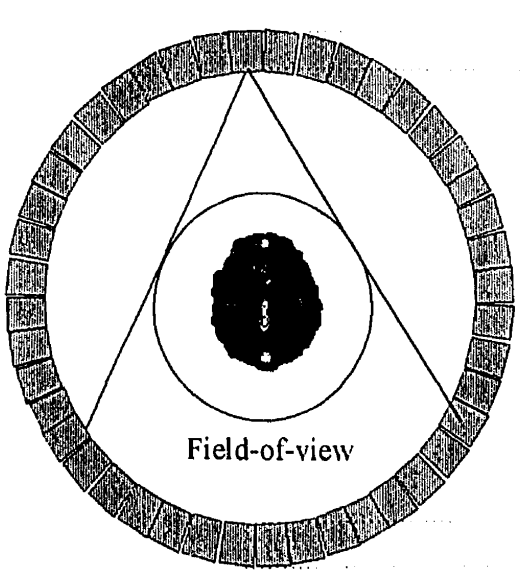

Field-of-view limits the project length, which sets the radial acceptance criteria

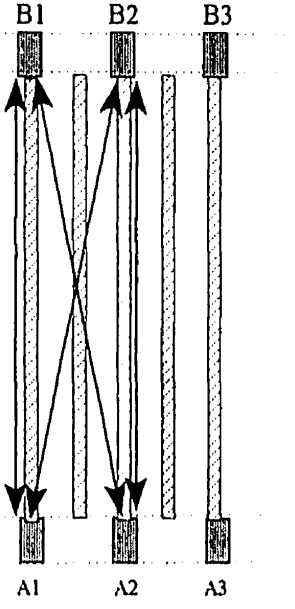

Coincidence in the direct planes (A1-B1), (A2-B2) form direct slices, Coincidence in the adjacent planes (A1-B2) & (A2-B1) form a cross slice

Figure 2.5 Axial and radial acceptance criteria. The former limits the projection length, and the later results direct and cross slices.

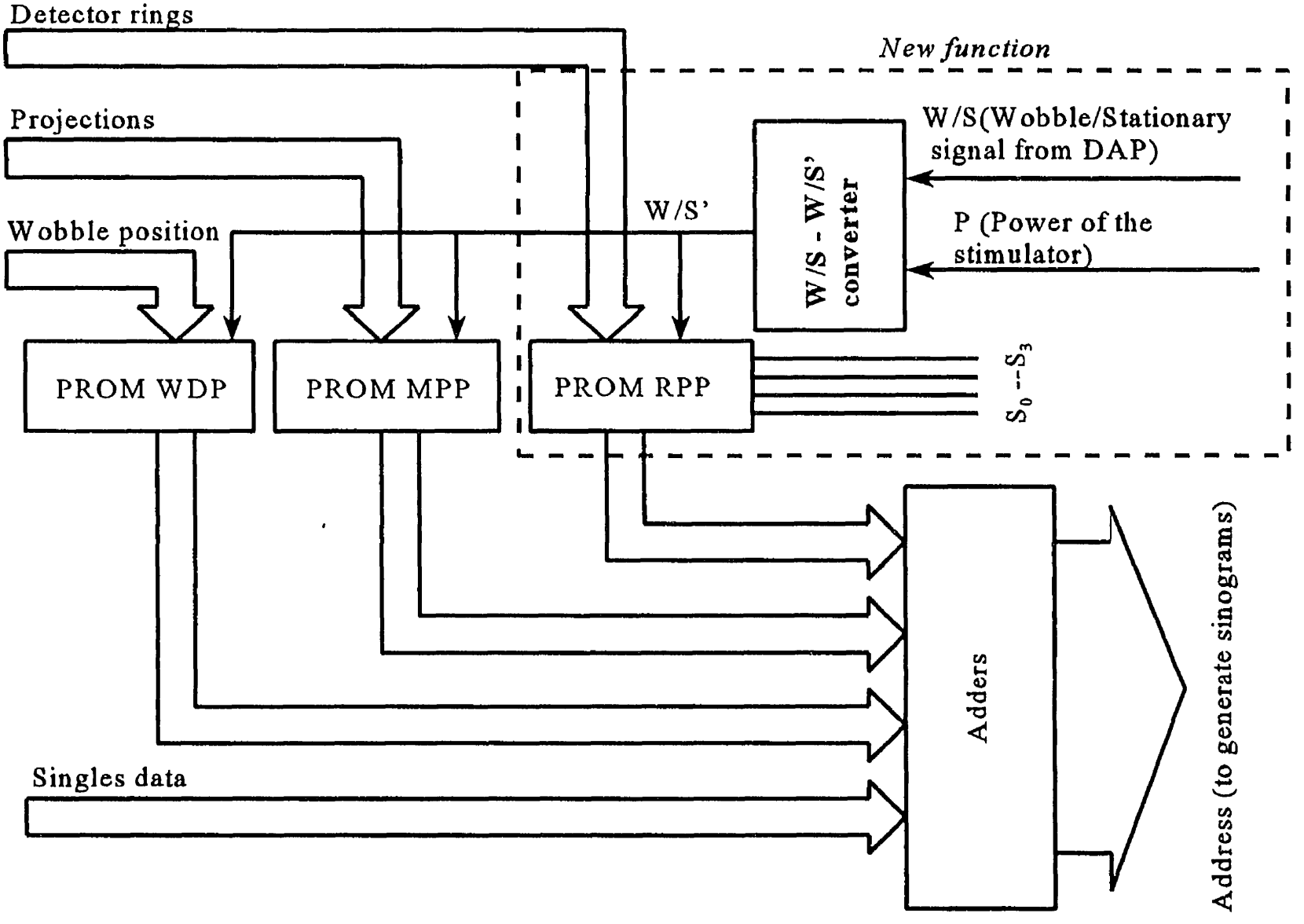

Figure 2.6 A diagram for the original and new PROM circuit board of the Scanditronix PC2048-15B PET scanner.

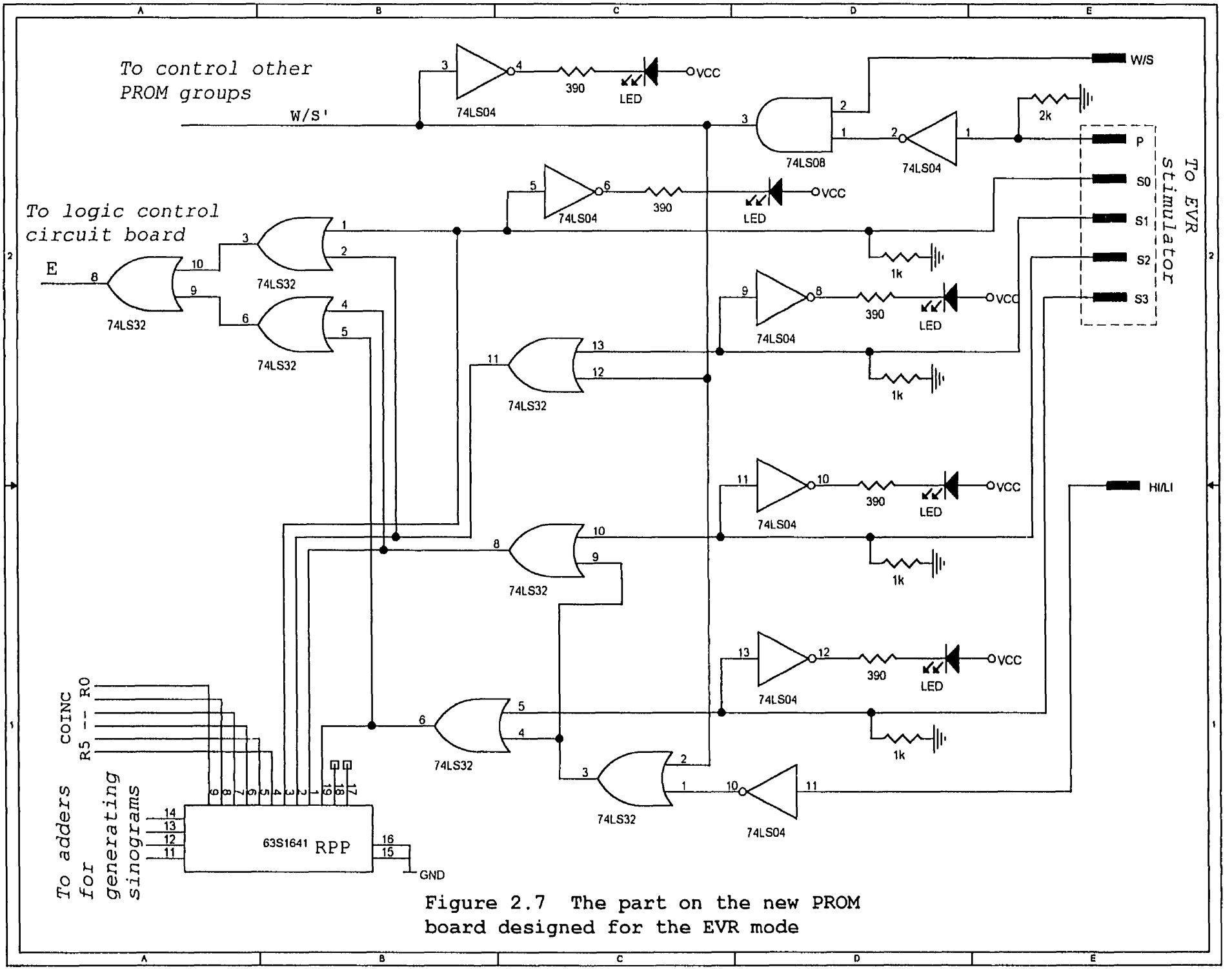

Figure 2.7 The part on the new PROM board designed for the EVR mode

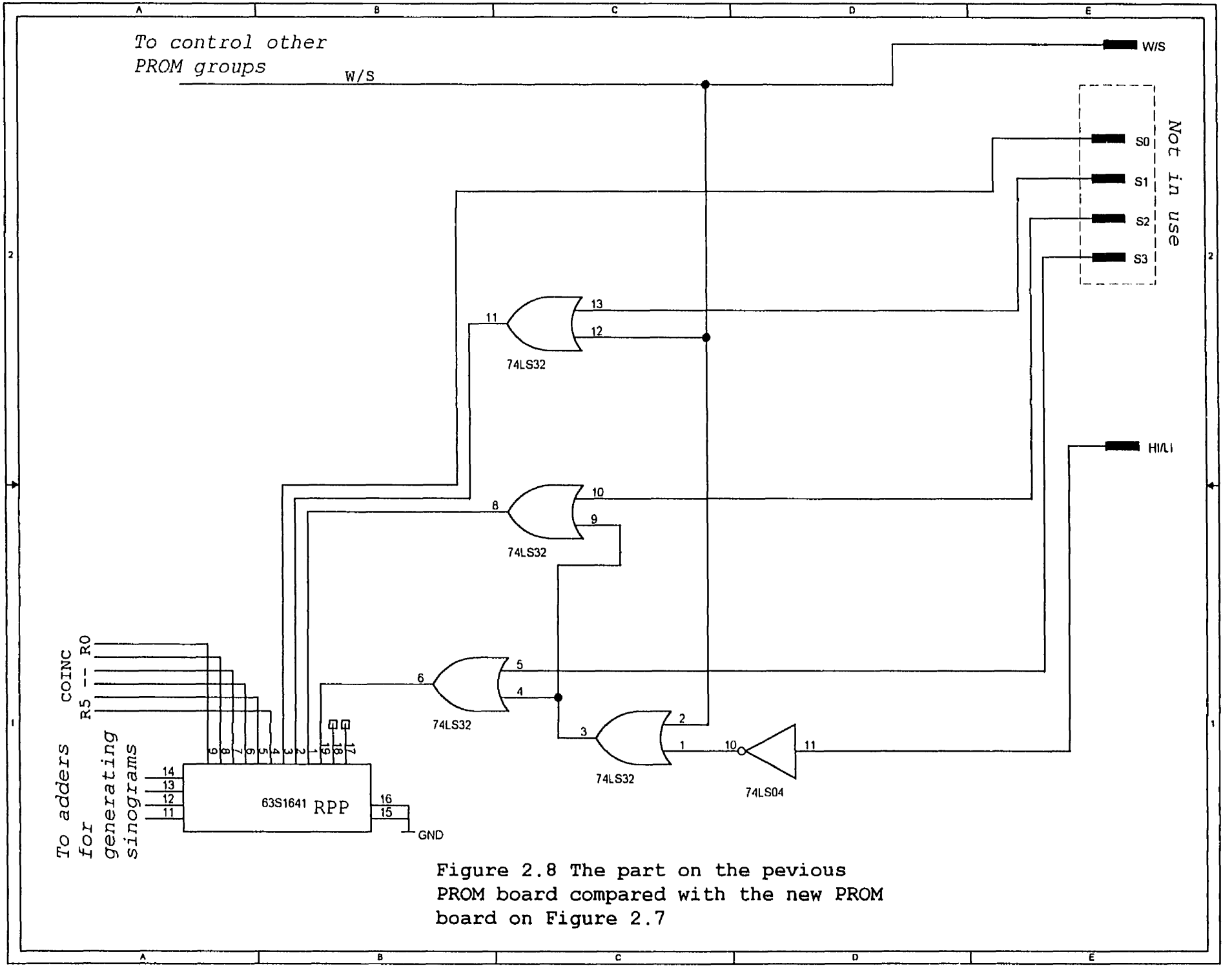

Figure 2.8 The part on the pevious PROM board compared with the new PROM board on Figure 2.7

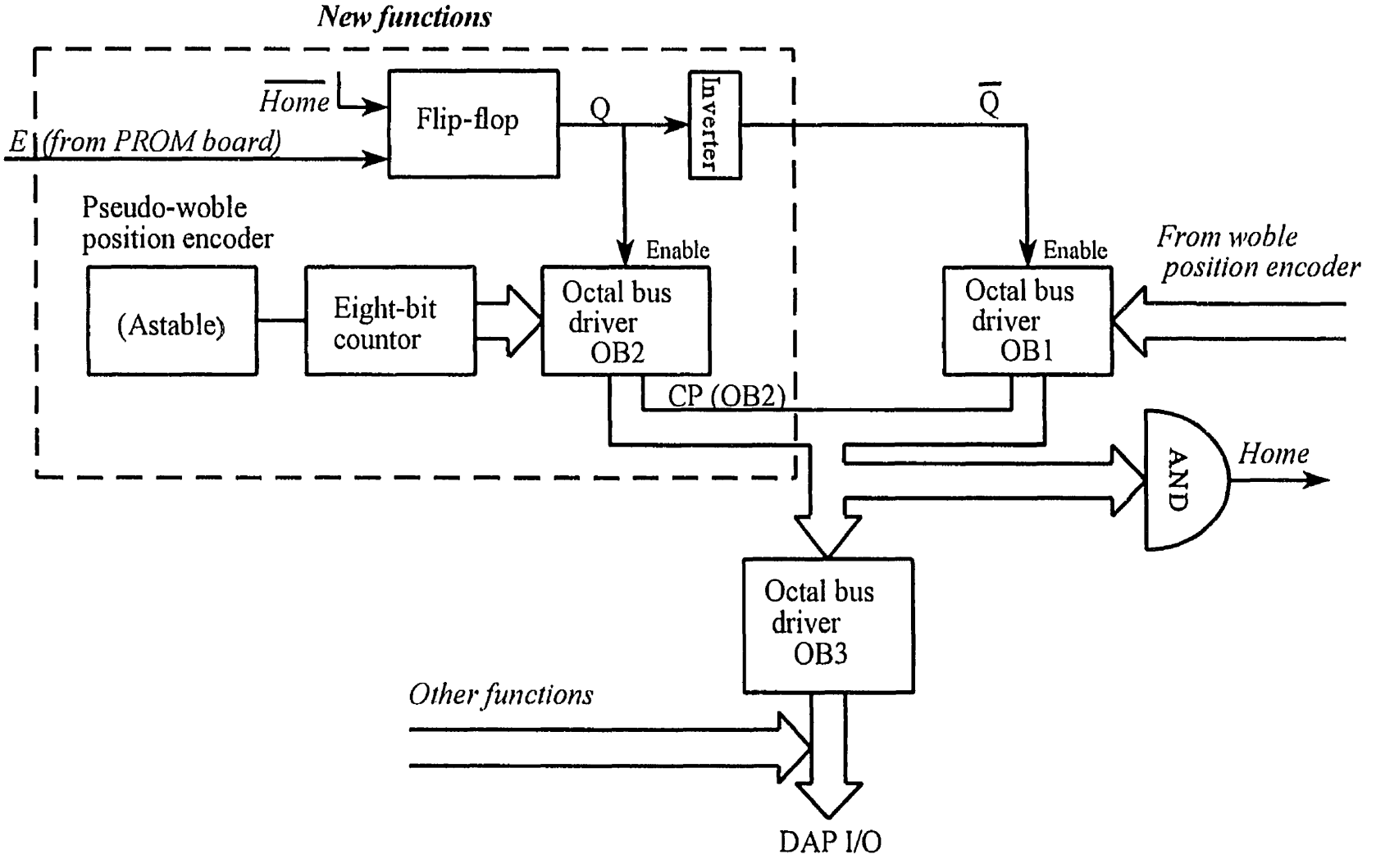

Figure 2.9 A diagram of the pseudo-wobble encoder and the logic to exchange scan modes on the Logic Control Circuit Board.

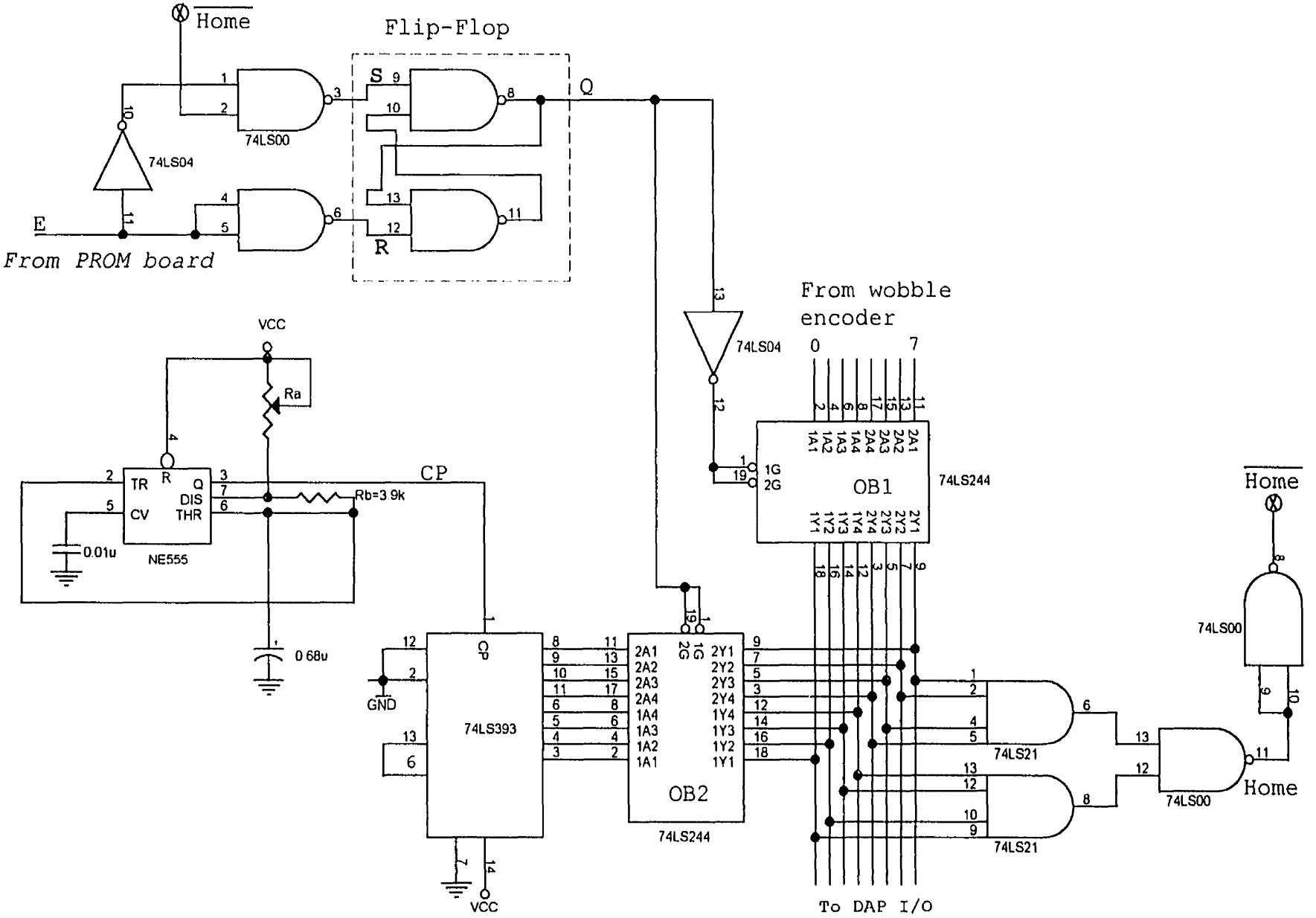

Figure 2.10 Pseudo-wobble encoder and the logic for exchanging scan modes. (On the Logic Control Circuit Board)

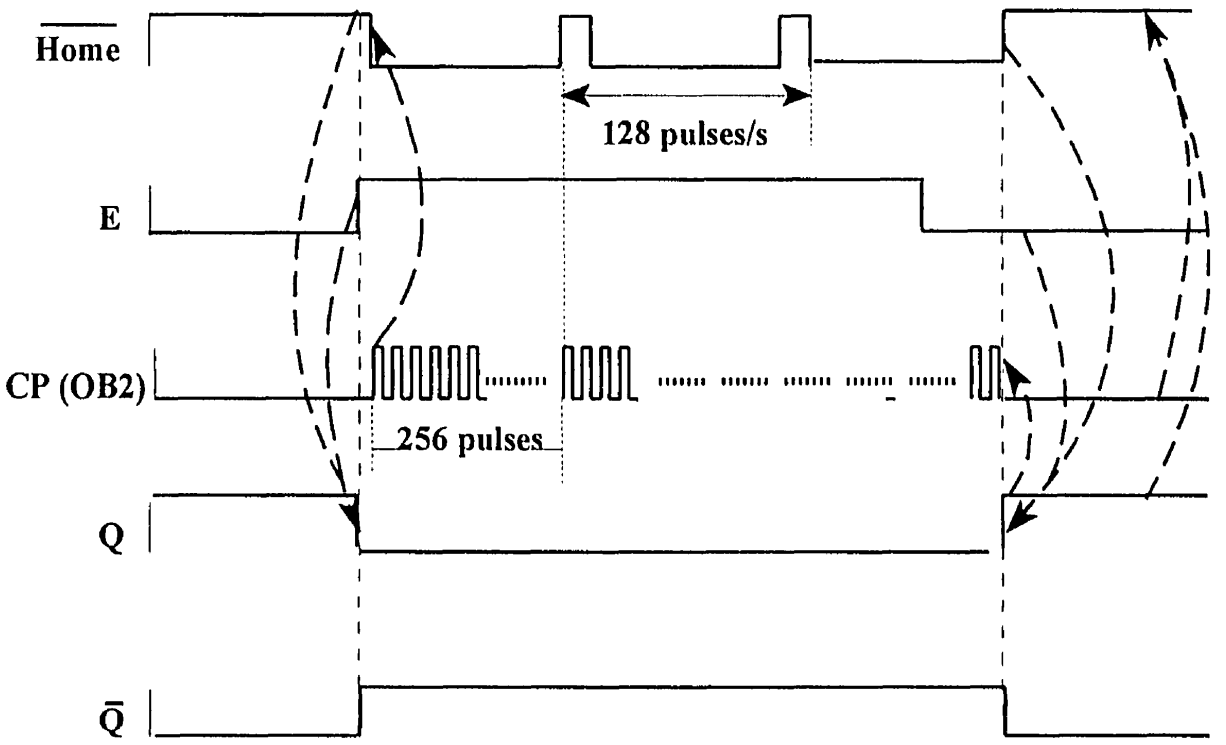

Figure 2.11 Time sequence of the logic exchanging modes of the scanner. The pseudo-wobble encoder will be on in the EVR mode when E is high.

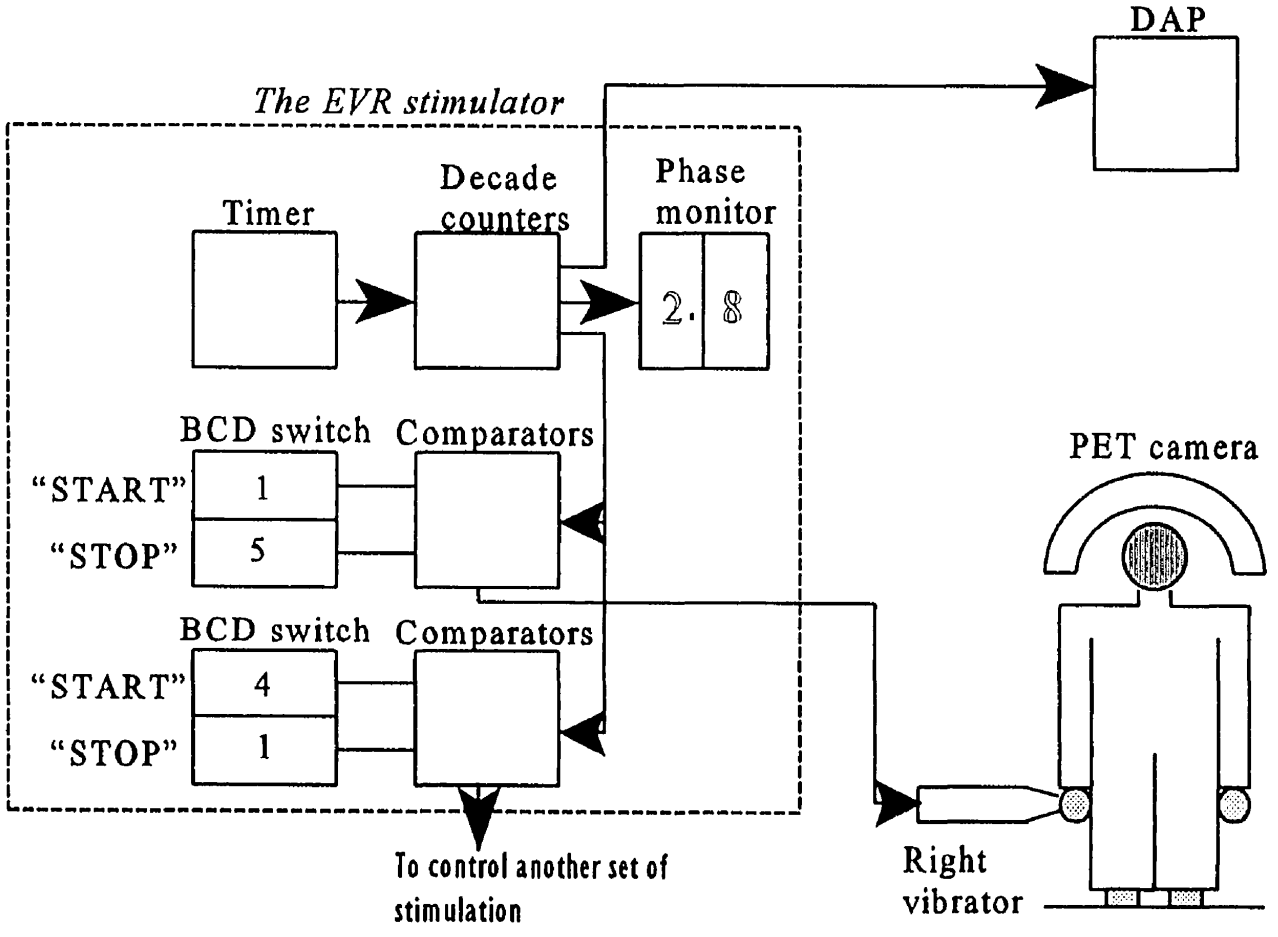

Figure 2.12 The diagram of the EVR stimulator and its application to PET studies with vibrotactile stimulation.

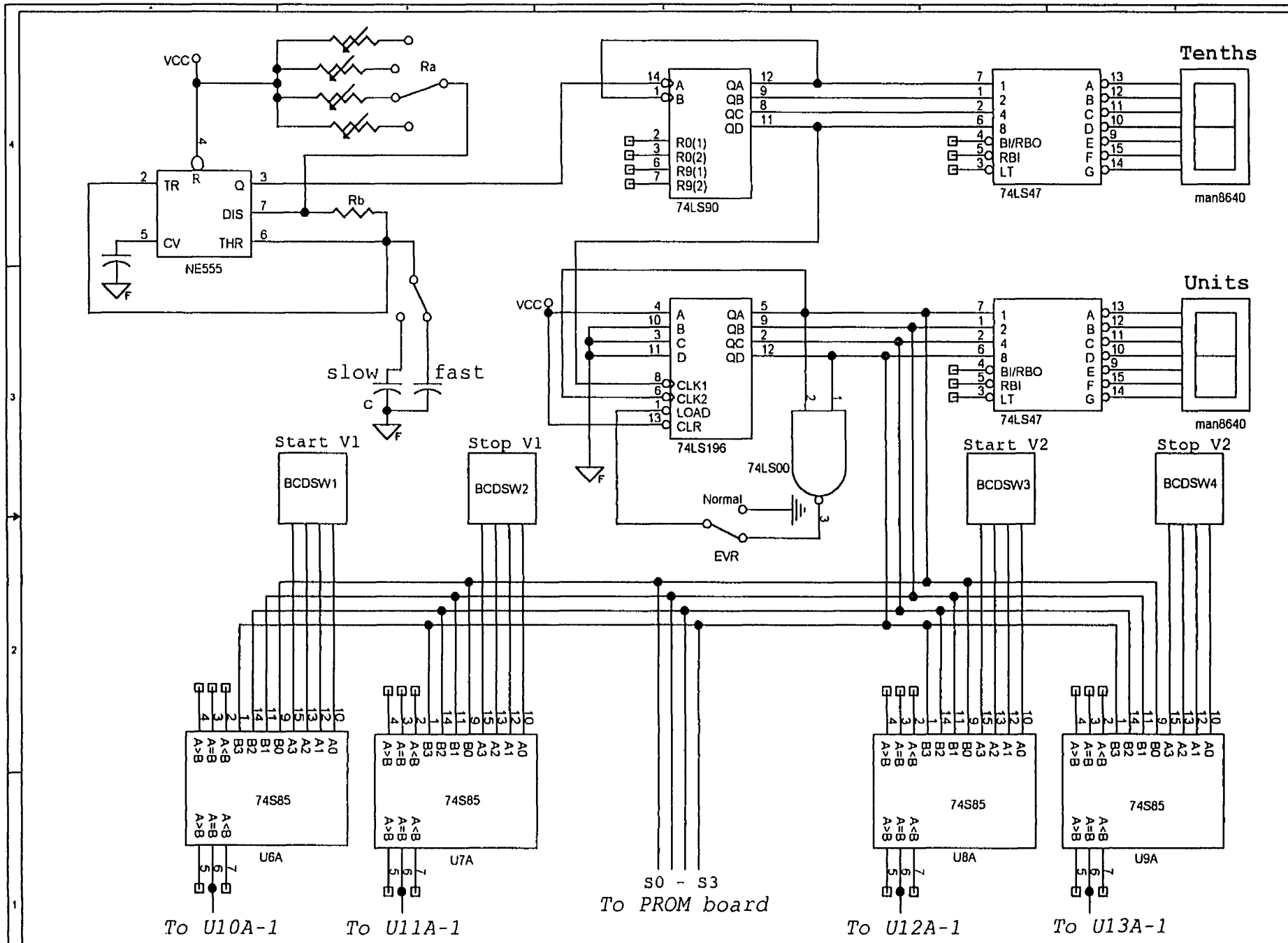

Figure 2.13 EVR Stimulator. Main circuit (page 1)

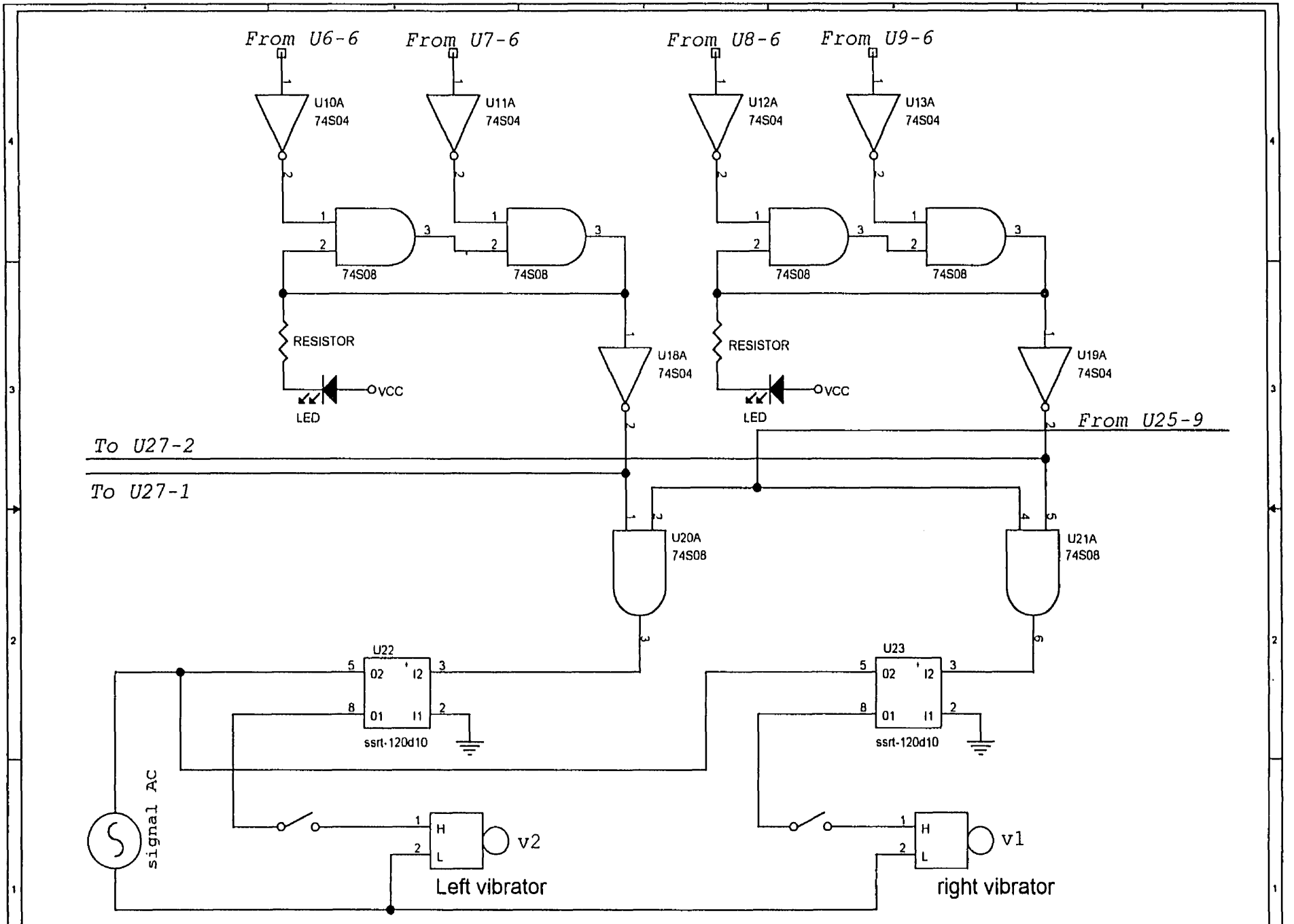

Figure 2.14 EVR Stimulator. Main Circuit (page 2)

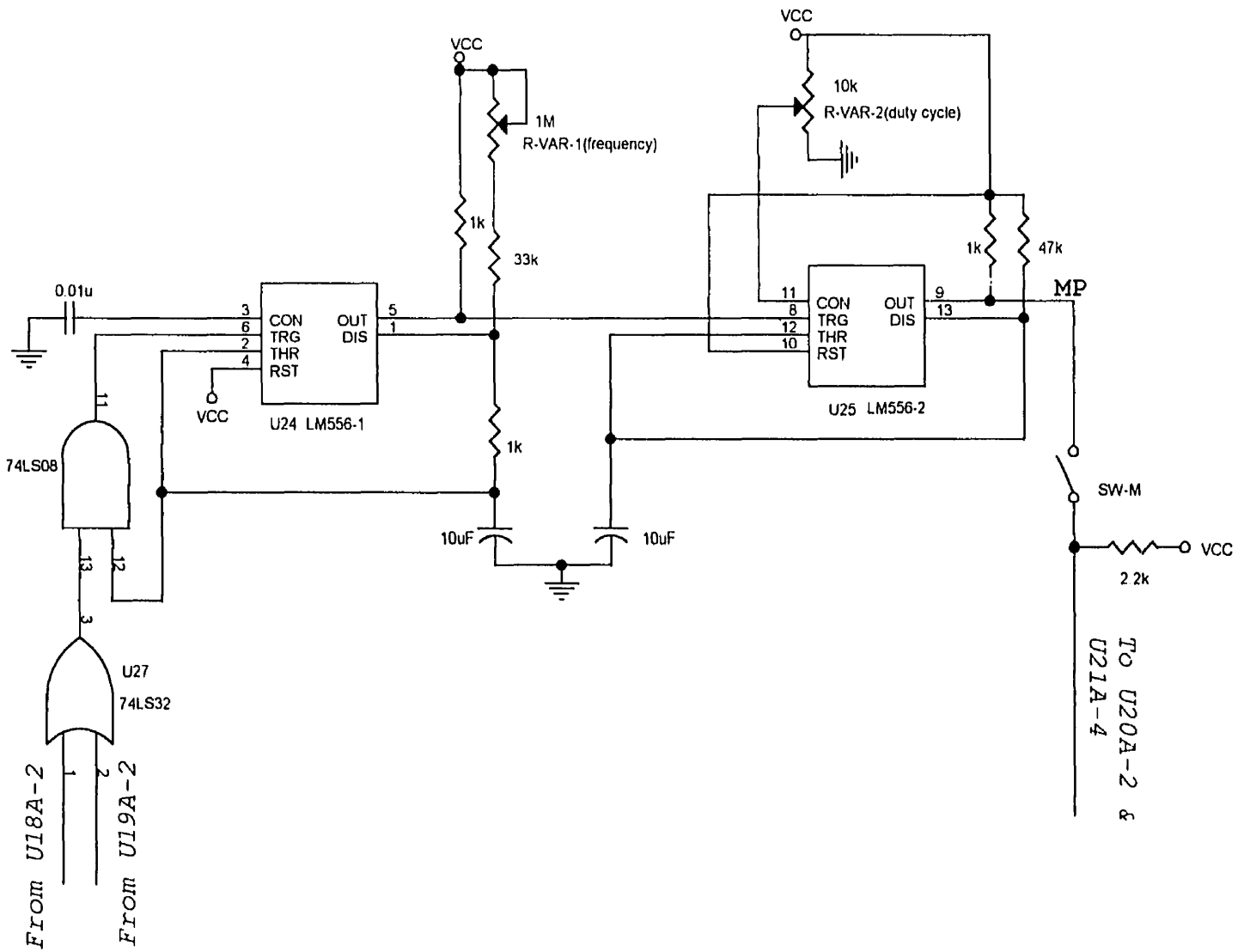

Figure 2.15 EVR Stimulator.
Modulation circuit (page3)

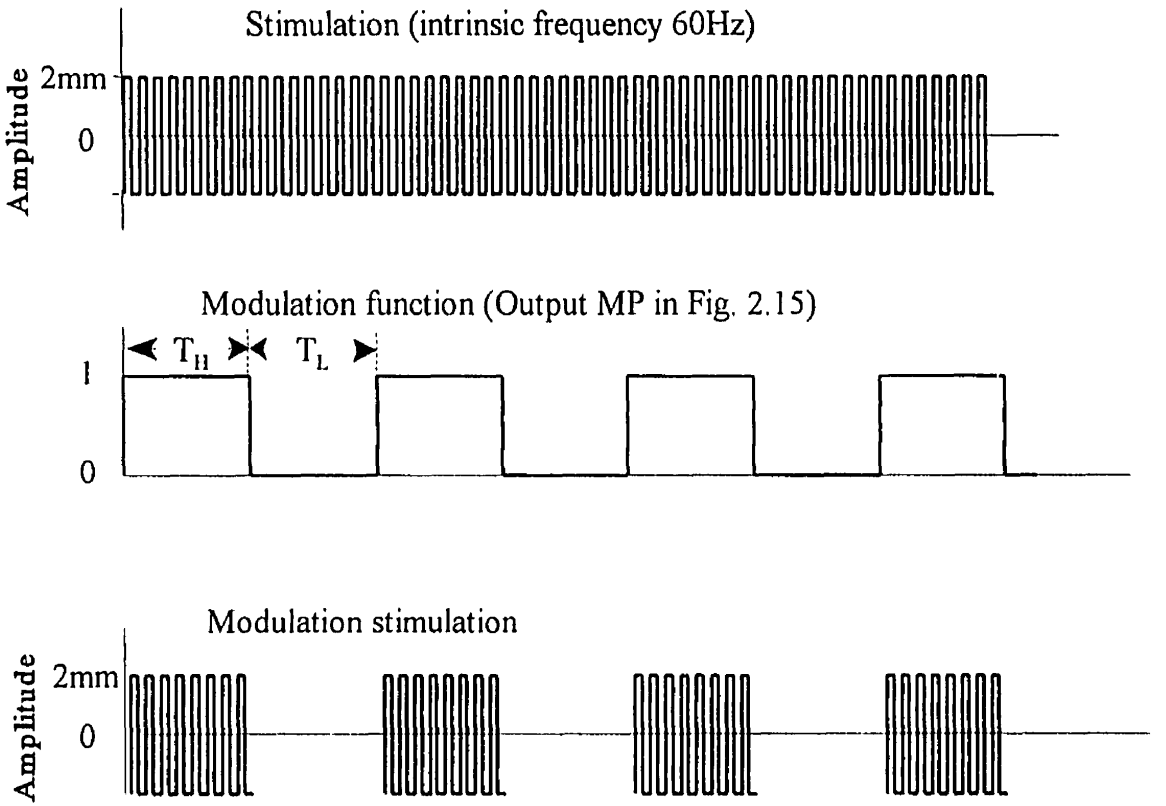

Figure 2.16 Specifications of the vibrotactile stimulation and its modulation. Where T_L and T_H are usually set to 1 second.

3. Software design for the EVR technique

>>

3.1. Overview of the software of Scanditronix PC2048-15B PET scanner

Apart from the hardware which acquires the data and stores it into sinograms, a PET scanner also requires a large amount of software to operate the hardware, to transfer the data into a file of a specific format on the host computer, to reconstruct the data to produce images, and to analyse the images according to the particular purpose of the study.

As shown in Figure 3.1, there are three major program packages which fulfil the basic functions of the PC2048-15B scanner: (1) PCAM for acquiring data; (2) REC for reconstructing image files from the raw data; (3) SEE for displaying and manipulating the images [Scanditronix PC-2048B software manual]. These three programs are employed for EVR scans in a conventional way without any modification. Because the sinograms of an EVR scan are written in a special structure by the new PROM circuit board when the gating function is applied (see section 2.2), a new program CONEVR was written to convert the raw data of an EVR scan into 8 separate data files. The structure of the converted data is the same as a normal stationary scan so that the data can be reconstructed in a conventional way.

The data structures of an EVR scan will be analysed in section 3.3 and the Program CONEVR will be discussed in section 3.4. However, it is necessary to introduce the acquisition program PCAM and its special requirements for the EVR mode first.

3.2. Data acquisition program PCAM and its special requirements for the EVR mode

PCAM sets its own parameters by loading and modifying a protocol which is a " standard" file (STD file). Some of the parameters are for the subject, including name, age and sex. Other parameters pertain to the settings of the scanner, such as the length of each frame of a scan, the total scanning time and the wobble speed. The raw data is acquired and stored to the DAP disk by running PCAM.

The main acquisition programs and all the utilities are files which must be loaded from the DAP disk. All the hardware of the scanner is controlled directly through DAP. The DAP disk is logically divided into a program disk and a data disk. A data file uses different size of disk space, depending on the field of view selected and the mode in which the acquisition system is operated. When the data is transferred from the DAP disk to the data disk on VAX, data files are reorganized, reformatted and a file header is added to each file. The header contains the information from the acquisition protocol and the parameters of the hardware settings such as the number of detectors per ring, number of projections per slice, sampling mode, data type (byte, word or long-word) and the scan type (emission, blank, transmission). It also records temporal information such as the time of injection (the time at which the radio-tracers are administered), the measurement time, the measuring starting time. These data are important for calculating the activity concentration, for random and dead-time corrections.

The acquisition protocol employed for an EVR study is the same as a normal wobble scan,

as long as the gating function is on and the wobble motor is turned off manually (for details, see section 2.2 and 2.3).

3.3. The structure of the data acquired in the EVR mode

Though we know that the new PROM circuit board gated by the auxiliary phase signal can shift memory regions according to the phases when acquiring data, the detailed structure of the data still needs to be revealed by experiments. For this purpose, some experiments are arranged like this:

A cylindric liquid phantom full of ^{68}Ge solution was put into the field of view of the PET camera. The size of the phantom was 175mm in outer-diameter, 200mm in height and a wall thickness of 5mm. The phase was set from 1 to 8 by using a manual switch to set the 4 gating inputs on the PROM circuit board to 0 or 1 (to set the phase number from 1 to 8). A 10 minute EVR scan was done for each phase, and the data were moved to the VAX. A stationary scan and a wobbled scan were also done with the same conditions.

The differences between the data structures among EVR, stationary and wobble scans were found by examining the data files. Table 3.1 is a comparison of the file structures. From the table we can see: Both stationary and wobbled scans have a four-block header (a block is 512 bytes) followed by 16 blocks of singles written in long-words(32bits), and then followed by sinograms written in words (16bits). The sinograms takes 720 blocks for a stationary scan and 3840 blocks for a wobbled scan.

The singles are written in an one dimensional array with a size of 2048, since there are 2048 crystals; The sinograms are written in fifteen (48×256) arrays, one following another.

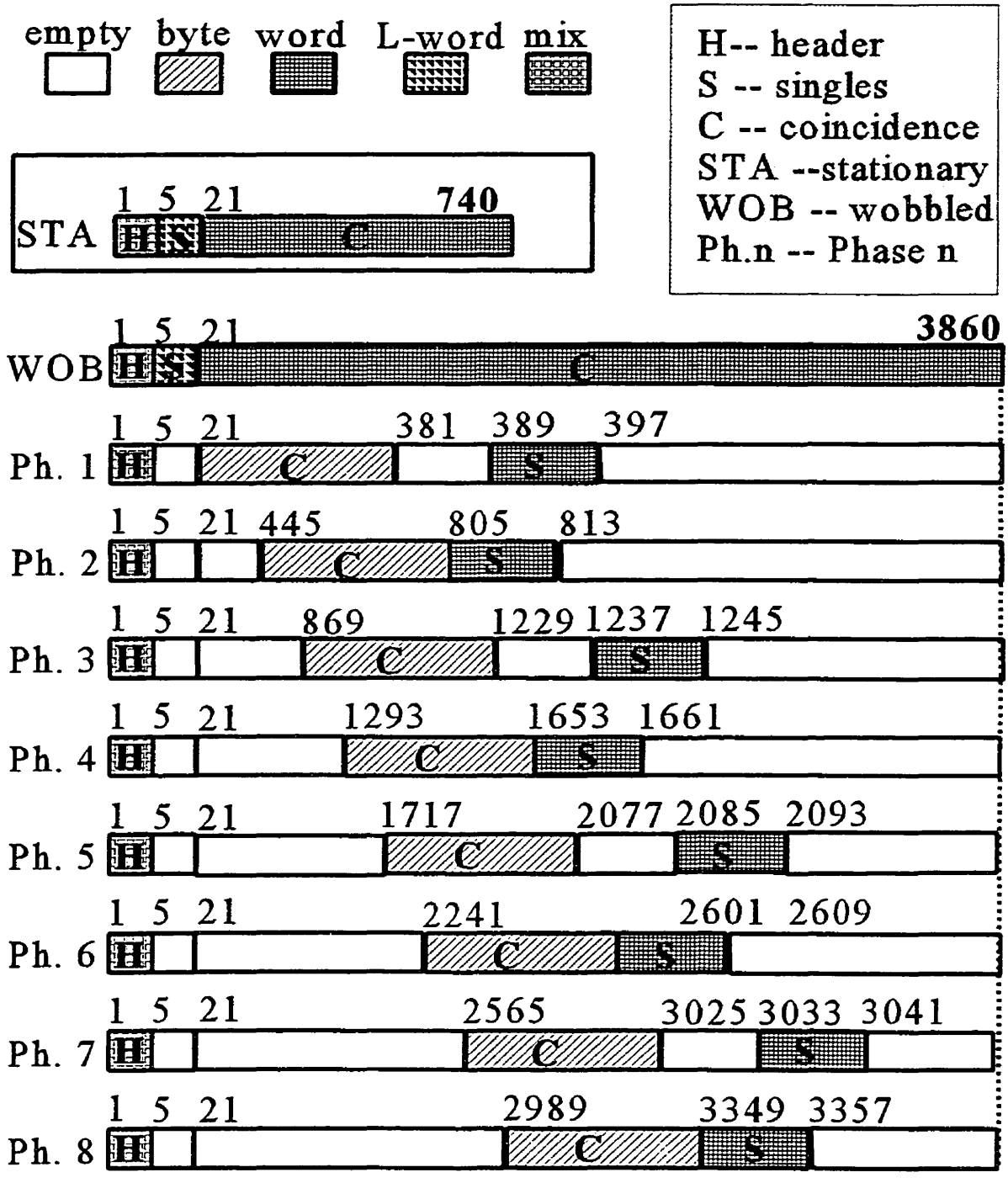

Table 3.1 The structure of the raw data file of an EVR scan compared with a stationary and a wobbled scan. The regular numbers are the beginning blocks of the contents, the bold ones are the sizes of the files. 1 block = 512 bytes. (Not to scale).

each array represents a sinogram for each slice, and the number of slices is 15; where 48 is the maximum projection length in numbers which represent d, 256 is the total number of detectors and also the maximum projection angle β in numbers (See Figure 2.3 & 2.5).

For EVR studies, we notice that the singles are written in words instead of long-words; the sinograms are written in bytes (8 bits) instead of words and they are written in locations which are special when compared with stationary and wobble scans.

The data structure of an EVR scan can be expressed in the following formula:

$$B_C=20+(I-1)\times 424+(S-1)\times 24 \tag{3.1}$$

$$B_S=20+(I-1)\times 424+360+\begin{cases} 8 & (odd\ phase) \\ 0 & (even\ phase) \end{cases} \tag{3.2}$$

For a stationary scan:

$$B_C=20+(S-1)\times 24 \tag{3.3}$$

$$B_S=4 \tag{3.4}$$

Where B_c is the block which precedes the first block of sinogram in the raw data file for phase number I and slice number S. B_S is the block which precedes the first block of the

singles data in the raw data file for phase number I. There are 24 blocks of coincidence data for each slice of each phase following 424 times the number of phase of blocks of zeros, after that, there are 360 blocks of zeros and then 8 blocks of singles data. we need to pay attention that there are 8 more blocks of zeros before the 8 blocks of singles data for the odd phases. which does not happen for even phases. It is noticed that phase 0 is not used, because the data does not follow the rules of Formula 3.1 & 3.2. Now the phases are limited to 1-8 for this configuration.

In addition to the scan data, some of the parameters in the file header for an EVR scan are written in a special way: The data type, projection length, sampling mode, measurement time and measuring starting time are recorded as they would be for a wobble scan, which are not true for an EVR scan. The data structure, including the header, needs to be reorganized and rewritten as 8 new files that are structured as ordinary stationary scan data files, and the temporal information also needs to be corrected to represent the real situation of each phase, so that the data may be read easily and reconstructed correctly with the program REC. Table 3.1 is a list of some critical parameters in the header of a file acquired from a stationary or wobbled scan.

Table 3.2 Some critical parameters for the stationary and wobbled modes

	data type	projection length	sampling mode
Stationary	0 (word)	48	0
Wobbled	0 (word)	256	5 (bins)

3.4. A program to generate reconstructible phase files

The program CONEVR is written for the purpose to rewrite the raw data of an EVR scan analysed above to 8 distinct files with the structure of the file of a stationary scan. The sinograms which are recorded according to Formula 3.1 are rewritten according to Formula 3.3, and the singles recorded according to Formula 3.2 are rewritten according to Formula 3.4. The parameters in Table 3.2 recorded as a wobbled scan need to be rewritten as a stationary scan for the file of each phase. The measurement time (T_{MI}) and measuring starting time (T_{SI}) of the file of each phase are calculated using the following formulae and written into the header of the new file:

$$T_{MI}=T_{MR}/(S_R/S_I) \tag{3.5}$$

$$T_{SI}=T_{SR}+(I-1)\ D \tag{3.6}$$

Where I is the number of the phase. T_{MR} is the measurement time recorded in the raw data, T_{SR} is the measurement starting time recorded in the raw data. S_R and S_I are the singles of the raw data and the new data respectively. D is the duration of each phase which are set by the EVR stimulator (see section 2.2 "EVR stimulator")

The time frame number in the string of the file name is changed so that the files for different phases can be identified by its name. As an example, a raw EVR data file named as

PCSOMANI____-COACT_____052549$0001.DAT;1

(PC+patient-name+context+ID-number +$+frame-number+.DAT;1)

can result in 8 files in series for the 8 phases, when running CONEVR:

PCSOMANI____-COACT_____052549$0011.DAT;1

PCSOMANI____-COACT_____052549$0021.DAT;1

PCSOMANI____-COACT_____052549$0031.DAT;1

PCSOMANI____-COACT_____052549$0041.DAT;1

PCSOMANI____-COACT_____052549$0051.DAT;1

PCSOMANI____-COACT_____052549$0061.DAT;1

PCSOMANI____-COACT_____052549$0071.DAT;1

PCSOMANI____-COACT_____052549$0081.DAT;1

This change not only links each file to its corresponding phase, but also makes it possible to merge the 8 files into one volume with a time dimension. Such a file can be read and subsequently analysed temporally (details see Section 7.2, "Image conversion and format ").

An EVR data file can be simply rewritten by running CONEVR by inputting the raw data file name and the phase duration. Total singles of the raw data and each phase, total coincidence of each phase, measurement time and measuring starting time can be displayed when running CONEVR. The role CONEVR plays can be seen in Figure 3.1, which can be treated as another package of the software systems. Figure 3.2 is a flow chart of the program CONEVR.

The rewritten data files are ready for reconstruction.

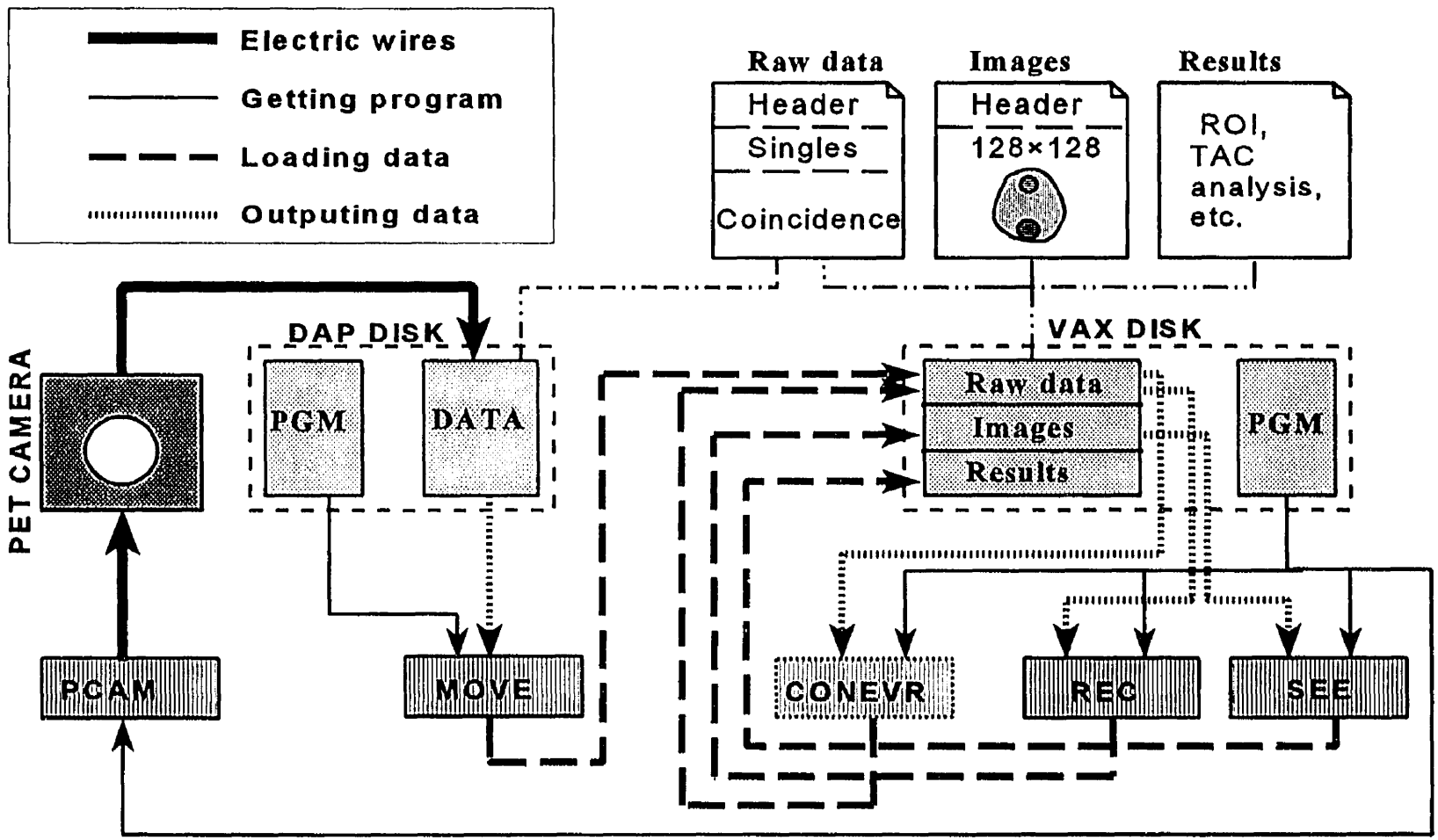

Figure 3.1 Software systems of Scanditronix PC2048-15B scanner and the added program CONEVR for converting the data of EVR scans.

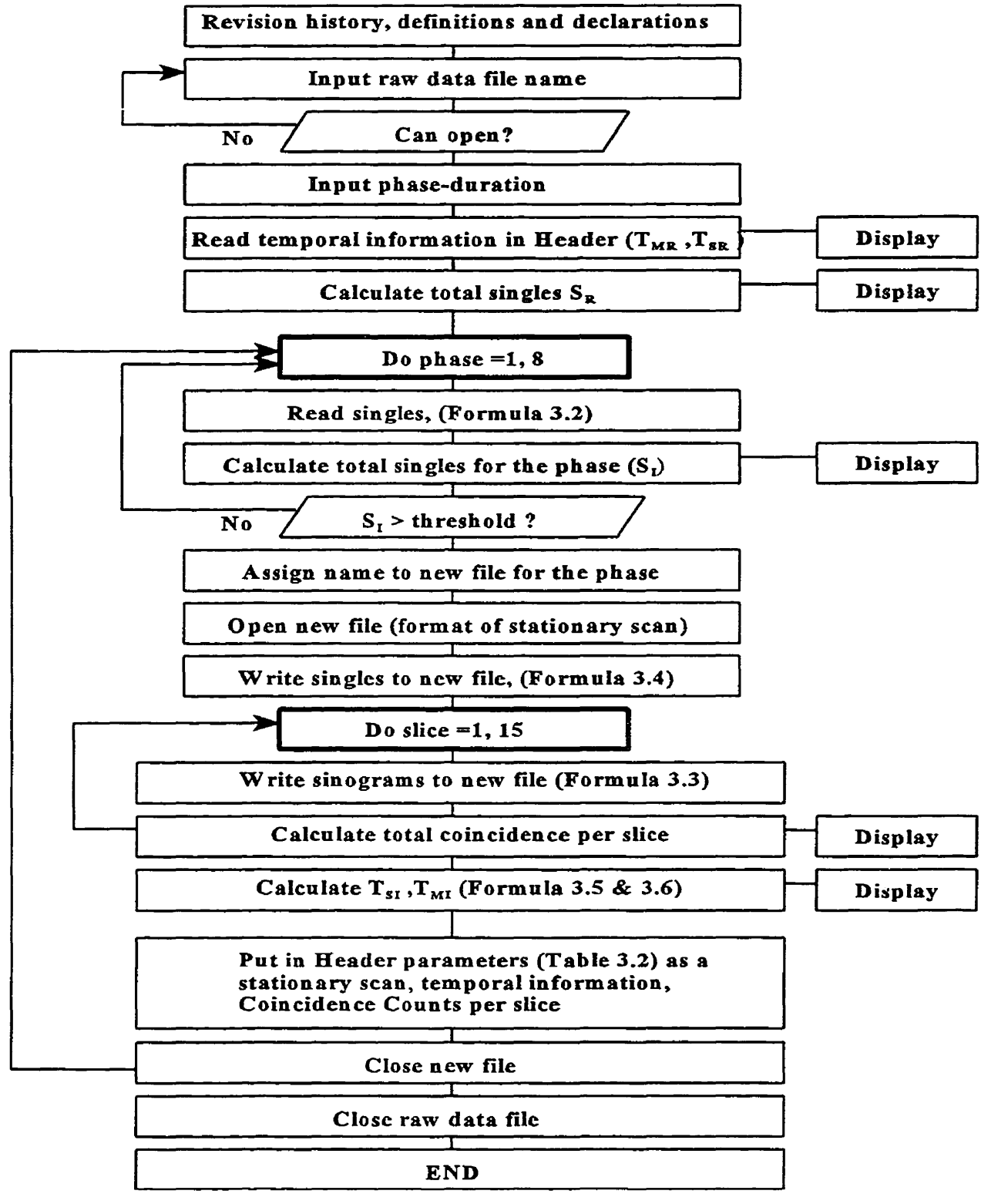

Figure 3.2 The flow chart of CONEVR program.

4. Simulation and phantom tests

>>

Strict testing of the hardware and software was required before performing any studies with human subjects. Phantom tests simulating the conditions of a real EVR study are indispensable to test the mechanical, electronic and software aspects of the system to ensure that they function reliably and produce images with the required precision.

Testing with a stationary radioactive rod source, an orbiting radioactive rod source and a brain phantom filled with radioactive solution were done in order to ensure that (1) the coincident and single events were rewritten properly; (2)the gating technique functions properly; (3)the parameters in the file-header of each phase file were written properly to permit the REC program to read them and to generate images which represent the reality quantitatively with the resolution of the scanner.

4.1. Testing the sinograms with a radioactive rod source

4.1.1. Materials and methods

In order to examine if the coincidence data in sinograms were written properly, a ^{68}Ge radioactive rod source was put at a position in the field of view of the scanner along the axial direction (as shown in Figure 4.1). A scan was acquired in an EVR mode, transferred to the data disk on the VAX and converted by CONEVR program. The sinograms were examined with the SEE display program.

4.1.2. Results

Figure 4.2 shows the 15 pairs of sinograms of the data of phase 5. We can see that the sinograms of the radioactive rod were written in a sine shape according to the rule in formula 2.3, which means the coincidence data were acquired by the hardware and restructured by the software correctly.

The sinograms of the data of other phases (which are not presented here) were examined and found out to be identical to phase 5. This is because the source was stationary.

4.2. Testing the gating function with a rotating radioactive rod source

4.2.1. Materials and methods

The following tests employing an orbiting radioactive source have been done to test if the gating function, which accumulates the data into 8 separate bins, is reliable.

The set-up of the test and the diagram of the electronics are shown in Figure 4.3. The same rod ^{68}Ge radioactive source was mounted on an eccentric arm which was rotated by a small synchronous motor at a speed of 1 rpm. The rod source is parallel to the shaft of the motor along the axial direction of the camera. The orbit of one point on the source follows a circular path centred on the axis. A shaft encoder was employed to detect and record the angular position of the shaft by producing 256 index pulses and one origin pulse per revolution. The "index" signal were counted by two eight-bit counters in series, so that only the 4 highest bits are used to encode the angular position of the source by outputting 8

numbers (0 - 7) to identify 8 different periods in each revolution. The "origin" signal resets the counters at the end of every revolution. A logic adder is used to add 1 to the inputs to (S0, S1, S2, S3) so they repeat from 1 to 8 instead of 0 to 7 in each revolution according to the requirement of the EVR mode (for details, see Section 3.3). The output of any combination of the eight bits were connected to the four bits S0, S1, S2, S3 on the PROM board (Figure2.7) so that the gating of the PROM was synchronized with the rotation of the source. The data was acquired with the scanner on the EVR mode, transferred, converted with the program CONEVR and reconstructed to a series of 8 normal 15-slice images with the program REC.

In a ten-minute EVR scan, the source rotated for several revolutions, and it was expected that the 8 phases of the images of the radioactive source should have produced a series of images of arcs with the same radioactivity concentration on the circumference of a circle, where the length of each arc should have been 1/8 of the circumference without gaps or overlaps between adjacent arcs.

4.2.2. Results

Figure 4.4 shows the images of the 8 phases of slice 6 of the orbiting radioactive source. It is shown that each image is produced from the data from the source as it sweeps through a 45-degree segment of its orbit. No spillage of data was observed. It maybe noticed that the arc of the first phase starts from a 22.5 degree from the horizontal line. This is simply because the starting point was chosen arbitrarily in the experiment.

The images of other slices were examined and the same expected pattern was observed. These results show that the gating technique works as expected.

4.3. Testing the normalization with a ^{18}F-FDG filled Hoffman brain phantom

4.3.1. Materials and methods

A Hoffman phantom study was done to test the normalization which is determined by (1) the rearrangement of the singles data; (2) the calculation of the temporal duration of each phase (for details, see Chapter 3 "Software").

A Hoffman brain phantom [Hoffman brain phanton manual] is a cylindrical phantom composed of many thin layers of plexiglass with different pattern of holes on each layer. When filled with radioactive solution, the distribution of the radioactivity concentration is similar to that of a real brain and macroscopically simulates a brain's gray/white matter distribution. For this particular experimental setup, a Hoffman phantom was filled with 5mCi of ^{18}F-FDG solution diluted with filtered water. Air bubbles were removed from the solution, and the phantom was well sealed and placed within the field of view of the PET camera. A 10-minute EVR scan was done with a phase-duration of 20 seconds. The phase-duration was not relevant in this study, since the phantom was in a static state, so that the activity concentration should remain constant between phases after the correction of the decay of the isotope.

4.3.2. Results

Figure 4.5 shows the 8 images of 8 phases of one slice (8th slice is chosen) from the above experiments. The circle on each image includes the same arbitrary region of interest (ROI). Figure 4.6 shows the averaged activity concentration in the ROI (y coordinate) as a function of the number of the phases (x coordinate). With a linear fitting y=ax+b in least-squares sense, the coefficient a = -0.0044×10^4 and b = 4.0312×10^4 result in a 0.1% difference on averaged activity concentration between phases. This insignificant difference means the normalization was properly done with the program CONEVR. However, the images are usually re-normalized at the stage of data analysis of activation studies, which will optimize the variations introduced at this stage of data conversion (for details, see Section 7.5 "Resampling and normalization").

4.4. Testing the reliability of the logic controlling with a ^{18}F-FDG filled Hoffman Brain Phantom

Some more scans were done with the same Hoffman phantom to test the controlling logic (for details, see Chapter 2 section 3 "Modification of the logic control circuit board"). Wobbled, stationary and EVR protocols were selected in a random order to acquire data. Images were reconstructed and examined, and no abnormality was found during the acquisition process and image reconstruction.

After all these simulation tests, the EVR technique is ready for trials of activation studies with human subjects.

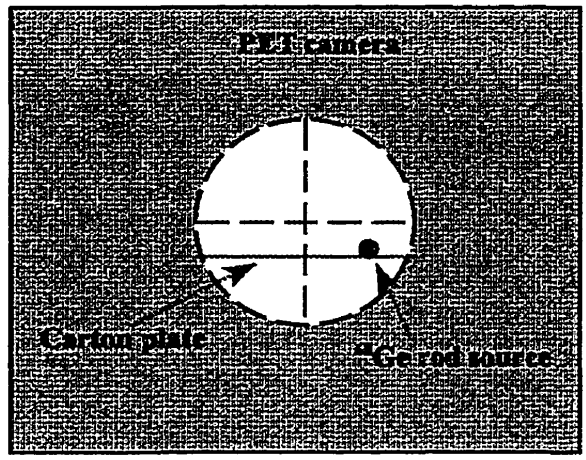

Figure 4.1 Front view of the position of the radioactive rod source in the sinogram test.

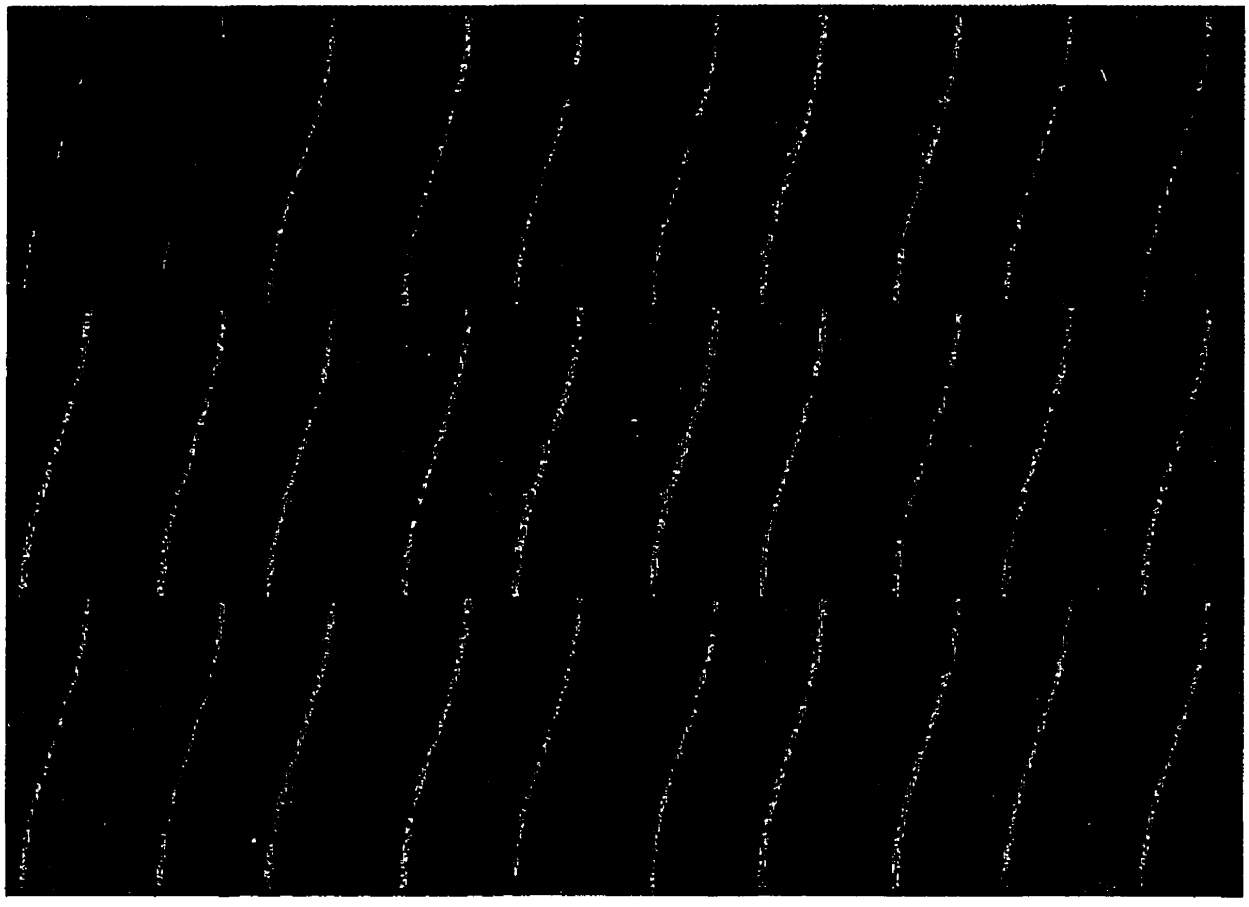

Figure 4.2 The sinograms of the 15 slices of one phase of the EVR scan with a radioactive source at the position as shown in Figure 4.1. Each is written in a pair (ref. Figure 2.3). The sine waves in the sinograms correspond to formula 2.3, which proves that the CONEVR rewrites the coincident events properly.

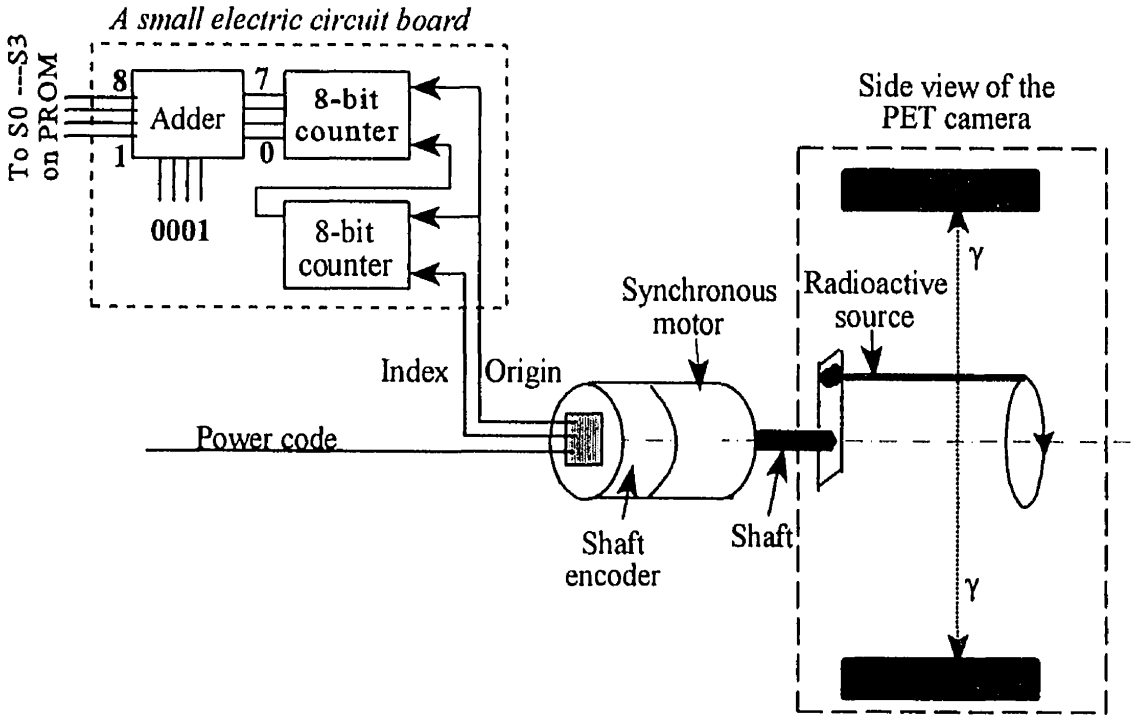

Figure 4.3 The experimental setup of the test for the gating function with a rotating radioactive rod source and a shaft encoder .

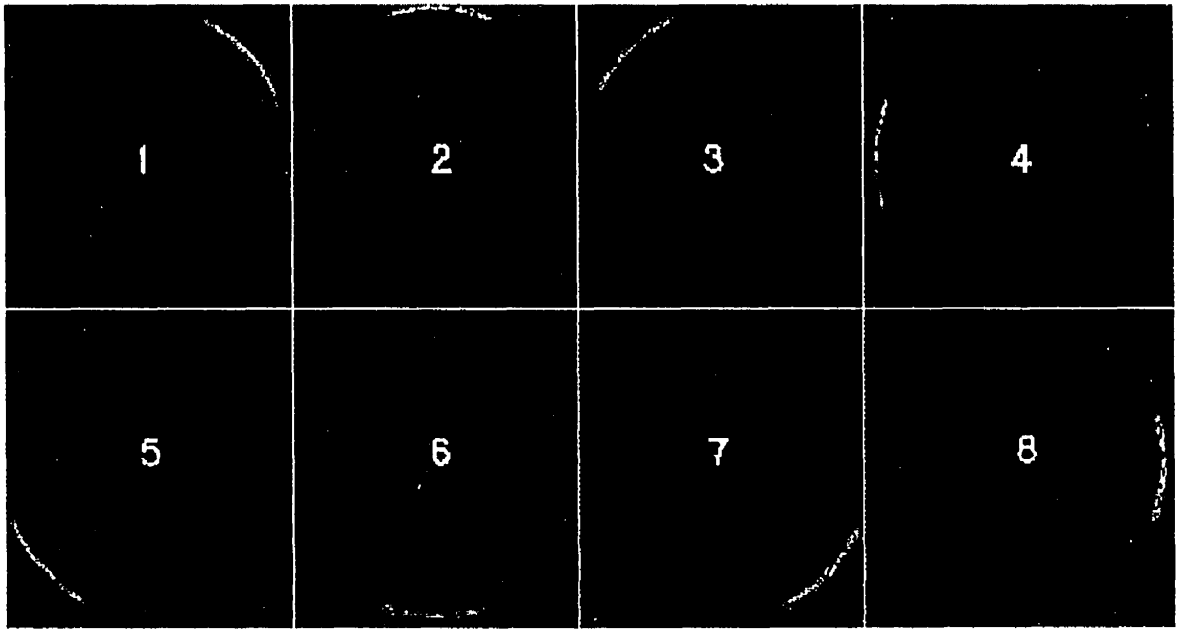

Figure 4.4 A series of 8 images of the 7th slice acquired during the gating function simulation test with a rotating radioactive rod source mounted on a shaft encoder.

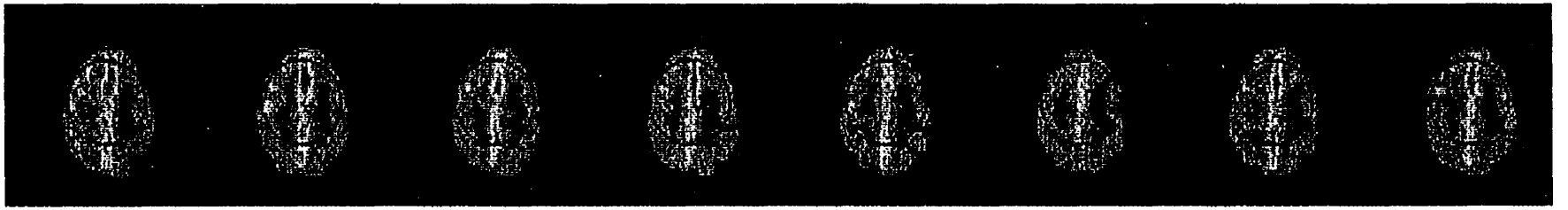

Figure 4.5 Eight phases of the image of the 8th slice of a Hoffman phantom filled with 5mCi ^{18}F-FDG solution. The circle defines an arbitrary ROI for study.

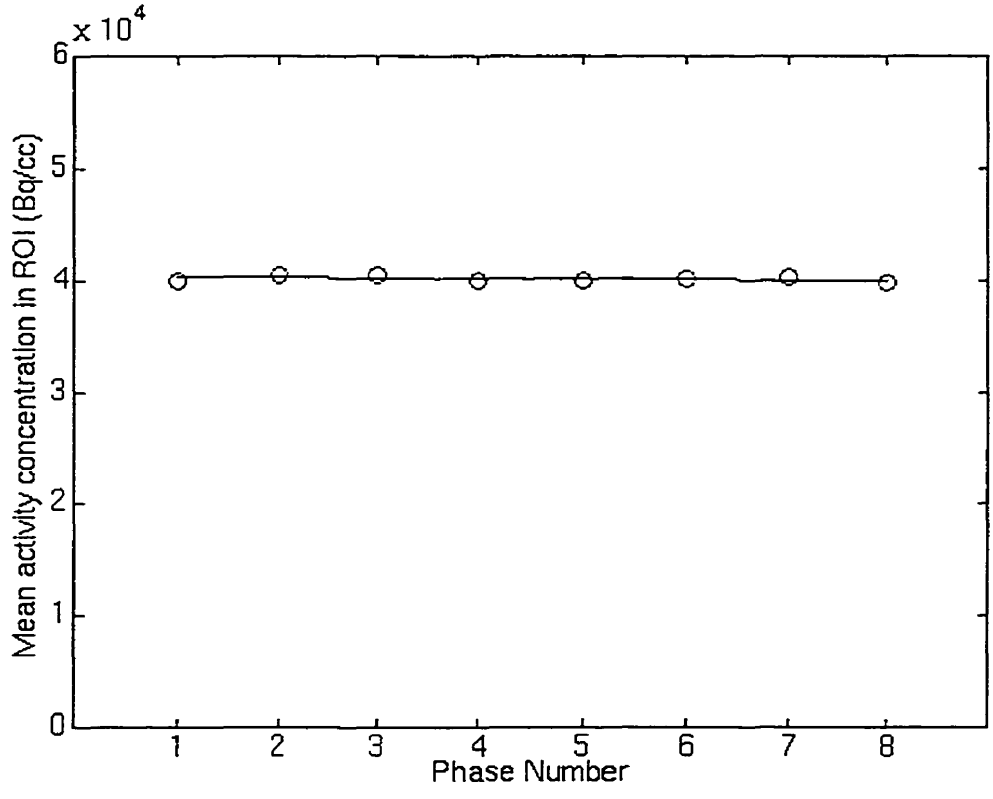

Figure 4.6 The average activity concentration in the ROI in Figure 4.5 as a function of the number of the phases. The line is a linear fit of the 8 values.

5. ^{11}C labelled CO gas system

>>

The EVR technique was first applied to the measurement of the cerebral blood volume using ^{11}C labelled CO as the tracer. A ^{11}C-CO generating system was built for this study and may be used for other studies later. The ^{11}C-CO system consists of two main parts as shown in Figure 5.1 and 5.2. The tracer is first produced in the production unit and passed along a delivering line approximately 50 metres long to the receiving unit where it is stored and administered to the subject.

5.1. The gas production unit.

The radioactive ^{11}C-CO gas is produced with an IBA/Siemens negative ion cyclotron. The nominal beams of the cyclotron are 100μA for protons and 60μA for deuterons [Diksic M, 1996]. One of the targets of the cyclotron is used to produce ^{11}C-CO gas. The newly built ^{11}C-CO gas production line consists of the target, a trap to condense the radioactive CO_2, an oven to convert CO_2 to CO and another trap to remove CO_2 residue from the output of the CO gas. The ^{11}C-CO gas manufacturing process is described below:

(1) Protons generated from an ion source in the centre of the cyclotron are accelerated to an energy of about 18MeV. The proton beam bombards a gaseous nitrogen target mixed with 0.15% oxygen. The gas is compressed to 0.3 liters in the target box using a pressure of

20atm. The $^{14}N(p,\alpha)^{11}C$ nuclear reaction will take place in the target box to produce the positron-emitting ^{11}C isotope. Then, the following chemical reaction takes place with the energy of the proton beam deposited in the target box:

$$C + O_2 + energy = CO_2 \qquad (5.1)$$

The amount of CO_2 produced is controlled by the beam intensity and the bombarding time.

(2) The gas in the box then contains N_2, and a small percentage of O_2 and ^{11}C-CO_2. The composition of the gas is:

50mCi of ^{11}C-CO_2 containing $3.3X10^{12}$ molecules

0.3L N_2 at 20atm and 20 °C containing $1.5X10^{23}$ molecules

0.15% O_2 containing $2.3X10^{20}$ molecules

In order to convert ^{11}C-CO_2 into a bolus of ^{11}C-CO efficiently, the tiny amount of ^{11}C-CO_2 in the box needs to be purified by removing the N_2. This is achieved by passing the hot gas into a trap which is a coil made of a stainless steel tube. The trap is dipped into liquid nitrogen which is at -195 °C and the CO_2 and O_2 condense in the coil. The nitrogen will pass through the tube and be ventilated. It takes about 2 minutes for all the radioactive gas to be condensed. Table 5.1 is a comparison of the temperatures at which nitrogen, oxygen and carbon dioxide change state:

Table 5.1 Temperatures at which CO_2, O_2 and N_2 change state at 1atm.

Material	Temperature	Phases of states
CO_2	-78.5°C	gas-solidate
O_2	-182°C	gas-liquid
N_2	-195°C	gas-liquid

(3) The coil is then raised out of the liquid N_2 and allowed to reach room temperature to gasify the condensed material. High pressure helium gas is then released to direct the material into a charcoal filled oven. The oven is heated to 900°C producing the following chemical reaction:

$$CO_2 + C + energy \rightarrow 2CO \tag{5.2}$$

$$O_2 + C \rightarrow 2CO \tag{5.3}$$

The converting efficiency is dependent on the surface area of the charcoal and the amount of ^{11}CO and O_2 molecules passing through the oven per unit time (which is dependent on the flow of the gas). The Flow rate, temperature, and temperature uniformity in the oven are

critical for efficient CO production. These variables are controlled using needle valves and a temperature controller [Jolly D, 1995].

$$CO_2 + NaOH \rightarrow NaHCO_3 \qquad (5.4)$$

(4) The gas from the oven is passed through a soda lime trap to remove any CO_2 residue: Failure to remove the $^{11}CO_2$ residue will result in contaminating the CBV images obtained by ^{11}CO. We would then obtain a CBF distribution overlapped on the desired CBV distribution.

Pure CO including the radioactive CO is mixed with helium gas (which is inert). The gaseous mixture may then be administered to the subject.

With this ^{11}CO generating system, 70mCi of ^{11}CO gas is able to be produced stably using a 15μA ×5 minute proton beam. This is more than is required for one subject since 25mCi is the limit for a human subject [see appendix, EVR consent form].

5.2. The gas receiving and administering unit

The gas receiving and administering unit consists of a gas reservoir with a radioactivity monitor, a medical air supplier and a mouthpiece for inhalation. The process is described below:

(1) The gas from the production unit is a mixture of helium and CO. The gas is delivered from the production unit through a delivering line in the ceiling to a rubber bag (capacity of 3 litres) next to the PET scanner. This takes about 12 minutes.

(2) The gas in the bag is mixed with medical air (Medical air is purified air produced in

the hospital for clinical use). The activity is monitored with a γ-ray counter underneath the bag. After the activity reading reaches the amount required by the scan protocol, the rest of the gas in the delivering line is vented via the exhaust duct. The gas in the bag is ready to be administered to the subject.

(3) A mouth-piece, (which is connected to the bag through a valve), is then given to the subject. The subject's nose is clipped in order to prevent gas leaking into the PET room. The investigator will give instructions to the subject to inhale the gas in one or several breaths.

The scans can proceed 4 minutes after inhalation of the gas. By this time ^{11}CO equilibrium is established throughout the body [Phelps ME, 1978].

5.3. CO risk considerations:

Several considerations are necessary in order to safely and efficiently administer the radioactive gas to the subject:

1) A total amount of 0.02 litre CO is administered with 3 litres of normal air to a subject during one study. Only 0.7% of the inhaled gas is CO, corresponding to approximately 5×10^{20} molecules (An adult takes in 10^{23} -10^{24} oxygen molecule per minute during natural breath , and the CO competes with O_2 to combine to red blood cells). This is well below the toxic level. The total amount of CO is derived as follows:

$$V_{CO} = 0.3\%\times 20atm\times 0.3l = 0.02l. \quad (at\ 1atm) \tag{5.5}$$

The target box has an original pressure and volume of 20atm and 0.3 l. 0.3% of the volume is CO produced from 0.15% O_2.

2) 25mCi of ^{11}C produces a whole-body exposure of 5.1 mSv, which is within the limit allowed by the Ethics Committee at the MNI. The details of which are in the EVR consent form in the appendix.

3) The amount of the radioactivity administered to the patient is carefully monitored by the γ-ray counter. This avoids over-dosing the subject.

4) The gas system is well sealed in order to minimize the background radiation in the PET room.

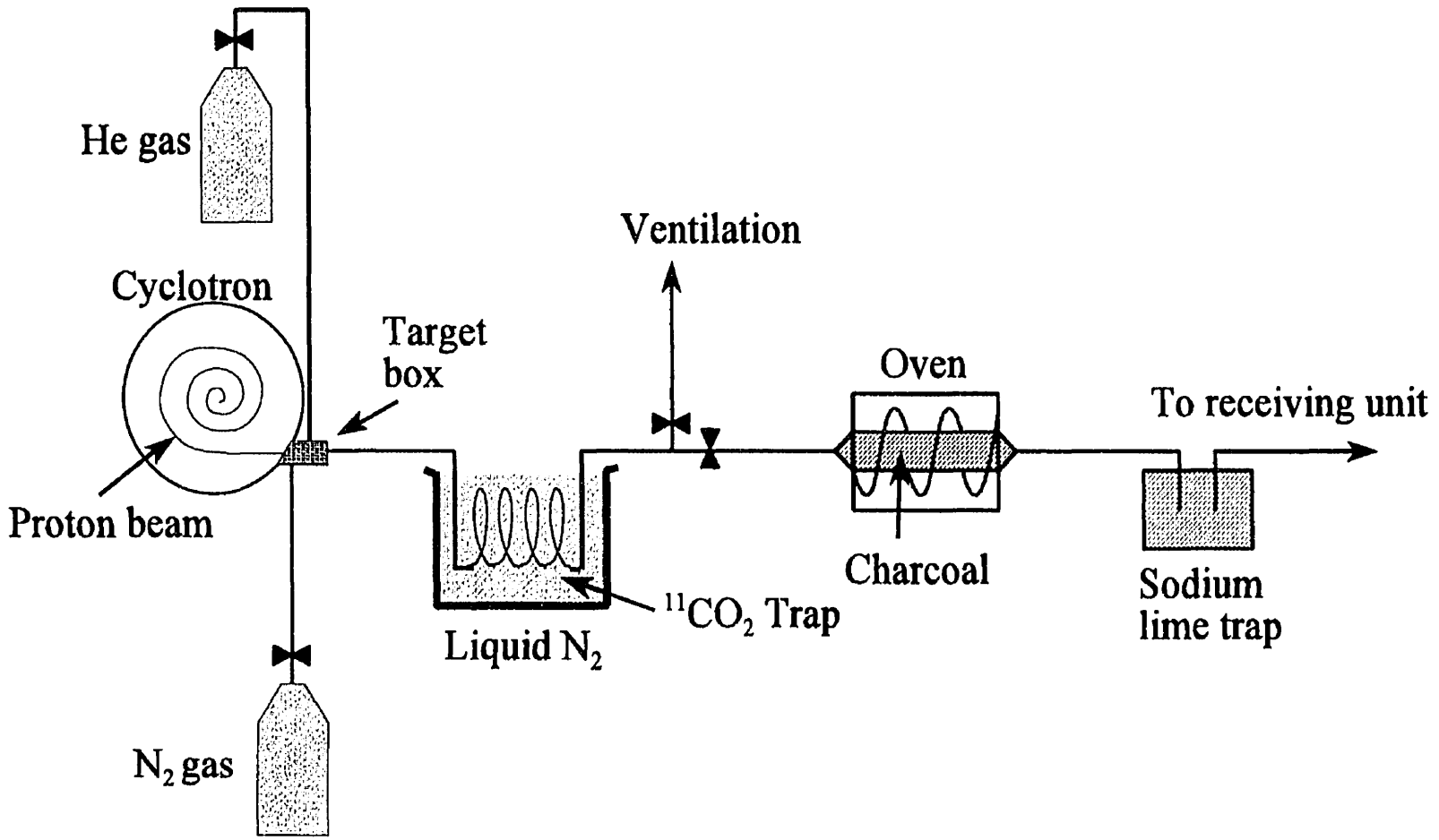

Figure 5.1 The system to generate and deliver the ^{11}C-CO gaseous tracer. (Not to scale).

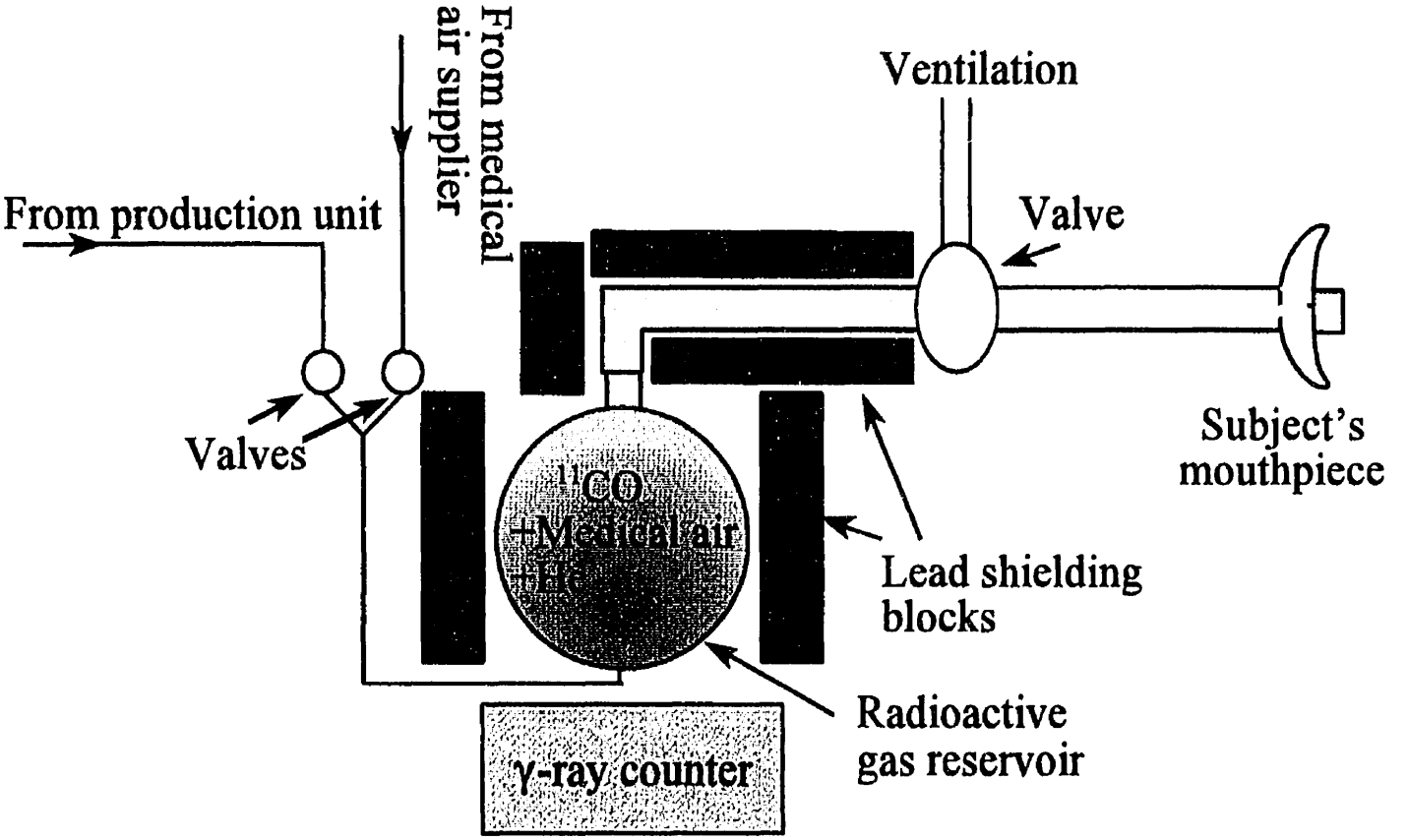

Figure 5.2 The system to receive and administer the ^{11}C-CO gaseous tracer. (Not to scale)

6. Experimental setup of an EVR activation study with vibrotactile stimulation and ^{11}C-CO gaseous tracer

>>>

6.1. Subject selection

Eight healthy human subjects were selected as volunteers. No preference for handedness or sex is given to the subjects. The average age of the subjects was 23. Consent forms approved by the Montreal Neurological Institute Ethics Committee were given to each subject so that he/she can fully understand the procedure and the level of risk due to the radiation. The consent forms were signed by the subjects, the main investigator, a medical doctor and a witness prior to conducting the study (see EVR consent form in appendix).

6.2. Experimental procedure

6.2.1. The EVR CBV activation protocol with phase-dependent stimulation

(1) A head-restraining mould was made to prevent the head of the subject from moving while in the scanner.

(2) The scanning level was selected to locate the region of activation in the optimized area of the field of view of the scanner. This positioning was verified by doing a brief transmission scan to show the location of the head on the display.

(3) The wobble position was reset to "Home", and the wobble motor was turned off

manually. This is critical for the EVR acquisition protocol. (for details, see Section 2.3 "New PROM board" and 2.4 "Modification of the Logic Control board")

(4) A ten minute transmission scan was done for the purpose of attenuation correction. (A blank scan was done in advance, at the beginning of the day).

(5) The EVR stimulator was connected to the scanner, powered up and switched to the EVR state. (Refer to Figure 2.13). The finger-tips of the right hand of the subject were taped loosely to touch the head of the mechanical vibrator. The application of stimuli was sequenced by the EVR stimulator to switch on and off according to the pattern in Figure 6.1. The stimulation was on during phase 1 to 4 and off during 5 to 8. A phase duration of 5 seconds was selected, allowing 30 cycles of data to be acquired.

(6) ^{11}C labelled CO gas was produced and contained in a rubber bag (See Chapter 5, "CO gas generating system). Enough ^{11}C-CO gas should be delivered into the rubber bag so that an activity of 25mCi be administered to the subject. The gas, mixed with medical air, then was inhaled by the subject using the multiple inhalation method described below.

(7) The scan was started 4 minutes after the inhalation, with the stimulation on..

(8) The stimulation was stopped and the vibrator was removed from the hand of the subject. A 60-minute rest-state scan was then acquired.

(9) At the end of the study, the state of the scanner was reset to the original state.

(10) An MRI (Magnetic Resonance Imaging) image was acquired to provide an image which contains the detailed anatomical structure of the subject's brain for data analysis and physical interpretation of the results.

(11) The acquired data from the activation and rest-state were reconstructed to generate

images for subsequential analysis (for details, see next chapter).

This protocol was applied for 4 of the 8 subjects scanned.

6.2.2. The stationary CBV activation protocol with continuous stimulation

The purpose of the this protocol was: 1) to estimate the detectability of the activation in the images resulting from this particular kind of study; and to 2) to contribute to the assessing of the significance of the activation in the average images from multiple subjects [Worsley, 1992], particularly when the SNR of an image of a single subject is very poor.

The procedure is the same as the EVR CBV activation protocol described above, except that (1) the stimulation is on constantly during the 20-minute activation scan (Figure 6.1); (2) The data are acquired in stationary mode instead of the EVR mode.

This protocol was applied to the other 4 of the 8 subjects before the EVR CBV protocol.

6.3. Multiple inhalation method

One major factor limiting the SNR of CBV images is the low efficiency of the uptake of the gaseous radioactive tracer. Most of the previous studies employing ^{11}C CO tracer used the single bolus inhalation method [Phelps 1987, Grubb 1987, Martin 1987, Cherry 1993]. It was found that merely 1/3 of the ^{11}C activity in the administered gaseous bolus combined with red blood cells, and the rest was quickly exhaled [Grubb RB, 1987]. This low efficiency did not pose a problem for global CBV measurement, but was apparently critical when detecting local CBV variations induced by a stimulation by subtracting a rest-state image from

an activation image, because the magnitude of CBV changes are much smaller than that of CBF changes [Fox PT, 1986], and CBV images are much noisier than CBF images [Cherry 1993].

In order to improve the efficiency of the tracer uptake, a multiple inhalation method was devised, as described below.

There is a valve connecting the subject's mouthpiece with either (1) the CO reservoir or (2) the exhaust duct (see Figure 5.2). The valve can be set in one of the two positions to allow the subject to either (1) breathe ^{11}CO from the rubber bag or (2) breathe normal air through the exhaust duct. The position of the valve is adjusted while the subject breathes as the follows steps:

Step 1: Put the valve at position 2;

Step 2: Exhale (for 5 seconds);

Step 3 Put the valve at position 1;

Step 4 Inhale (for 5 seconds);

Step 5: Hold breath (for 5 seconds);

Step 6: Exhale into the bag (for 5 seconds);

Step 7: Put the valve at position 2;

Step 8: Natural breath (10 seconds).

The above process is repeated for a total of 4 cycles. During the 4th cycle, step 6 is omitted so that the residue radioactive gas can be ventilated to maintain the background radiation in the scanning room as low as possible.

Table 6.1 is a record of the percentage uptake of the tracer activity in the first 3 breaths

for all of the 8 subjects. The percentage uptake was calculated by the following formula:

$$P=\frac{A_{after}-A_{before}}{A_0}\times 100\% \qquad (6.1)$$

Where, P is the percentage uptake of the radioactive tracer, A_0, A_{before}, A_{after} are the readings of the total radioactivity delivered to the bag, before and after each breath. The reading of the activity was from the γ-ray counter. The radioactivity uptake is increased with a factor of 2 (from 1/3 to 74%) when compared with the single bolus method. thus the SNR can increase a factor of $\sqrt{2}$=1.4 (Formula 1.10).

Table 6.1 The percentage uptake of ^{11}C-CO with the multiple inhalation method

	Tracer uptake ratio (%)			
Subjects	**Breath 1**	**Breath 2**	**Breath 3**	**Total**
1	41	28	12	81
2	27	28	25	80
3	38	38	12	78
4	24	19	10	53
5	55	25	15	95
6	30	3	13	46
7	29	31	24	84
8	44	18	14	76
Average	36 ± 10	23±11	16±5.7	74±16

There is more CO_2 breathed in by a subject than that of natural breaths, since the breaths

from the 2nd to 4th contains the CO_2 which has been exhaled into the bag from the preceding breaths. But there is no radioactive CO_2 among it to contaminate the CBV images with radioactive H_2CO_3 CBF distribution, because the breathed-in ^{11}C-CO can not be transformed into ^{11}C-CO_2 immediately by biochemical reactions in the human body. So this method can be used in the future CBV studies.

Theoretically more breaths could be taken by subjects to increase the uptake ratio beyond 75%. It is necessary, however, to balance the time for equilibrium (~4 minutes for ^{11}C [Phelps ME, 1978]) with the total uptake of radioactivity to achieve an required optimal stable distribution when the scan starts.

6.4. Other factors affecting the quality of images

6.4.1. Subject condition

We found that the subjects who are young, and who exercise regularly are more capable of taking in radio-isotopes efficiently. The cooperation of the subjects with the instructor who provides verbal instructions is also critical. Currently, our data is limited to 8 subjects. We expect to amass more data from additional studies involving inhalation to understand these aspects more thoroughly.

6.4.2. Subject movement

For most of the EVR scans, a video monitoring system [Picard Y, 1997] was employed

to monitor and record the position of the heads of the subjects. It was found that 6 of 8 subjects moved their heads less than 3mm, other two subjects moved more than 5mm, however. The effect of the head movement can be partially corrected by acquiring multiple short frames, registering and summing them together [Scanditronix PC2048-15B Software Manual].

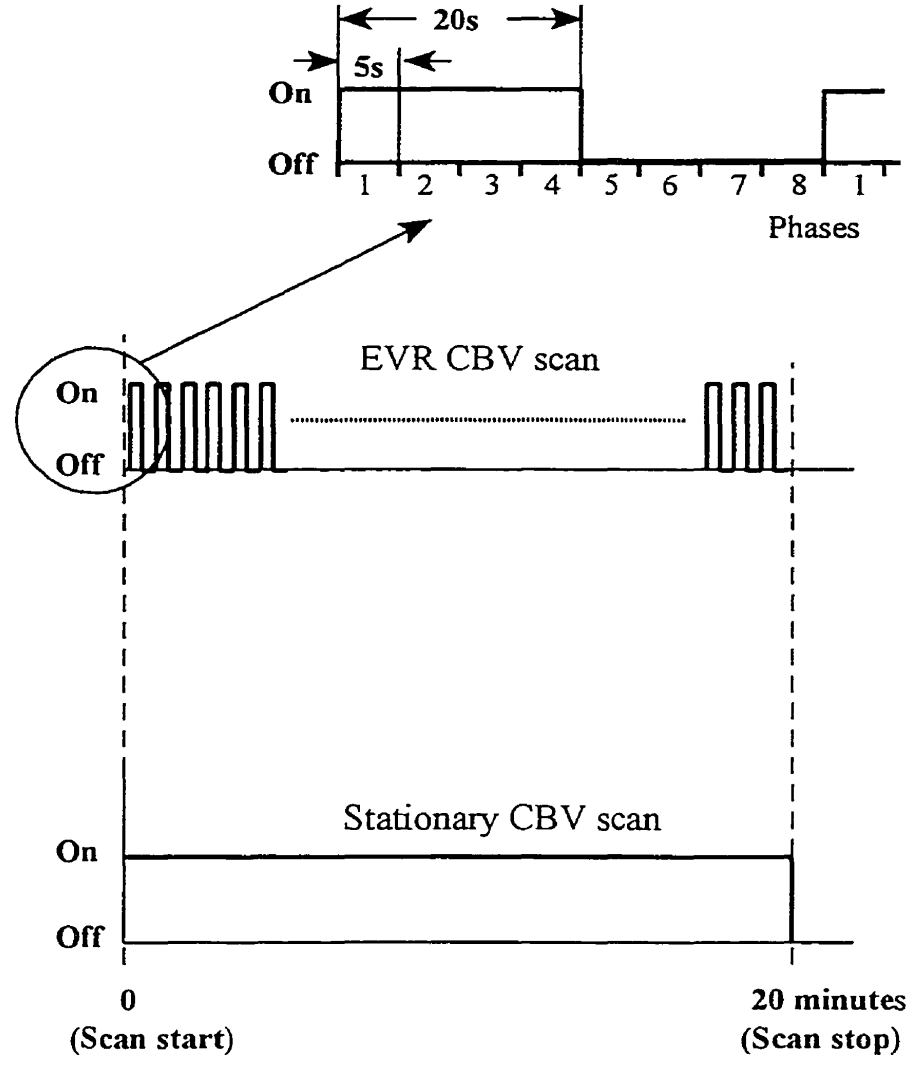

Figure 6.1 The pattern of the stimuli of the EVR CBV scan and the stationary CBV scan.

7. Data analysis and results of the EVR cerebral activation studies with vibrotactile stimulation

7.1. Image reconstruction

The data acquired for the activation and rest-states studies were reconstructed by the program REC (See Chapter 3, "Software"). Hanning-type of back-projection filters of two widths were used for reconstruction [MATLAB reference book]: A 10 mm-width was used for registration. Since two volumes of PET CBV images, PET CBV and MRI images needed to be registered manually, blood vessels serve as very good landmarks on both PET CBV and MRI images (for details, see section 7.3 "Image registration and transformation"). A 10mm filter provide good vessel contrast for PET CBV images acquired with 25mCi ^{11}C-CO. An 18mm filter was used for image analysis purposes. The choice to use the wide filter was necessary because of limitations of the algorithm used to transform the images from native space to Talairach space (Talairach space is a standardized sterotaxic coordinate framework [Talairach J, 1988]. Images of different subjects are transferred onto this space by geometric scaling and resampling. This enables the same structures within different subjects to be spatially matched.) Because this transformation is linear, it does not eliminate the variation in the relative sizes and shapes of various cortical features between subjects. The averaging of images from a number of subjects in Talairach space, as a result, produces misleading "structure" in the resultant image when the cortical features are incongruous between

subjects. A filter sufficiently wide to eliminate this spatial variation removes this artefact and allows one to define the optimized ROI.

7.2. Image Conversion and format

The images were transferred from VAX to Sun/Unix workstations and written as 4-dimensional matrices. The images may be analysed in either native space or Talairach space. Analyses involving averaging images over multiple subjects are performed only in Talairach space. The following tables are specifications for the PET and MRI images.

Table 7.1 specifications for the PET image files in native space

	X	**Y**	**Z**	**T (time)**
Dimensions	128	128	15	8
Size of unit	2mm	2mm	6.5mm	5s

Table 7.2 specifications for the PET and MRI images in Talairach space

	X	**Y**	**Z**	**T(time)**
Dimensions	128	128	80	8
Size of unit	1.72mm	1.34mm	1.5mm	5s

7.3. Image registration and transformation

Reconstructed CBV images need to be registered first to a certain volume of image from the same series of scans of the same subject in the native space, and are then registered to the MRI image of the same subject. This minimizes errors caused by the motion of the subject between scans. In order to do statistical analysis with many subjects, the PET and MRI images of each subject need to be transformed onto Talairach space. Figure 7.1 illustrates that any transformation is a combination of rotation, translation and scaling.

Each image can be treated as a three dimensional vector, and it can be converted to another vector by multiplying it by a transformation matrix. The following formulae express this transformation:

$$[M_{S_i \to S_j}][V] = [V'] \tag{7.1}$$

$$[M_{S_j \to S_i}] = invert\ [M_{S_i \to S_j}] \tag{7.2}$$

$$[M_{S_i \to S_k}] = [M_{S_i \to S_j}]\ [M_{S_j \to S_k}] \tag{7.3}$$

where S_i, S_j, S_k are different spaces representing any space of $PET_{act,n}$ (the PET image of the nth activation scan), PET_{base} (The PET images of the rest-state scan), MRI (MRI image), or TAL (Talairach space). **[V]** represents an image in the space of S_i, which is transformed into **[V']** in space S_j. $[M_{S_i \to S_j}]$ is the transformation matrix from space S_i to S_j, which can be

obtained by registering two volumes of images.

The registration between two CBV PET images of the same subject can be done manually with a registration program called "Register" (available at FTP site of ftp.bic.mni.mcgill.ca). Since the high activity in blood vessels in CBV images is readily identified, CBV images of the same subject can be easily registered by matching the large vessels. In the same way, a CBV PET image and an MRI image of the same subject can be registered. An accuracy of 2.5mm can be easily achieved in this process. Figure 7.2 is an illustration showing that how a CBV PET image is registered to a MRI image of the same subject. MRI to Talairach space transformation requires 3-dimensional linear scaling, which is done by an automated feature matching program [Collins DL, 1994].

After obtaining all the transformation matrices by the above registration, the PET and MRI images of all of the subjects were transformed into Talairach space using formulae (7.1), (7.2) and (7.3) and were subsequently analysed.

7.4. Assessing Significance of the activation sites and making ROIs

The significance of the activation sites was assessed using statistical analysis according to the mathematic model developed by Worsley et al.[Worsley K, 1992]. In the model, the subtracted PET images (rest-state images subtracted from the activation images) are averaged among subjects, the averaged image is standardized to have unit variance, and the local maxima are searched. The model then provides means of deciding which of the local maxima are statistically significant. The program DOT, which has been developed according to this model, can generate a T-image in the brain volume in Talairach space [Milot S, 1996].

A T-image is the average subtracted image divided by the pooled standard deviation. Regions with high T correspond to the regions of high mean activation.

Figure 7.3 shows T-images produced from activation and rest-state scans of the 8 subjects (4 from the EVR CBV scans and another 4 from the normal CBV scans. The reason to include the 4 normal CBV scans is to increase the significance of the activation site against noise). The T-image shows that the somatosensory right hand area is significantly activated. Figure 7.3 is a comparison of the activation sites of the CBV PET images in this study and CBF PET images in some previous studies [Reutens D, 1997]. The same kind of stimulation was involved in both studies. It can be seen that the increase of CBV happens in the same area of that of the CBF study, except that the size and magnitude of the activation is smaller.

The ROI for study is made to include a volume at the peak in the somatosensory area. The T value in the volume is greater than the half of the maximum.

7.5. Resampling and normalization

From Formula 1.12, We can derive the following:

$$\Delta CBV(i)=K(C'_{act}(i)-C'_{base}) \tag{7.4}$$

$$C'_{act}(i)=\frac{C_{act}(i)}{\int_{t_1}^{t_2} C_{bl}(t,i)dt}, \qquad C'_{base}=\frac{C_{base}}{\int_{t_1}^{t_2} C_{bl}(t)dt} \tag{7.5}$$

where

$C'_{act}(i)$, C'_{base} are normalized regional activity concentration for phase i of the activation and base-line states, respectively. K is a calibration factor. The results of the integration in the denominators of Equation 7.5 should not vary depending on the phase or the activation, since the increase in regional blood activity is negligible in comparison to the global blood activity.

In practice, this study is concerned with relative changes in regional activity, and the absolute quantities in Equation 7.5 are not determined directly. Relative regional activities are determined by normalizing the images by their mean pixel value:

$$C'_{pixel} = \frac{100\ C_{pixel}}{Mean(C_{pixel})} \qquad (\ C'_{pixel}\ can\ be\ C'_{act}(i)\ ,\ C'_{base}) \tag{7.6}$$

where

$$Mean(C_{pixel}) = \frac{\sum_{slice\ 15}^{slice\ 75} \sum_{(within\ Mask)} C_{pixel}}{\sum_{slice\ 15}^{slice\ 75} \sum_{(within\ Mask)} pixels} \tag{7.7}$$

where C_{pixel} is the value represents the activation concentration in a given pixel, and C'_{pixel} is its normalized value. The average is taken from slice 15 to 75 instead of from 1 to 80 because some of the bottom slices and top slices have discrepancies after registration and transformation. Note that only counts within a specified mask contribute to the sum. The

mask excludes the counts outside the skull which originate from noise, exclude some brain structure with extremely low radioactivity concentration and excludes the sagittal sinus which have a blood concentration 20 times more than the normal cortices. A relatively small variation in the radioactivity concentration in the sagittal sinus would cause a significant variation of the calculated normalization factor. Figure 7.4 is an illustration of the discrepancy and the mask.

7.6. Fractional CBV changes in the ROI.

From Formulae (7.4) and (7.5) we can define Fractional CBV change (F) within the ROI for each subject (n):

$$F_n(i) = \frac{\Delta CBV_n(i)}{CBV_n} = \frac{\sum_{ROI} C'_{act,n}(i) - \sum_{ROI} C'_{base,n}}{\sum_{ROI} C'_{base,n}} \qquad (7.10)$$

The average among N subjects is:

$$\bar{F}(i) = \frac{\sum_{n=1}^{N} F_n(i)}{N} \qquad (n=1,2,.....,N) \qquad (7.11)$$

where F_n (i) is the Fractional CBV change during phase i for subject n; $\bar{F}(i)$ is the mean Fractional CBV change of phase i; $C'_{act,\,n}$ is the normalized activity concentration of the image during phase i for nth subject; $C'_{base,\,n}$ is the normalized activity concentration of the image corresponding to the rest-state for the nth subject.

7.7. Results

Figure 7.5 shows the fractional CBV change for single subjects. The error bars are calculated by conducting the same ROI analysis as above by choosing ROIs of the same volume on 8 cortical regions which are not likely to be activated. The results represents the statistical noise in the 8 ROIs, and the standard deviation for the 8 values can apply as an error bar. This figure indicates that evoked vascular response can be seen in single subject studies.

Figure 7.6 shows the average of the fractional CBV changes among the 4 subjects. The curve of the EVR is clearly demonstrated. A rise time of $k_r = 7.3 \pm 1.9$s and a decay time of $k_f = 13.2 \pm 2.2$s by fitting the curve with two exponentials with Levenberg-Marquardt Method [Numerical Recipes in C]: the rising curve with $F=F_{max}(1-e^{-t/k_r})$ $(1 \le p \le 4)$, and the decay curve with $F=F_{max}e^{-t/k_f}$ $(4 \le p \le 8)$, . Here F_{max} is the maximum fractional change of CBV, p is the phase.

7.8. Discussion

In fitting to determine the rise and decay time, an assumption was made that the activation achieved its maximum at phase 4 (15 seconds after stimulation). The assumption was based on the results from the previous human and animal studies and modelling [Frostig RD, 1990; Kwong K, 1992; Narayan SM, 1995] in which the rise time varies from 2 to 9 seconds.

A curve with a rise-time of 7.3s, will reach 87% of its maximum at 15 seconds (at the beginning of phase 4) and 93% at 20 seconds (at the end of phase 4). This may suggest that the standard deviations of the above results have been underestimated.

The above time-course results quite agree with those measured using fMRI on human subjects with visual and hand squeezing tasks [Kwong K, 1992]. It also agrees with those of animal studies [Frostig RD, 1990; Narayan SM, 1995]. The magnitude of the fractional CBV change, the location and size of the activation site also agrees with the previous studies [Fox PT, 1986].

The above results were obtained from studies on 4 different subjects, and a clear response curve was found from the average of their data. Theoretically, the precision can be improved by using more subjects and trying different phase-durations.

CBV in the brain is less uniformly distributed than CBF (Figure 7.7). Patient movement can cause significant artifacts. As an example, blood vessels are less than 3mm in diameter. A misregistration of 3mm will result in a negative peak beside a positive peak instead of cancelling the two peaks when subtracting two images. For this reason, a wide reconstruction filter is used for analysis with image subtraction. Fortunately, the time-course measurement by the EVR technique is much less influenced by the motion artifacts than the magnitude

measurement. The image differences caused by patient motion between phases are offset by the short phase-duration and the large number of repetitions. (the 5 second phase-duration is considered to be very short compared to the 20-minute scan time. The number of cycles 30, is considered to be large). We can describe the effects of the patient motion in the following way:

$$F'_n(i)=F_n(i)+C_n \tag{7.11}$$

Where $F'_n(i)$ is the calculated fractional CBV change for subject n, phase i, in which the activation and baseline images have some mismatch caused by patient motion, and the movement (< 5mm) is much smaller than the size of the ROI(~ 30mm). $F_n(i)$ is the ideal fractional CBV change. The difference C_n is independent of the phases. We can derive:

$$\begin{aligned}\bar{F}'(i)&=\frac{\sum_n F'_n(i)}{N}\\&=\bar{F}(i)+\bar{C}\end{aligned} \tag{7.12}$$

where

$$\bar{C}=\frac{\sum_n C_n}{N} \tag{7.13}$$

By differentiating equation (7.12), we get

$$\frac{d\bar{F}'(i)}{di}=\frac{d\bar{F}(i)}{di} \tag{7.14}$$

we can see that $F'_n(i)$ and $F_n(i)$ have the same time-course, though the magnitude is different.

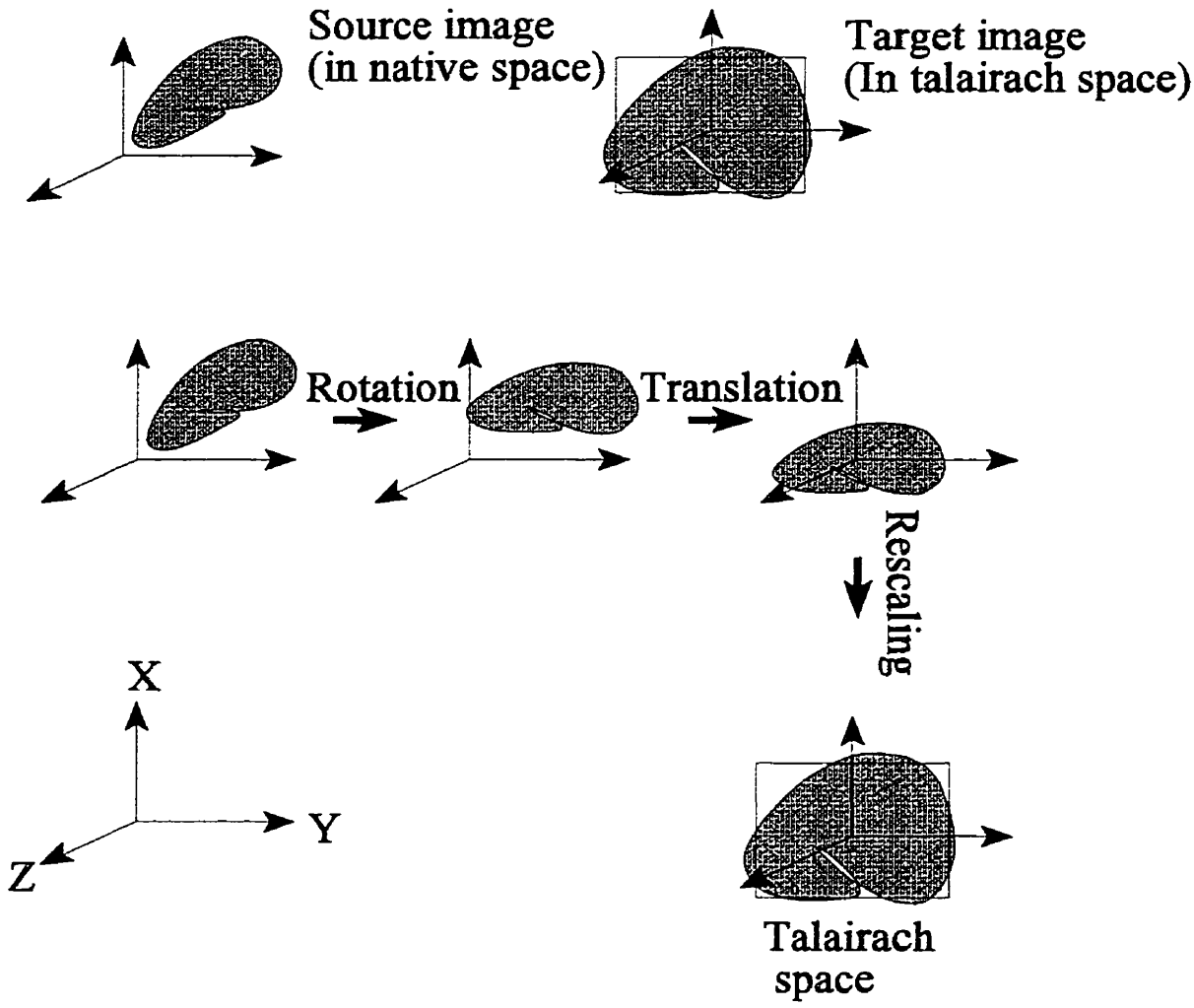

Figure 7.1 The tranformation processes required for PET activation studies.

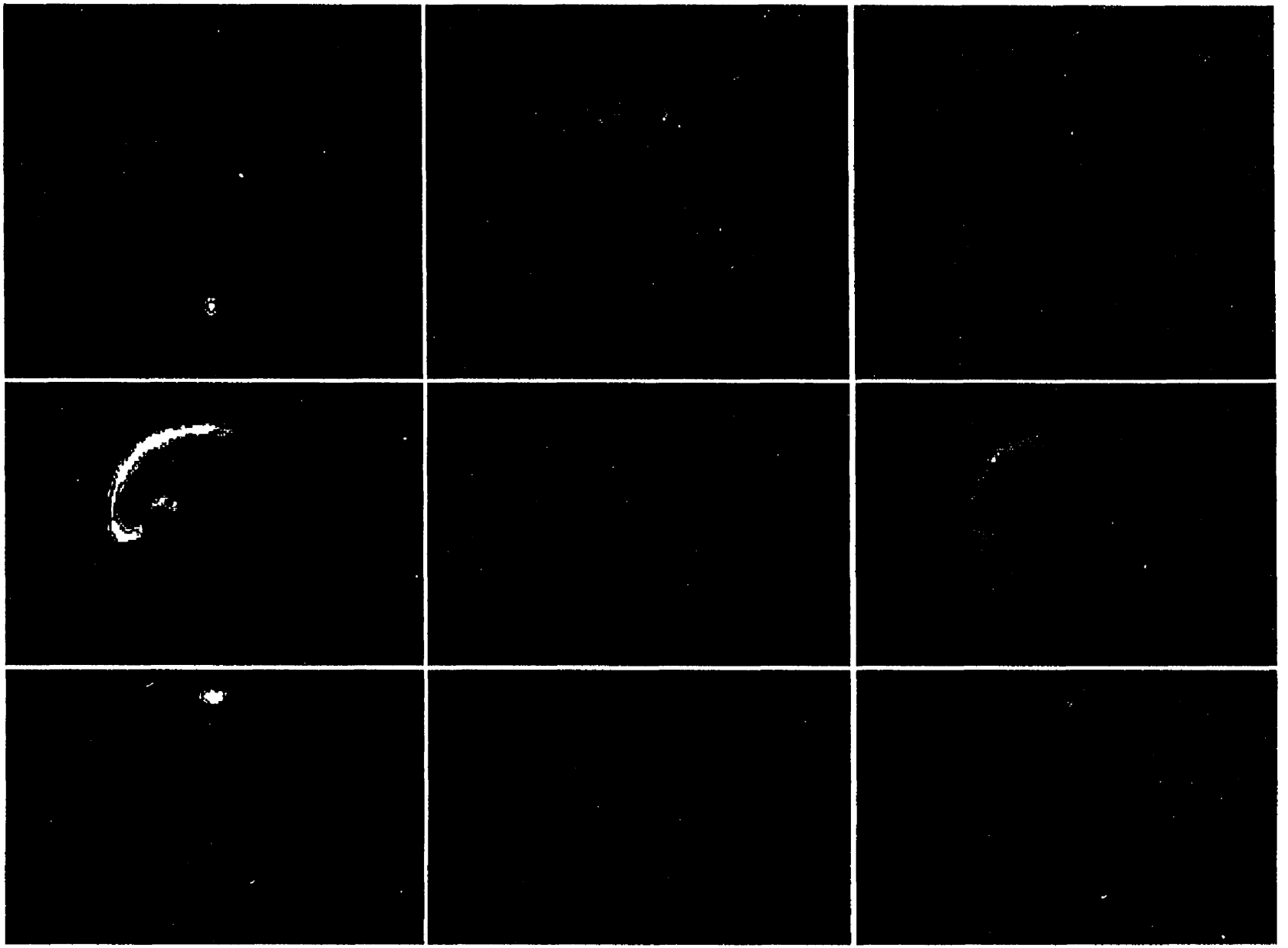

Figure 7.2 A CBV image coregistered with an MRI image using Register program. From left to right are CBV, MRI, and the coregiastration of both images. From top to bottom are transverse, sagittal and coronal planes which join at the cross.

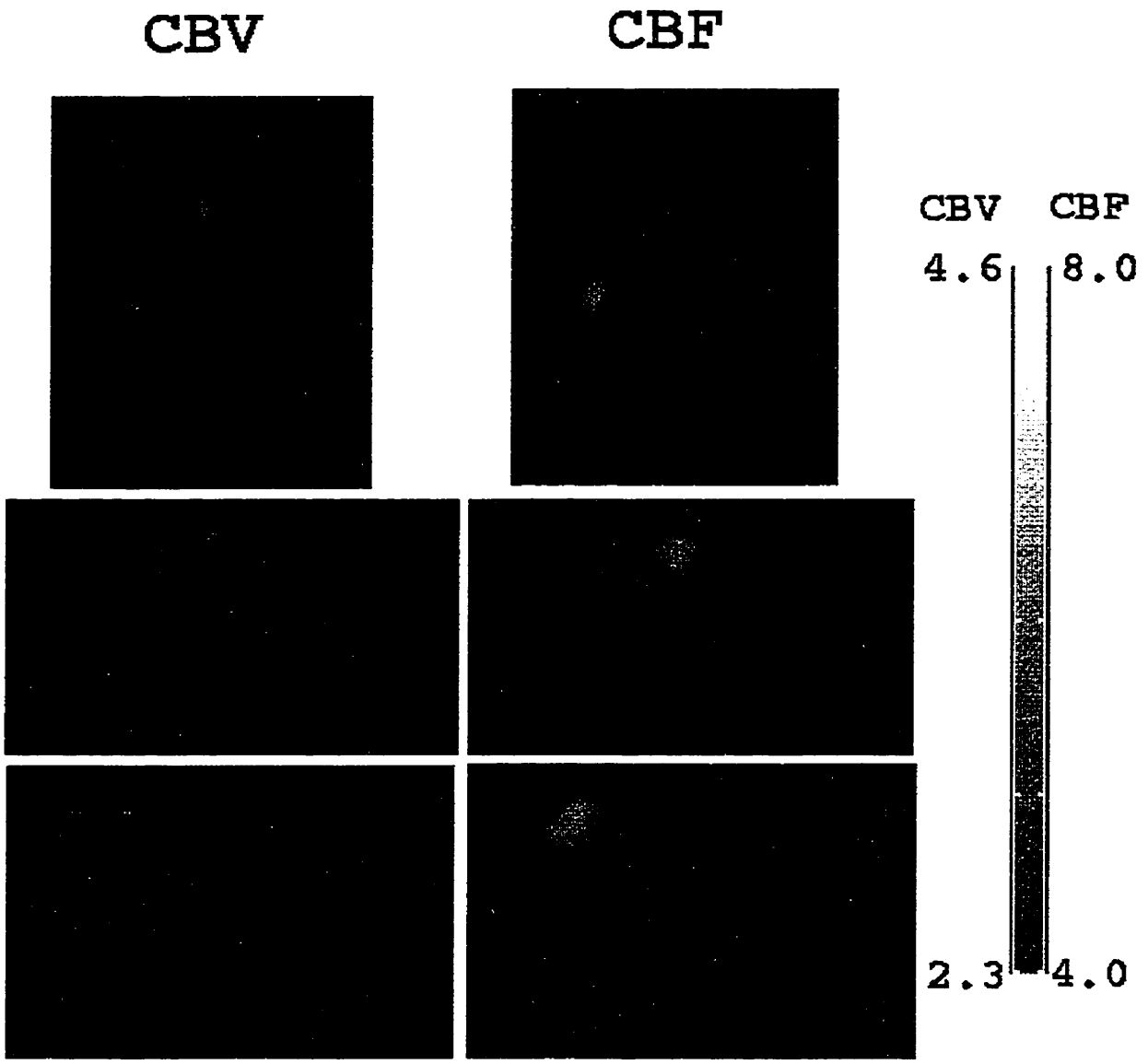

Figure 7.3 T-images of CBV and CBF PET activation studies with vibrotactile stimulation coregistered with MRI images. The CBF data is taken from a vibrotactile activation study on 8 subjects with 6×40mCi ^{15}O-water tracer injected to each subject.

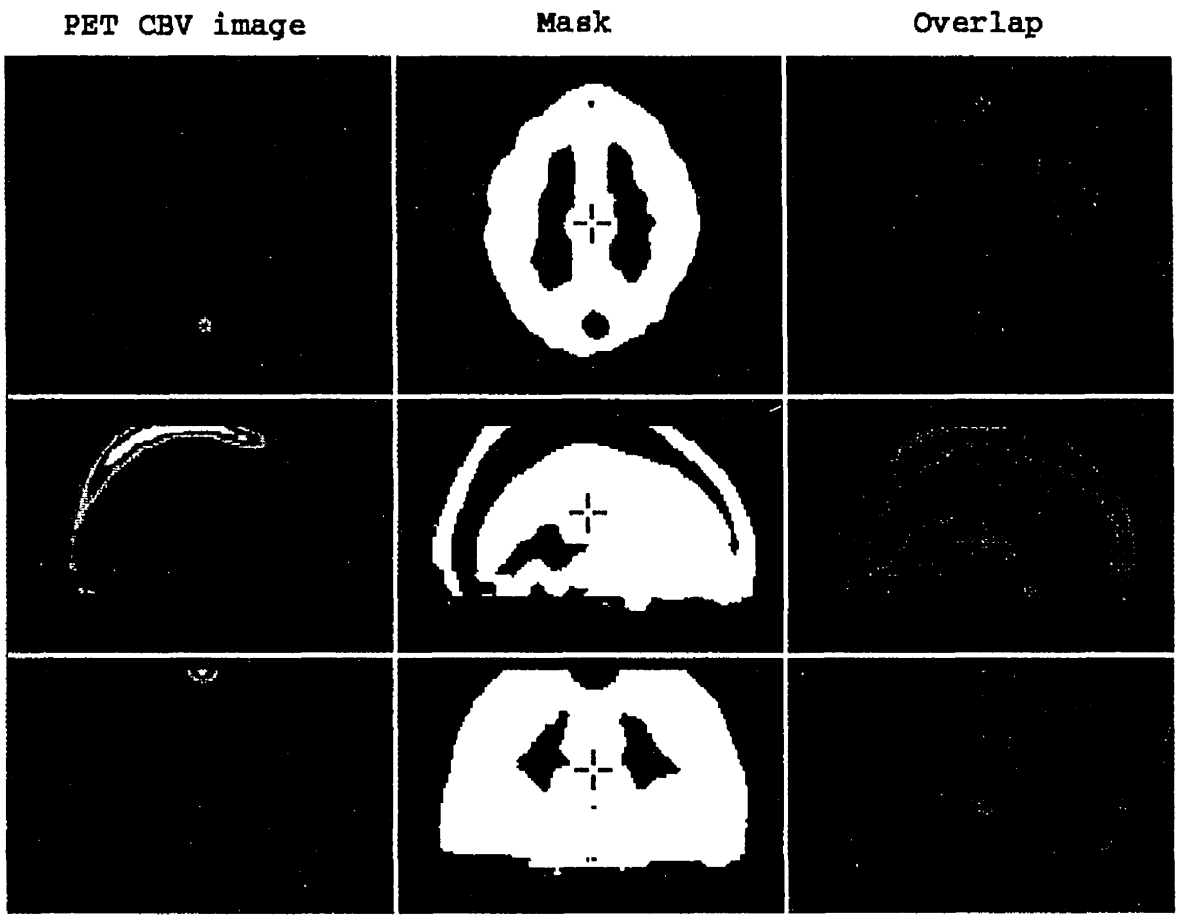

Figure 7.4 LEFT: CBV PET images averaged over 4 subjects; **MIDDLE:** The mask which excludes areas with very high and very low radioactivity concentration; **RIGHT:** Coregistered image and mask. (All in Talairach space)

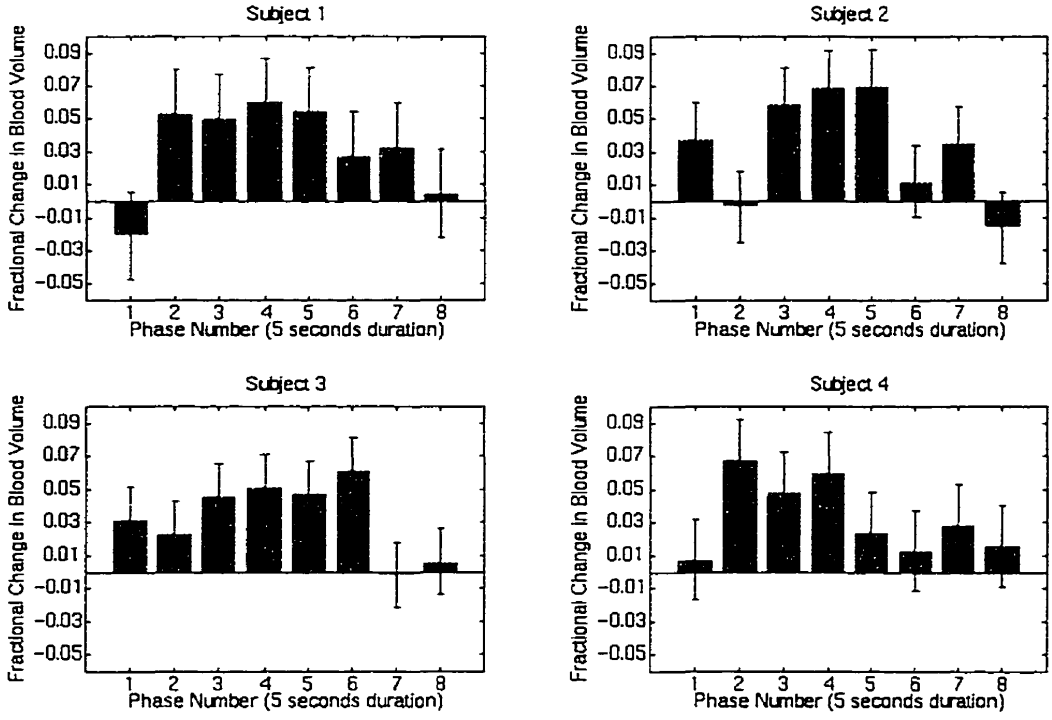

Figure 7.5 Fractional change of CBV for the EVR studies for 4 individual subjects.

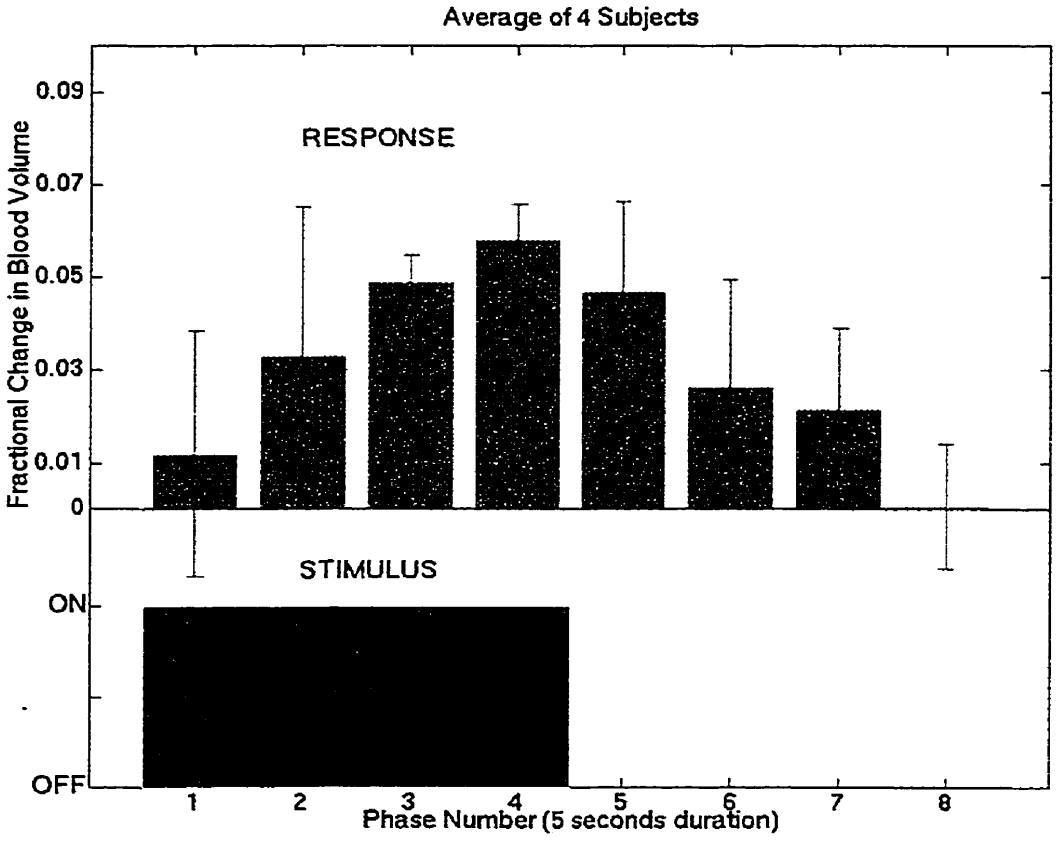

Figure 7.6 The average fractional change in CBV from the EVR scans of the 4 subjects .

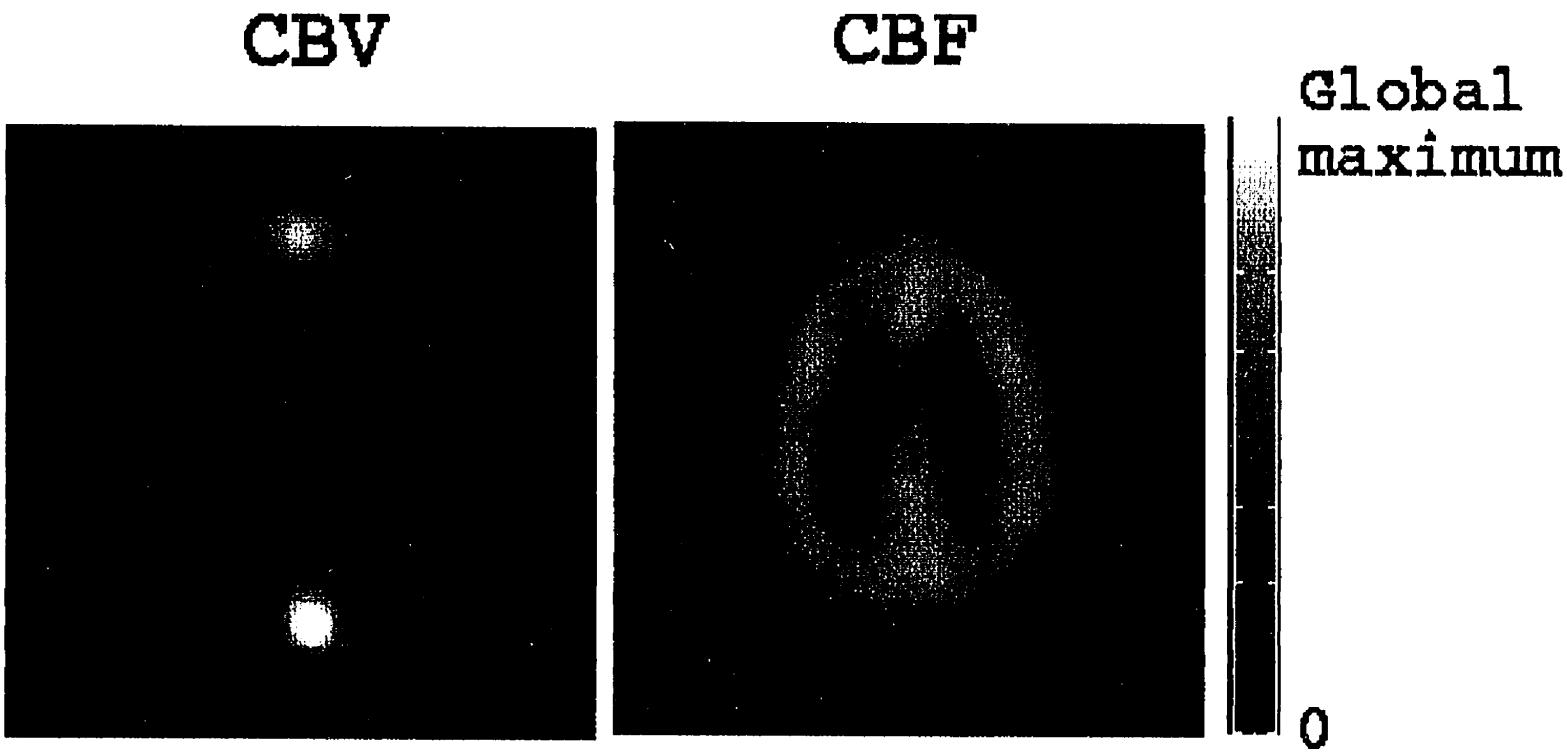

Figure 7.7 A comparison of the uniformity of the radioactivity concerntration. Both images are from the same slice of a subject. 25mCi ^{11}C-CO, 40mCi ^{15}O-H_2O were administered to the same subject for the CBV, CBF studies respectively.

8. Conclusion

A technique to measure evoked vascular response (EVR) was developed for the Scanditronix PC2048-15B PET scanner, which has opened a temporal window for PET. Following simulation and phantom tests, the technique was first applied to CBV activation studies on 4 subjects by employing vibrotactile stimulation, where 25 mCi of ^{11}C labelled CO gaseous tracer was administered to each subject. Fractional CBV change in the somatosensory right-hand area shows clear evoked vascular response when averaging the data of 4 subjects. A rise time of 7.3±1.9s and a decay time of 13.2±2.2s were determined which agree well with the previous studies on human subjects, animals and modelling.

The technique offers the advantage of selecting any phase-duration from milliseconds to minutes in order to study vascular or neuronal responses. It can be further applied to activation studies with other types of stimulation such as visual, auditory or olfactory stimulations. It has the ability to synchronize one or two sets of stimulation with the acquisition, which enables EVR studies with mixed stimulation [Stein BE, 1995; Small DM, 1996]. The technique also has the ability to vary the frequency of the stimulation, facilitating frequency-dependent activation studies [Kwong K, 1992; Fox PT, 1985; Sadato N, 1996].

Other than activation studies, the technique can be easily adapted to studies requiring gated memories to distinguish different temporal periods of brain function. As an example,

during sleep studies with PET, different activities are going on in different periods of sleep [Hong CC, 1995; Kempenaer C, 1994; Hofle N, 1997]. A technique which can clearly separate events happened during REM (Rapid Eye Movement) period from other periods can be very helpful. The EVR technique can play such a rule by storing data in different files corresponding to different periods during sleep by gating the EVR mode with EEG signals.

The gating hardware and software have been adapted in conjunction with a technique to correct head motion of subjects during PET studies by storing data in different memory regions according to the head position [Picard Y, 1997].

The EVR technique is being incorporated currently to the new scanner ECAT HR+, which has a sensitivity 4 times higher than the Scanditronix PC2048-15B and a potential to allocate 32 phases [Moreno-Cantu, 1996; Thompson CJ, 1997]. This may permit the EVR technique to be applied to a single subject with good temporal resolution. This provision would be clinically very useful.

9. References

>>

1 Allemand R, Gresset C, Vacher J, "Potential advantages of a cesium fluoride scintillator for a time-of-flight positron camera " J. Nucl. Med. 21, pp 153-155 (1980)

2 Applegate C, Fox PT, Raichle ME, "Habituation of cerebral blood flow response to cutaneous vibration", Neurology, 38, S363 (1988)

3 Barrio JR, Huang S-C, Yu D-Y, Melega WP, Quintana J, Cherry SR, Jacobson A, Namavari M, Satyamurphy N, Phelps ME, " Radiofluorinated L-M-tyrosine: New in vivo probes for central dopamine biochemistry", J Cereb. Blood Flow Metab. 16, pp667-668 (1996)

4 Cherry SR, Woods RP, Hoffman EJ, and Mazziotta JC," Improved methodology for cerebral activation studies in a single subject using ^{15}O-Water and PET". IEEE Trans Nucl Sci V40:4 pp960-962 (1993)

5 Collins DL, Neelin P, Peters TM, Evans AC, " Automatic 3D intersubject registration of MR volumetric data in standardized Talairach space", J Comput. Assist. Tomogr., Vol 18, pp192-205 (1994)

6 Cumming P, Leger G, Kuwabara H, Gjeddle A, "Pharmacokinetics of plasma 6-[^{18}F]fluoro-L-3, L-dihydroxyphenylalanine ([^{18}F]FDOPA) in humans", J Cereb. Flow Metab., 13, pp668-675 (1993)

7 Dagher A, Thompson C J, "Real time data rebinning in PET to obtain uniformly sampled

projections", IEEE Transactions on Nuclear Science, Vol. NS-32, No.1 February (1985)

8 DI Chiro G, et al. " ^{18}F-2-fluoro-2-deoxyglucose positron emission tomography of human cerebral gliomas", J. Cereb. Blood Flow Metab, Vol. 1, suppl. 1, pp S11-S12 (1981)

9 Diksic M, MRC group grant application "Physiology and pathophysiology of neuronal activation", A.C. Evans and colleagues, 12.1, September (1996)

10 Doyon J, Owen AM, Petrides M, Sziklas V and Evans AC, " Functional anatomy of visuomotor skill learning in human subjects examined with positron emission tomography", European Journal of Neuroscience, Vol. 8 pp637-648 (1996)

11 Drevets WC, Burton H, Videen TO, Snyder AZ, Simpson J R, and Raichle M E: "Blood flow changes in human somatosensory cortex during anticipated stimulation", Nature, Vol. 373, 19 January, pp 249-252 (1995)

12 Evans AC, Marrett TS, Collins DL, Peter T M, "Anatomical-functional correlative analysis of the human brain using three dimensional imaging systems", Proceedings of International Society of Optical Engineering: Medical Imaging III, New port Beach,CA, pp264-274 (1989)

13 Evans AC, Thompson CJ, Marrett S, Meyer E, Mazza M. " Performance evaluation of the PC2048: A New 15-Slice Encoded-Crystal PET Scanner for Neurology Studies". IEEE Transactions on Medical Imaging, Vol.10, No.1, March, pp 90-98 (1991)

14 Fox PT, Raichle ME, "Focal physiological uncoupling of cerebral blood flow and oxidative metabolism during somatosensory stimulation in human subjects", Proc. Natl. Acad. Sci. USA, Vol. 83, February, pp 1140-1144 (1986)

15 Fox PT, Miezin FM, Allman JM, Van Essen DC, and Raichle M E. "Retinotopic

organization of human visual cortex mapped with Positron-Emission Tomography". The Journal of Neuroscience, March, Vol 7,(3), pp 913-922 (1987)

16 Fox PT, Burton H, Raichle ME, " Mapping human somatosensory cortex with Positron Emission Tomography", J. Neuroserg. Vol. 67, July, pp (1987b)

17 Fox PT, Mintun MA, Reiman EM. "Enhanced detection of local brain response using intersubject averaging and change distribution analysis of subtracted PET images" Journal of Cerebral Blood Flow Metabolism. Volume 8, pp 642-653 (1988)

18 Frostig RD, Lieke EE, Ts'o DY, Grinvald A, "Cortical functional architecture and local coupling between neuronal activity and the microcirculation revealed by in vivo high-resolution optical imaging of intrinsic signals ", Proc. Natl. Acad. Sci. USA, 89, pp 6082-6086 (1990)

19 Fujita H, Meyer E, Kuwabara H, Marrett S, Gjedde A, "Comparison of apparent V_0 images for water, oxygen and CO in PET", J Nucl. Med.34, s199 (1993)

20 Jolly D, Private communication, June 1995.

21 Grady CL, Haxby JV, Horwitz M, Gillette J, Salerno JA, Gonzalez-Aviles A, Carson RE, Herscovitch P, Schapiro MB, Rapoport SI, " Activation of cerebral blood flow during a visuoperceptual task in patients with Alzheimer-type dementia", Neurobiol. Aging Vol. 14, pp35-44 (1993)

22 Grubb RL, Raichle ME, Eichling JO, Ter-Pogossian MM, " The effect of changes in P_aCO_2 on cerebral blood flow, blood volume and vascular mean transit time", Stroke, 5, pp630-639 (1974)

23 Grubb RL, Raichle ME, Higgins CS, and Eichling JO. "Measurement of regional cerebral

blood volume by emission tomography" Annals of Neurology, Volume 4, Number 4, October, pp 322-328 (1978)

24 Grubb RL, Ratcheson RA, raichle ME, Kliefoth AB, Gado MH, "Regional cerebral blood flow and oxygen utilization in superficial temporal-middle cerebral artery anastomosis patient: an exploratory definition of clinical problems ", J. Neurosurg. 50, pp 733-741 (1979)

25 Herscovitch P, Markham J, Raichle ME, "Brain Blood flow measured with intravenous H2O. I. Theory and error analysis", J. Nucl. Med. Vol. 24, No. 9, (1983)

26 Hoffman brain phantom manual: Data spectrum's three-dimensional Hoffman brain phantom user's manual, Data spectrum corporation 437 dimmocks mill RD, Hillsborough, NC 27278.

27 Holte S, Eriksson L, Larson JE, Ericson T, Stjernberg H, Hansen P, Bohm Chr, Kesseelberg M, Rota E, Herzog H, Feinendegen L, " A preliminary evaluation of a positron camera system using weighted decoding of individual crystals", IEEE Trans. Nucl. Sci., Vol. 35, No. 1 (1988)

28 Hong CC, Gillin JC, Dow BM, Wu J, Buchsbaum MS, "Localized and lateralized cerebral glucose metabolism associated with eye movements during REM sleep and awareness: a positron emission tomography (PET) study", Sleep, Vol. 18, pp570-580 (1995)

29 Hurtig R, Hichwa RD, O'Leary DS, Boles Ponto L, Narayana S, Watkins G, Andreasen NC, "Effects of timing and duration of cognitive activation in [^{18}O] water PET studies", J Cereb. Blood Flow Metab., Vol. 14, No.3 (1994)

30 Kato T, Kamei A, Takashima S, and Ozaki T: " Human visual cortical function during

photic stimulation monitoring by means of Near-Infrared Spectroscopy". J Cereb Blood Flow Metab, Vol.13, No.3, pp 516-520 (1993)

31 Kempenaers C, Mendlewicz J, " Rythmie du sommeil paradoxal chez une adulte", Neurophysiologie Clinique, Vol. 24(2), pp167-173 (1994)

32 Kwong KK, Belliveau JW, Chesler DA, Goldberg IE, et.al. "Dynamic magnetic resonance imaging of human brain activity during primary sensory stimulation", Proc. Natl. Acad. Sci. USA, Vol 89, June, pp 5675-79 (1992)

33 Lange N, Zegar SL, " Non-linear Fourier time series analysis for human brain mapping by functional magnetic resonance imaging", Applied Statistics (1996)

34 Leblanc R, Meyer E, Bub D, Zatorre RJ, Evans AC, "Language localization with Activation Positron Emission Tomography Scanning", Neurosurgery, Vol. 31, No.2, August, pp 369-372 (1992)

35 Lou HC, Edvinsson L, Mackenzie ET, "The concept of coupling blood flow to brain function: Revision required?" Ann. Neurology Vol. 22, No. 3, Sept., pp (1987)

36 Maini CL, Turco GL, Castellano G, Liboni W, Podio V, Chianale G, Gornaglia G, " Cerebral blood flow and volume in symptom-free migraineurs, A SPECT ? Study", Nuklearmedzin, 29(5), November, pp 214-214 (1990)

37 Martin W, Power WJ, Raichle ME. "Cerebral blood volume measured with inhaled $C^{15}O$ and PET", J Cereb. Blood Flow Metab., Vol 7, No 4, pp 421-426 (1987)

38 MATLAB reference book: MATLAB high-performance numeric computation and visualization software, reference guide. The Math Works Inc. 1995

39 Meyer E, Perguson SSG, Zatorre RJ, Alivisatos B, Marrett S, Evans AC, Hakim AM,

"Attention modulates somatosensory cerebral blood flow response to vibrotactile stimulation as measured by Positron Emission Tomography", Ann. Neurology, Vol. 29, No. 4, pp440-443 (1991)

40 Milot S, DOT User's Guide, Brain Imaging Centre in MNI, May 30, (1996)

41 Moonen C, Van Zijl P, Frank J, Le Bihan D, Becher E, " Functional magnetic resonance imaging in medicine and physiology", Science, Vol. 250, pp53-61 (1990)

42 Moreno-Cantu JJ, Thompson CJ, Zatorre RJ, "Evaluation of the ECAT EXACT HR$^+$ 3D PET scanner in ^{18}O-water brain activation studies", IEEE Nuclear Science Symposium Conference Record, November 2-9, vol. 2, pp1280 (1996)

43 Murase K, Private communication 1995.

44 Narayan SM, Santori EM, Toga AW, "Mapping functional activity in rodent cortex using optical intrinsic signals", Cerebral Cortex, Vol. 4, pp195-204 (1994)

45 Narayan SM, Esfahani P, Blood AJ, Sikkens L, Toga AW, " Functional increase in cerebral blood volume over somatosensory cortex", J. Cereb. Blood Flow Metab. Vol. 15, No. 5, pp 754-765 (1995)

46 Ngai AC, Ko KR, Morii S, Winn HR, "Effect of sciatic nerve stimulation on pial arterioles in rats", Am. J. Physiol. 254, H133-H139 (1988)

47 Numerical recipes in C, The art of scientific computing, second edition, William H, Press; Saul A, Tenkolsky; William T, Vettering; Brain P, Flannery, pp 683.

48 Ogawa S, Lee TM, Kay AR, Tank DW, " Brain magnetic resonance imaging with contrast dependent on blood oxygenation ", Proc. Nat. Acad. Sci. USA, Vol. 87, pp9868 (1990)

49 Owen AM, Doyon J, Petrides M, Evans AC, "Planning and spatial woring memory examined with positron emission tomography", European Journal of Neuroscience, Vol. 8, pp353-364 (1996)

50 Perry DW, Zattore RJ, Evans AC," Co-variation of CBF during singing with vocal fundamental frequency", Neuroimage, 3, S315 (1996)

51 Positron Emission Tomography PC2048-15B/PC4096-15B Software Manual

52 Positron Emission Tomography PC2048-15B/PC4096-15B Hardware Manual

53 Phelps ME, Huang SC, Hoffman EJ, and Kuhl DE. "Validation of tomograghic measurement of cerebral blood volume with ^{11}C-labelled carboxyhemoglobin" The Journal of Nuclear Medicine, Volume 20, Number 4, pp 328-334 (1979)

54 Raichle ME, Eichling JO, Straatmann MG, Welch MJ, Larson KB, Ter-pogossian MM, "Blood-brain barrier permeability of ^{11}C-labelled alcohols and ^{15}O-labelled water", Am. J. Physiol, 230, pp 543- 552 (1976)

55 Raichle ME, Martin WR, Herscovitch P, Mintun MA, Markhum J, "Brain Blood flow measured with intravenous H_2O. II. Implementation and validation" J. Nucl. Med. Vol. 24, Num. 9, pp790-798 (1983)

56 Roland PE, Eriksson L, Stone-Elander S, Widen L, " Does mental activity change the oxidative metabolism of the brain?" J. Neuroscience, 7(8), August, pp 2373-2389 (1987)

57 Roland PE, Gulyas B, " Visual imagery and visual representation ", Trends in Neuroscience, 17, pp281-297 (1994)

58 Reutens D, Private communication, 1997.

59 Sadato N, Ibanez V, Deiber M, Campbell G, Leonard M, Hallette M, "Frequency-

dependent changes of cerebral blood flow during finger movement", J Cereb. Blood Flow Metab., Vol. 16, No. 1 (1996)

60 Sandman CA, O'Halloran J P, Isenhart R. "Is there an Evoked Vascular Response?" Science, Vol. 224, 22 June, pp 1355-1357 (1984)

61 Segebarth C, Belle V, Delon C, Massarelli R, Decety J, Le Bas JF, Decorps M, Benabid AL, "Functional MRI of the human brain: predominance of signals from extracerebral veins", Neuroreport, Vol. 5, pp 813-816 (1994).

62 Seitz AJ, Roland PE, "Vibratory stimulation increases and decreases the regional cerebral blood flow and oxidative metabolism: A Positron Emission Tomography (PET) study", Act. Neurol. Scand. 86, PP 60-70 (1992)

63 Shockley RP, LaManna JC, "Determination of rat cerebral cortical blood volume changes by capillary mean transit time analysis during hypoxia, hypercapnea and hyperventilation. Brain Res. 459:1 (1988)

64 Small DM, Zatorre RJ, Jones-Gotman M, Petrides M, Evans AC, " Flavour processing: More or less than the sum of its parts?" Neuroimage, 3, S345 (1996)

65 Stein BE, Wallace MT, Meredith MA, Neural mechanism mediating attention and orientation to multisensory cues, in the cognitive neurosciences, In the Cognitive Neuroscience, M. Gazzaniga Ed., MIT Press, Cambridge, Mass.

66 Talairach J, Tournoux P, Co-Planar Stereotactic Atlas of the Human Brain, Stuttgart, Georg Thieme Verlag.

67 Talairach J, Tournoux P, "Co-planar sterotactic atlas of the human brain: 3-dimensional propotional system: an approach to cerebral imaging", Stuttgart:Verlag.

68 Ter-Pogossian MM, Ficke DC, Beecher DE, Hoffman GR, Bergmann SR, "The super PET 3000-E: A PET scanner designed for high count rate cardiac applications", J. of Computer Assisted Tomography, 18(4), pp 661-669, Jul-Aug (1994)

69 Thompson CJ, Yamamoto YL, Meyer E, "Positome II: A high efficiency positron imaging device for dynamic brain studies ", IEEE Trans. Nucl. Sci, NS-26, pp 583-586 (1979)

70 Thompson CJ, "Positron Emission Tomography, advances in scintillation cameras", Phys. Med, Vol. 4, No. 1 (Suppl.1), pp 23-26 (1988)

71 Thompson CJ, Murthy K, Picard Y, Weinberg IN, Mako R, "Positron emission mammography (PEM): A promising technique for detecting breast cancer", IEEE Trans. Nucl. Sci., Vol. 42, No. 4, pp1012-1017 (1995)

72 Thompson CJ, Private communication, 1997.

73 Thompson C J, "The effects of detector material and structure on PET spatial Resolution and efficiency", IEEE Transactions on Nuclear Science", Vol. 37, No. 2, April, pp 718-724 (1990)

74 TTL Data Book & TTL Data Book supplementary. Fairchild, Printed in USA, Dec. 1978.

75 Villringer A, Plank J, Stodieck S, Botzel K, Schleinkofer L, Dirnagl U, "Noninversive assessment of cerebral hemodynamics and tissue oxygenation during activation of brain cell function in human adults using Near Infrared Spectroscopy", Advances in Experimental medicine & Biology, 345, pp 559-565 (1994)

76 Wang B, Thompson C J, Mazza M. " Measurement of Evoked Vascular Response to cerebral activation with PET". Nuclear Symposium and Medical Imaging Conference, 1994 IEEE Conference Record, pp 1421-23 (1994)

77 Wang B, Thompson CJ, Reutens D, Jolly D, "Measurement of the evoked vascular response (EVR) to cerebral activation due to vibrotactile stimulation using gated ^{11}C-CO PET acquisition". Nuclear Symposium and Medical Imaging Conference, November, 1997, to be presented as a talk in November 13th, 1997.

78 Worsley KJ, Evans AC, Marrett S, Neelin P, "A three dimensional statistic analysis for CBF activation studies in human brain", J. Cereb. Blood Flow Metab. 12, pp 900-918 (1992)

79 Yamamoto YL, et al, Cerebral blood flow (Edited by M. Baldy-Moulinier). John Libbey, London, (1983)

80 Zatorre RJ, Jones-Gotman M, Evans AC, Meyer E, "Functional localization and lateralization of human olfactory cortex", Nature, Vol. 360, 26, November, pp 339-340 (1992)

81 Zatorre RJ, Evans AC, Meyer E, Gjedde A,"Lateralization of phonetic and pitch discrimination in speech processing", Science, Vol. 256, 8 May, pp846-849 (1992)

82 Zatorre RJ, Meyer E, Gjedde A, Evans AC," PET studies of phonetic processing of speech: Review, replication, and re-analysis", Cerebral Cortex, 6, pp21-30 (1996)

10. Appendix

>>

EVR Consent Form

POSITRON EMISSION TOMOGRAPHY (PET) AND MAGNETIC RESONANCE IMAGING (MRI) CONSENT FORM

MONTREAL NEUROLOGICAL INSTITUTE & HOSPITAL
McConnell Brain Imaging Centre, Departments of Nuclear Medicine& Neuroradiology

Title of Project: EVOKED VASCULAR RESPONSE STUDIES
Investigators: C. J. Thompson

1. REASON FOR THE STUDY

Positron emission tomography is a new test which provides pictures of the chemical activity and circulation of the brain. There are reasons to believe that these pictures will contribute to the understanding of certain neurological problems. This study will involve inhalation of a small amount of traces of carbon monoxide labelled with carbon ^{11}C [half life = 20 minutes]. The researchers hope that this study will contribute to the development of a new technique to localize parts of the brain which are used during the performance of specific tasks.

2. PROCEDURES

Your participation in this study will involve two sessions of about half a day each, probably on two separate days. The first involves a Positron Emission Tomography (PET) study, the second involves a Magnetic Resonance Imaging (MRI) study.

a) Positron Emission Tomography Procedures (PET Study)

1) You will be asked to lie on a couch; a head-holder will be made in order to keep head movement to a minimum.

2) A ten minute transmission scan will be done to localize the head in the scanner and help interpret the images.

3) You will take several breaths of air mixed with a trace amount of ^{11}C-labelled carbon monoxide. A twenty minute scan will be started a few minutes later. During this scan the fingers on the left and right hands will be tickled alternately with the mechanical vibrators. This will be done in the following sequence: left hand - nothing - right hand - nothing - left hand - etc. Later, another twenty-five minute scan will be done, during which only one of your hands will be tickled.
The order of the two scans may be interchanged.

4) We estimate that the study will take about an hour and a half, during which time you will be requested to lie still on the couch in the scanner.

5) All procedures during the PET study will be carried out by a qualified nuclear medicine technician, and supervised by a qualified nuclear medicine physician.

b) Magnetic Resonance Imaging Procedures (MRI Study)

You will be asked to lie on a couch that will be moved into a cylindrical opening where pictures of your head will be taken during a period of 30 to 40 minutes. The MRI machine will be quite noisy during the scan. To reduce the noise, you will be given earplugs.

3. CONTRAINDICATION

a) For PET Study

The following are contraindications for this procedure.

1) Pregnancy or Breast Feeding
2) Under 18 years old
3) Previous radiation doses received within the past year (over 20 mSv)

b) For MRI Study

The following are contraindications for this procedure.

1) Pacemaker
2) Aneurysm Clip
3) Heart/Vascular Clip
4) Prosthetic Valve
5) Metal Prosthesis
6) Pregnancy

4. ADVANTAGES OF THE PROPOSED STUDIES

Both PET and MRI studies are tests, not treatments. It is hoped that the information obtained will help our understanding of the function of the human brain. This may, in the long term, help the diagnosis and treatment of neurological disorders.

5. DISADVANTAGES OF THE PROPOSED STUDIES

a) PET

(I) Some discomfort may be caused by putting on the mouth-piece as well as immobility on the couch.

(ii) The main **Risk** of participating in this study is exposure to radiation from the short-lived tracer substances injected into your body, e.g:

i) 25 mCi of ^{11}C-labelled carbon monoxide (^{11}CO) will result in about 4.8 mSv of radiation to the whole body.

Therefore, during the study your body will be exposed to a radiation level of less than 5.0

mSv. This radiation dose is two times the radiation which you receive annually from natural background radiation (0.9 - 2.2 mSv) in various regions of North America. This is also 20% to of the annual dose limit allowed for those who work in a high radiation environment, such as, e.g., x-ray technicians. The degree of **Risk** associated with exposure to an additional less than 5.0 mSv of radiation is thought to be very low. This amount of additional radiation increases the risk of death from cancer by about 1 in 20,000 during a lifetime. Similar risks of death are associated with:

a) smoking 2 packs of cigarettes during a lifetime.
b) driving 2,000 miles by car (Montreal to Calgary).
c) flying 20,000 miles by air.
d) Lumbosacral spine x-ray once

Additional information available upon request

b) MRI

During this study, you will be exposed to a strong magnetic field. However, no long-term negative side-effects have been observed from this type of study. As mentioned above, the MR is very noisy and you will be given earplugs to reduce this effect.

6. EFFECTS OF PARTICIPATION IN THIS STUDY ON YOUR TREATMENT

Positron emission tomography or magnetic resonance imaging does not interfere with any treatment or other diagnostic tests.

7. CONFIDENTIAL NATURE OF THIS STUDY

The results of the testing will be kept confidential. No personal information will be released to third parties without your written approval. Your name, date of birth, address and telephone number may have to be forwarded to the Atomic Energy Control Board of Canada upon request.

8. INCIDENTAL FINDINGS

Any incidental findings regarding your own health will be communicated to you or to your physician at your request.

9. DISCONTINUATION OF THE STUDY BY THE INVESTIGATOR

At any time during the testing, the investigators have the right to terminate the study for

purely scientific reasons.

10. COMPENSATION

Upon completion of both MRI and PET studies you will receive $100.00 as compensation for your time and inconvenience. If studies have to be terminated for scientific reasons, compensation will be adjusted according to the fraction of the studies completed.

11. SUBJECTS STATEMENT CONCERNING WITHDRAWAL FROM THE STUDY

I understand that my participation in this research project is voluntary and I may withdraw at any time, including during the procedure, without prejudice to myself or my treatment.

QUESTIONNAIRE FOR MAGNETIC RESONANCE IMAGING

1. Previous surgery (type and date)_____.

2. Does the subject have any of the following?

	YES	NO
Cardiac pacemaker	____	____
Surgical clip on an aneurysm or other vessel	____	____
Surgical clip or valve on the heart	____	____
Prostheses (please specify type and location) _____	____	____
Implants (please specify type and location) _____	____	____
Metal or metallic fragments in any part of the body (please specify)_____	____	____

3. Is the subject pregnant? ____ ____

Is the subject currently taking prescription medication? ____ ____

SUBJECT'S DECLARATION OF CONSENT

I,_____, have read the above description with one of the above investigators, _____.

I fully understand the procedures, advantages and disadvantages of the study which have been explained to me. I freely and voluntarily consent to participate in this study.

I hereby certify that I have not participated in a PET investigation anywhere before.

Further, I understand that I may seek information about each test either before or after it is given, that I am free to withdraw from the testing at any time if I desire, and that my personal information will be kept confidential.

SIGNATURE _____ _____ _____
SUBJECT *DATE* *CONTACT NO.*

SIGNATURE _____ _____ _____
INVESTIGATOR *DATE* *CONTACT NO.*

SIGNATURE _____ _____ _____
WITNESS *DATE* *CONTACT NO.*

SIGNATURE _____ _____ _____
PHYSICIAN *DATE* *CONTACT NO.*

IMAGE EVALUATION TEST TARGET (QA-3)

150mm

6″

APPLIED IMAGE . Inc
1653 East Main Street
Rochester, NY 14609 USA
Phone: 716/482-0300
Fax: 716/288-5989